Chemical biological studies for the compounds exerting synthetic lethal effect in human tumor cells

March 2017

Yuki Shikata

A Thesis for the Degree of Ph.D in Science

Chemical biological studies for the compounds exerting synthetic lethal effect in human tumor cells

March 2017

Graduate School of Science and Technology

Keio University

Yuki Shikata

Abbreviations

2-DG	2-deoxyglucose
AC	adenylate cyclase
APC	adenomatous polyposis coli
cAMP	cyclic AMP
CCCP	m-chlorophenyl hydrazone
CI	combination index
ECAR	extracellular acidification rate
ESI	eeyarestatin I
GO	gene ontology
PARP	poly (ADP-ribose) polymerase
PKA	protein kinase A
PTX	paclitaxel
VCP	valosin-containing protein
Wnt	wingless/int-1
XN	xanthohumol

Chapter 1 Introduction

1.1 Chemotherapy and Targeted therapy

Cancer is one of the life-threatening diseases caused by uncontrolled cell growth and the potential to metastasize anywhere in the body. There are approximately 8.2 million cancer related deaths all over the world in 2012, and annual cancer cases is expected to rise 14 million in 2012 to 22 million within the next two decades[1,2]. A large number of cancer researchers have worked on a cure for cancer so far, and a wide variety of anticancer agents have ever been developed and clinically approved. One of the best features of cancer cells is that they grow faster than normal cells to form a tumor, therefore, DNA and microtubules have thought to be an effective target for anticancer agents, such as an alkylating agent cyclophosphamide (Endoxan)[3], antimetabolites fluorouracil (5-FU) and 6-mercaptopurine (Leukerin)[4], a topoisomerase II inhibitor etoposide (Lusted)[5], and a tubulin depolymerization inhibitor paclitaxel (Taxol)[6]. These chemotherapy agents interfere with cell division, thus, cancer cells are sensitive to them. Chemotherapy agents are now used for a wide variety of human tumors, however, they have been confronted with serious side effect problems that they could also damage to human normal cells.

In the last two decades, a lot of genes responsible for tumorigenesis have been discovered, including oncogene, tumor-suppressor genes, and stability genes[7]. These genes are related to the signaling pathways regulating cell growth, proliferation, and apoptosis, thus, their mutations contribute to cancer development. Therefore, a specific molecular target or signaling pathway that have a crucial role in tumorigenesis due to the mutation of such genes have thought to be attractive for anticancer agents, termed "targeted therapy"[8]. Many molecularly targeted agents have ever been developed and clinically approved, such as a Bcr-Abl inhibitor imatinib (CGP 57148; Gleevec) for chronic myeloid leukaemia (CML)[9], an anti-HER2 antibody trastuzumab (Herceptin) for

HER2-positive breast cancer[10,11], an anti-EGFR antibody cetuximab (Erbitax) for EGFR-positive colorectal cancer[12], and a VEGFR and PDGFR inhibitor sorafenib (Nexavar) for clear-cell renal-cell carcinoma and hepatocellular carcinoma[13,14]. Because these molecularly targeted agents target a mutated protein that activates in only cancer cells, they are expected to show the high specificity to cancer cells and less harmful to normal cells than chemotherapy agents, and indeed, they exhibit the dramatic clinical responses to each cancer. Furthermore, a target of the molecularly targeted agent could be a biomarker to predict its efficacy. However, there are also problems that some of the molecularly targeted agents have reported to exhibit severe side effects because of their 'off-target', and that cancer can develop a tolerance to them due to activating another survival signaling pathway and suppressing apoptosis pathway[15]. Therefore, another strategies are required to discover the more effective targets for overcoming such problems.

1.2 Synthetic lethality

To circumvent above problems, another idea was spotlighted that "synthetic lethality" might be useful for discovering more effective anticancer agents[16]. The concept of synthetic lethality was first described in the study of fruit fly *Drosophila melanogaster*[17-19]. If two genes (A and B) have a "synthetic lethality relationship", the simultaneous inhibition or mutation of both genes induces cytotoxicity, whereas that of either gene alone does not effect on cell viability[20]. Based on this principle, inhibitor of A could induce cell death selectively in tumor cells harboring the mutation of B, on the other hand, it would not effect on the normal cells harboring wild type B (Figure 1-1). Previously, many gene pairs exhibiting synthetic lethality have been reported[21], such as

PARP inhibition for breast and ovary cancer harboring mutated *BRCA* gene[22,23], CDK4 inhibition for non-small cell lung carcinoma harboring mutated *KRAS* gene[24], PLK1 inhibition for colorectal cancer harboring mutated *KRAS* gene[25], GSK3β inhibition plus TRAIL treatment for *MYC*-overexpressing cancer cells[26], MK2 inhibition for p53-deficient cancer cells[27], *TSC2* inhibition for *RB1* mutant cancer cells[28], and *SKP2* inhibition for *RB1*-deficient human retinoblastoma cells[29].

It is insufficient to understand how many gene pairs exist in human cells, but several studies have been reported that nearly all genes are related to synthetic lethal interaction in the budding yeast *Saccharomyces cerevisiae*[30,31], therefore, many gene pairs in human cells are expected to have synthetic lethality relationships[32]. As described above, the anticancer agents that exhibit synthetic lethal activity would have great potential to target selectively and treat cancer. However, only a few synthetic lethal agents have been reported to be in clinical development now because it is difficult to find the most effective target that have clear correlation with the mutation of synthetic lethal gene.

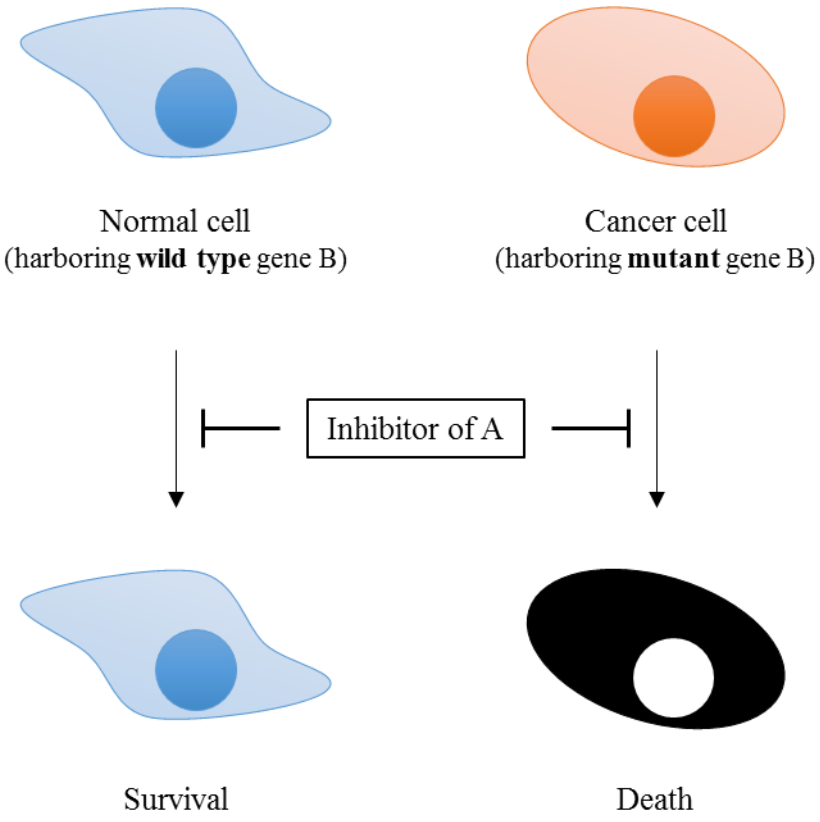

Figure 1-1. The principle of synthetic lethality

1.3 Valosin-containing protein and cancer

Valosin-containing protein (VCP), also known as p97, belongs to the ATPase associated with diverse cellular activities (AAA) ATPase family, which convert the energy generated from ATP hydrolysis into mechanical force to extract molecules from membranes or disassemble multiprotein complexes[33]. VCP forms a doughnut-shaped homo-hexameric complex[34], and plays crucial roles in a wide variety of cellular functions, such as autophagosome maturation[35,36], endoplasmic reticulum-associated degradation (ERAD)[37], the ubiquitin-proteasome system[38,39], the enhancement of NF-κB signaling[40,41], DNA repair[42], and cell cycle regulation[43]. Each monomer is composed of three domains: N domain is involved in interaction with co-factors and adaptor proteins, and D1 and D2 domains are responsible for ATPase activity. The D1 domain also mediates interactions among the monomers and promotes hexamer assembly[33]. Further, it has been reported that the D2 domain mediates the major ATPase activity of VCP, whereas the D1 domain has very low activity[44] (Figure 1-2).

Several clinical studies have reported that VCP may play crucial roles in cancer cells, and elevated VCP is correlated with progression, prognosis, and recurrence of gastric carcinoma[45], pancreatic ductal adenocarcinoma[46], and prostate cancer[47]. Therefore, VCP has been considered as a promising target for therapeutic intervention, and several VCP inhibitors have been reported, including D1 domain inhibitor eeyarestatin I[48,49] and D2 domain inhibitors 2-anilino-4-aryl-1,3-thiazoles[50], Syk inhibitor III[51], and N^2,N^4-dibenzylquinazoline-2,4-diamine (DBeQ)[52]. Furthermore, our laboratory previously identified xanthohumol (XN), a prenylated chalcone present in hops (*Humulus lupus* L.)[53], as a N domain inhibitor, which binds directly to N domain of VCP and modulates autophagy by inhibiting VCP functions[54] (Figure 1-2). However, no approved drugs are

available in the clinic for treatment *via* targeting VCP.

In Chapter 2, I investigated the molecular mechanisms governing the contribution of VCP to the antitumor activity of XN. XN harbors anti-tumorigenic effects toward different types of cancer cells[55] *via* intracellular reactive oxygen species (ROS) induction[56], NF-κB and Akt inhibition[57,58], ER stress induction[59] and disruption of the BIG3-PHB2 interaction[60]. VCP can also play crucial roles in cancer progression and prognosis, therefore, I hypothesized that the antitumor effects of XN can be attributed to the inhibition of VCP function. In this study, I performed genome-wide shRNA screening and identified adenylate cyclase (AC) pathway related genes which have synthetic lethality with VCP inhibition. Our findings suggested that targeting both VCP and the AC pathway is a potential chemotherapeutic strategy for the subset of tumor cells.

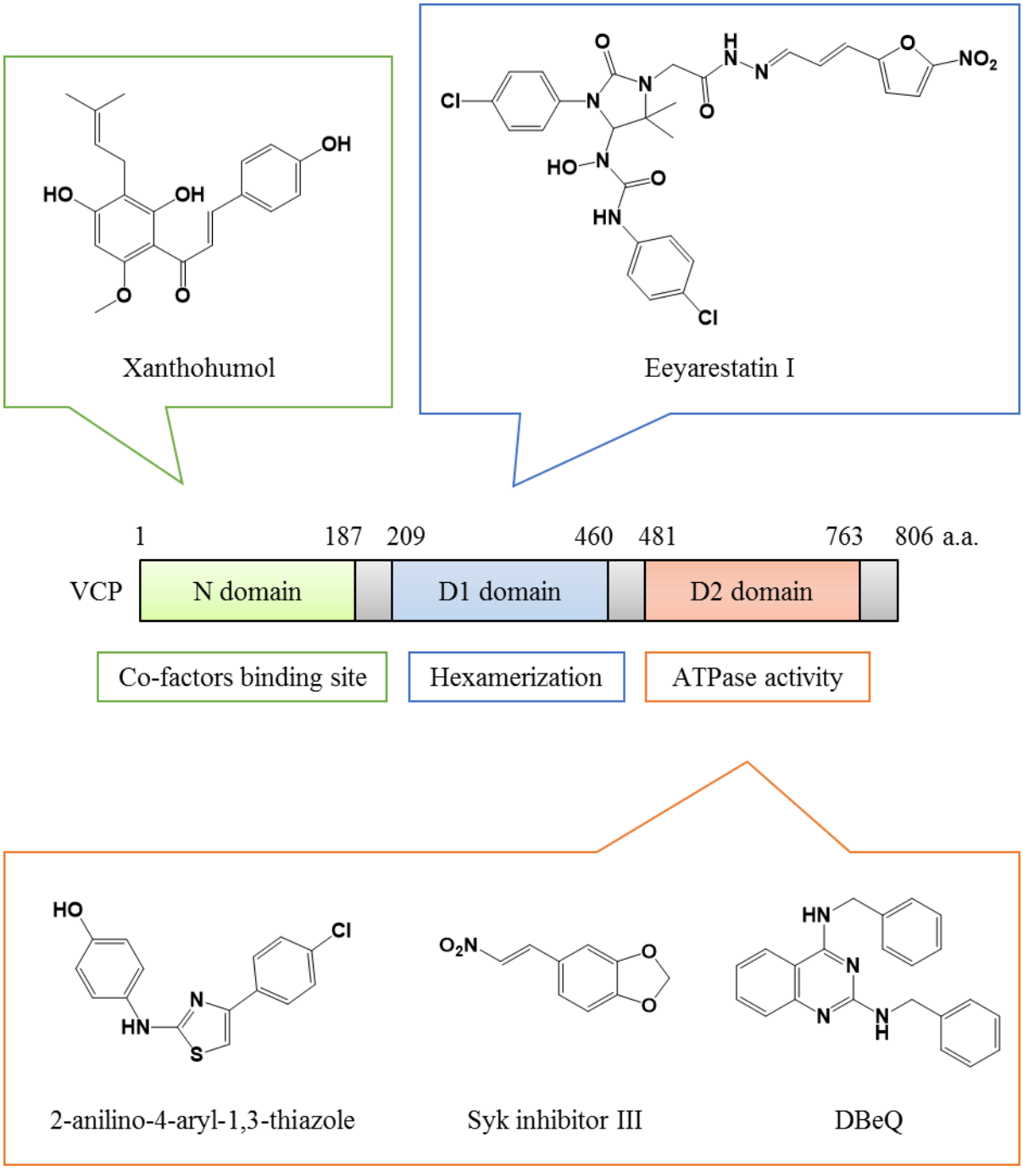

Figure 1-2. VCP inhibitors

1.4 Wnt signaling pathway and cancer

The wingless/int-1 (Wnt) signal transduction pathway plays a central role for the cell proliferation, survival, differentiation, and apoptosis. Wnt ligand stimulus allows β-catenin to accumulate in cytosol and translocate to nucleus, and promotes cell proliferation[61]. In the absence of Wnt ligand, β-catenin expression was downregulated by the "destruction complex" consisting of Axin, adenomatous polyposis coli (APC), casein kinase 1α (CK1α), glycogen synthase kinase 3β (GSK3β)[62]. Forming a scaffold with Axin and APC facilitates the phosphorylation of β-catenin by CK1α (at Ser45) and GSK3β (at Ser33, Ser37, and Thr41). Subsequently, β-TrCP, an F-box protein composed of ubiquitin protein ligase, recognizes the phosphorylation of β-catenin at Ser33/37, leading to promote the ubiquitination and proteasomal degradation of β-catenin, and the free β-catenin levels therefore remain low[62,63]. T-cell factor 4 (TCF4), a transcriptional factor of Wnt signaling pathway, is suppressed by several co-repressors such as transducing-like enhancer of split (TLE) and groucho, and the expressions of Wnt target genes are tightly regulated[64] (Figure 1-3).

On the other hand, in the presence of Wnt ligand, it interacts with the receptor, Frizzled and low-density lipoprotein receptor-related protein-5/6 (LRP5/6), and CK1 and GSK3 subsequently phosphorylate PPPSPXS site of LRP5/6, leading to recruit Axin to cell surface and inhibit its function[65,66]. Further, LRP5/6 promote Axin degradation, and then, β-catenin can escape from degradation by the destruction complex and be stable in cytosol[67]. The free β-catenin translocates to nucleus, where it associates with member of the TCF family to regulate the expressions of Wnt target genes. In the nucleus, β-catenin interacts with TCF4 transcription factor instead of co-repressors, and recruit several co-activators, such as creb binding protein (CBP), B-cell CLL/lymphoma 9 (BCL9), and

pygopus, leading to activate the Wnt target genes including cyclin D1 and c-Myc[61,67,68] (Figure 1-3).

Typically, this signaling pathway is tightly regulated, however, when β-catenin is mutated, it would be hyperactive and drive oncogenesis as a result of the aberrant cell growth signaling. Many studies have reported that β-catenin is mutated in a wide variety of tumors, such as up to 10% of all sporadic colon carcinomas[69,70], 20% of hepatocellular carcinomas[70,71], ovarian cancer[72], and prostate cancer[73]. Further, according to the Catalogue of Somatic Mutation in Cancer (COSMIC: Sanger Institute), approximately 10% of all human tumors harboring active-mutations in β-catenin[74]. The mutation in the N-terminus of β-catenin resulting from point mutations or in-frame deletions of serine or threonine residues phosphorylated by CK1α or GSK3β stabilizes β-catenin and allow it to escape from the proteasomal degradation system and to activate Wnt signaling pathway constantly[70,75,76]. Other than β-catenin, it has been reported that APC is mutated in up to 80% of sporadic colon carcinomas[61,77,78], and Axin 1 is mutated in some liver cancer and medulloblastomas[61,79,80]. Both APC and Axin are negative regulator of the Wnt signaling pathway, and the truncated mutations of them fail to form a scaffold of destruction complex, leading to stabilize β-catenin and aberrantly activate the Wnt signaling pathway.

As described above, activation of β-catenin plays a critical role for the pathogenesis of human tumors. Therefore, this pathway has been considered as a promising target for therapeutic intervention, and several molecularly targeted agents have been developed and entered a Phase I study for solid tumors before[81,82], such as a Porcupine inhibitor LGK974[83,84], a pan-Frizzled antibody vantictumab (OMP-18R5)[85,86], a Wnt ligand antibody OMP-54F28[87], and a CPB inhibitor PRI-724[88,89]. However, no approved drugs are available in the clinic for treatment *via* targeting of the Wnt signaling

pathway. In addition, most of these agents induced growth arrest in tumor cells targeting Wnt signaling pathway, thus, tumor cells do not die, and they could acquire resistance.

In Chapter 3, I performed the screening for the compounds, which exhibit synthetic lethality with β-catenin mutation. I have previously reported that MEK1/2 inhibitors induced cell growth arrest in β-catenin wild type tumor cell lines, whereas they induced apoptosis in β-catenin mutant tumor cell lines *in vitro* and *in vivo* [90], however, the molecular mechanisms still remained elusive. Therefore, I screened the compound other than MEK1/2 inhibitors, and identified nonactin, an antibiotic mitochondrial uncoupler, as a hit compound. Furthermore, I investigated the mechanism how nonactin, as well as other mitochondrial uncouplers, exhibited the synthetic lethality with β-catenin mutation.

Finally, in Chapter 4, I summarized the results, significance and speculation about this study described in Chapter 2 and 3, and also described a potential of the concept of synthetic lethal for discovering more effective anticancer agents.

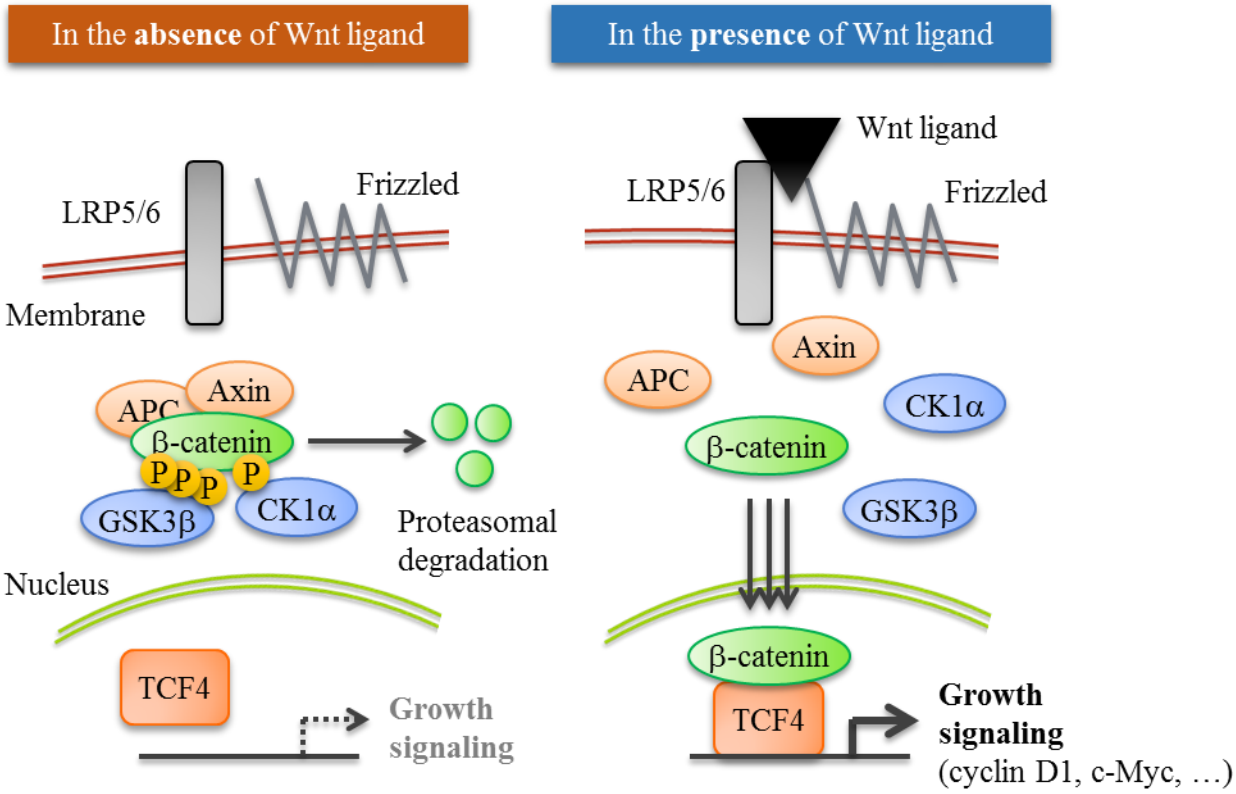

Figure 1-3. The Wnt signaling pathway

Chapter 2 Protein kinase A inhibition facilitates the antitumor activity of xanthohumol, a valosin-containing protein inhibitor

2.1 Introduction

Xanthohumol (XN) is a prenylated chalcone present in hops (*Humulus lupus* L.) and beer[53]. XN has received much attention in recent years, including reports of its various biological properties, such as anti-inflammatory[91], anti-oxidant[92], anti-angiogenic[57], and antibacterial[93] effects. Further, XN harbors anti-tumorigenic effects toward different types of cancer cells[55] *via* intracellular reactive oxygen species (ROS) induction[56], NF-κB and Akt inhibition[57,58], ER stress induction[59] and disruption of the BIG3-PHB2 interaction[60].

I previously reported that XN binds directly to valosin-containing protein (VCP) and modulates autophagy by inhibiting VCP functions[54]. VCP, also known as p97, belongs to the ATPase associated with diverse cellular activities (AAA) ATPase family and has a wide variety of cellular functions, such as autophagosome maturation[35,36], endoplasmic reticulum-associated degradation (ERAD)[37], and the enhancement of NF-κB signaling[40,41]. Therefore, our finding that XN modulated the function of VCP may explain how XN exhibited the above-mentioned biological effects, such as autophagosome maturation, ER stress induction, and NF-κB inhibition. Additionally, because clinical studies have identified a correlation among elevated VCP expression and the progression, prognosis and metastatic potential of gastric carcinoma[45], pancreatic ductal adenocarcinoma[46], and prostate cancer[47], the antitumor effects of XN can be attributed to the inhibition of VCP function. However, the molecular mechanisms governing the contribution of VCP to the antitumor activity of XN still remained elusive. In this study, I performed genome-wide shRNA screening and identified the adenylate cyclase (AC) pathway as genes relating to the antitumor activity of XN against human tumor cells. This pathway regulates various cellular functions *via* activating PKA-

dependent phosphorylation[94]. However, there are no reports that show the relevance of AC/PKA pathway inhibition to the antitumor activity of XN targeting VCP.

2.2 Results

2.2.1 Xanthohumol exhibited antitumor activity *in vitro* and *in vivo*

First, I examined the effect of xanthohumol (XN) on eighteen different human tumor cell lines chosen in a random manner. Each cell was treated with XN for 48 h and the sub-G_1 populations were determined *via* flow cytometry. Z-score values were then calculated using EC_{50} values of cell viability and plotted on a waterfall plot. As shown in Figure 2-1, seven cell lines, including SW480, SW48, DLD-1, SW620, A2058, LS-174T, and HCT116 cells, were highly sensitive to XN. However, there were not significant difference in VCP expression levels between XN-sensitive cells and the other cell lines (Figure 2-2). Subsequently, I detected the expression levels of cleaved-PARP by western blot to confirm the apoptosis-inducing ability of XN. As shown in Figure 2-3, when XN-sensitive SW480 and HCT116 cells and XN-insensitive HT29 and A549 cells were treated with indicated concentrations of XN for 24 h, the expression levels of cleaved-PARP increased in XN-sensitive SW480 and HCT116 cells, but not inHT29 and A549 cells. I correlated these results with a waterfall plot analysis.

I next investigated the antitumor effects of XN against XN-sensitive cells *in vivo*. Human colorectal tumor HCT116 and SW480 cells were injected subcutaneously into nude mice to establish xenograft models. Mice were randomized into four groups of five, after which the vehicle or XN was administered by intraperitoneal injection. As shown in Figures 2-4 and 2-5, tumor growth inhibition was observed in each xenograft model in a dose-dependent manner, without significant body weight loss (Figure 2-6). Furthermore, I evaluated for its effect on Ki67 labeling index as a tumor proliferative index using immunohistochemical (IHC) methods. A significant reduction of Ki67 labeling index in

tumor was observed in dose-dependent manner (Figure 2-7). These results indicated that XN exhibited antitumor activity against several human tumor cell lines *in vitro* and *in vivo*.

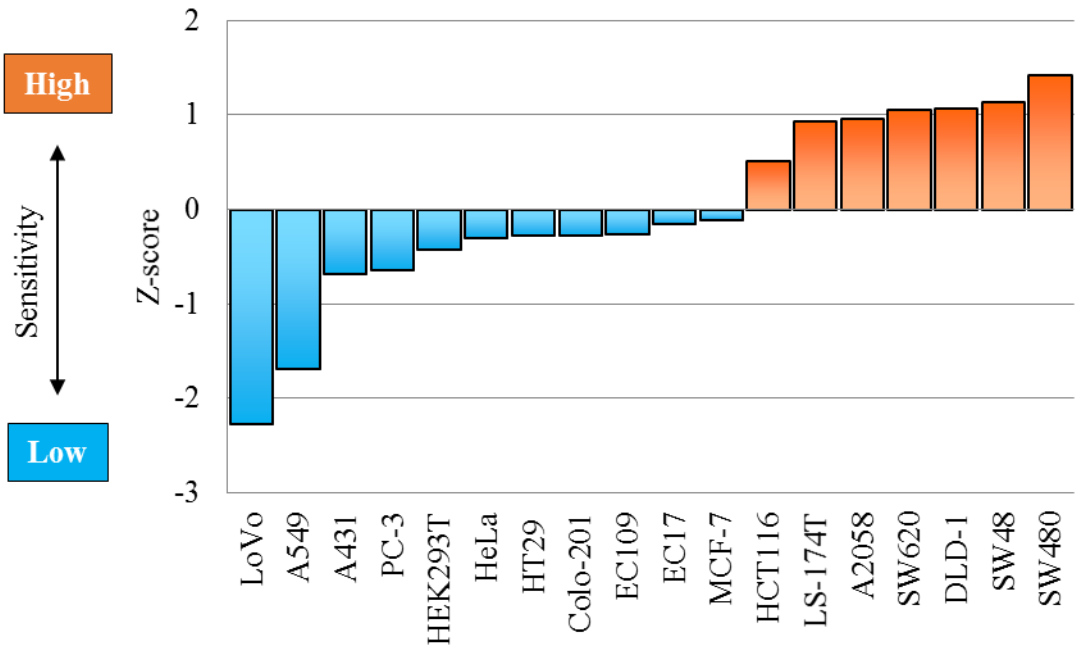

Figure 2-1. Sensitivity to xanthohumol

The effects of xanthohumol (XN) on several types of human tumor cell lines and xenograft models were examined. The sub-G_1 populations were determined 48 h after XN treatment *via* flow cytometry. Z-score values were calculated as described in the Materials and Methods and plotted on a waterfall plot.

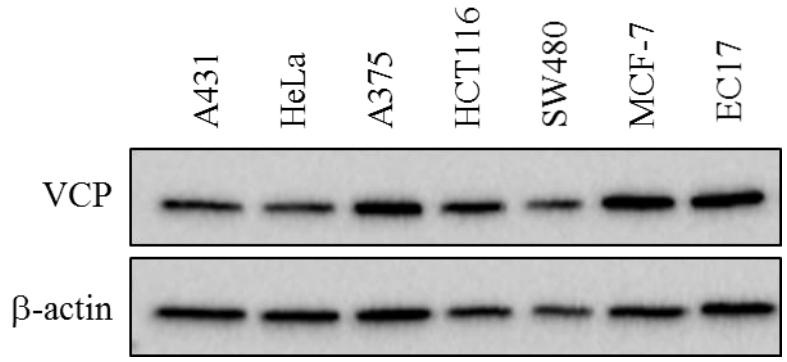

Figure 2-2. The expression levels of VCP

The expression levels of valosin-containing protein (VCP) in several human tumor cells were detected by western blot.

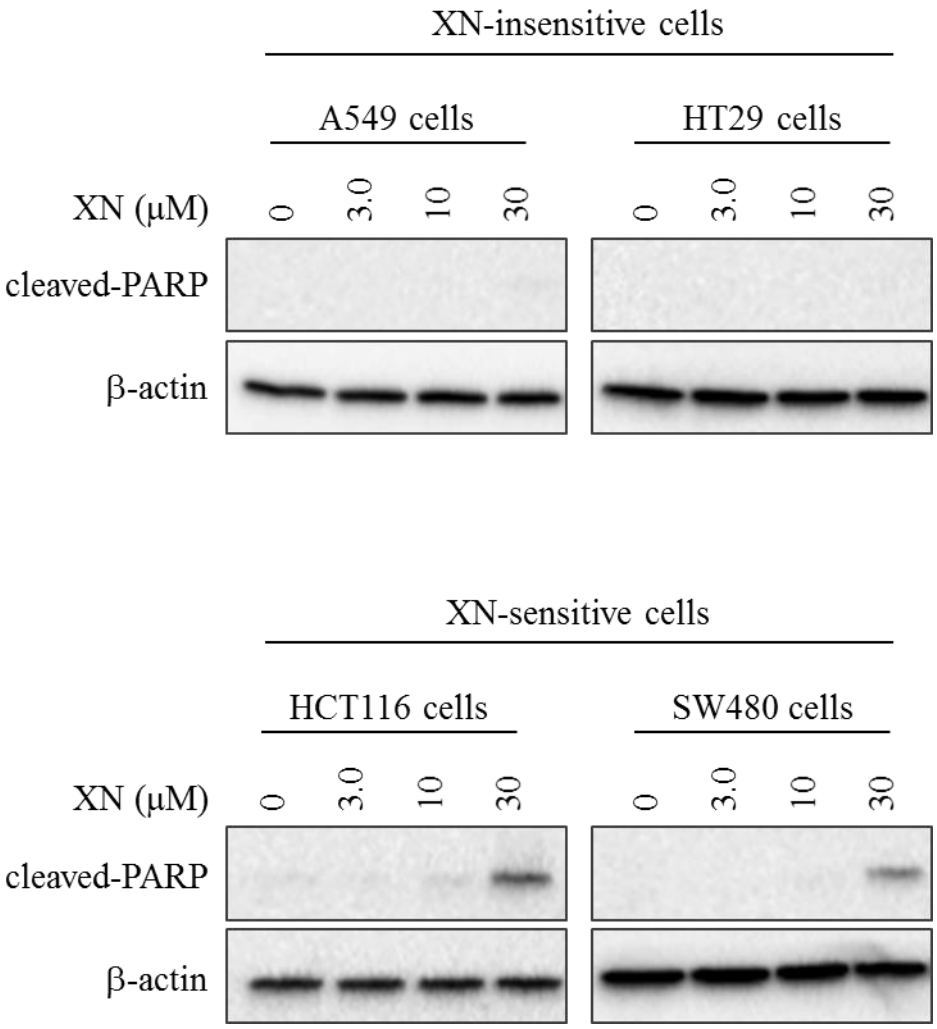

Figure 2-3. PARP-cleavage induced by XN

XN-sensitive SW480 and HCT116 cells and XN-insensitive HT29 and A549 cells were treated with XN for 24 h, and the expression levels of cleaved-PARP were detected by western blot.

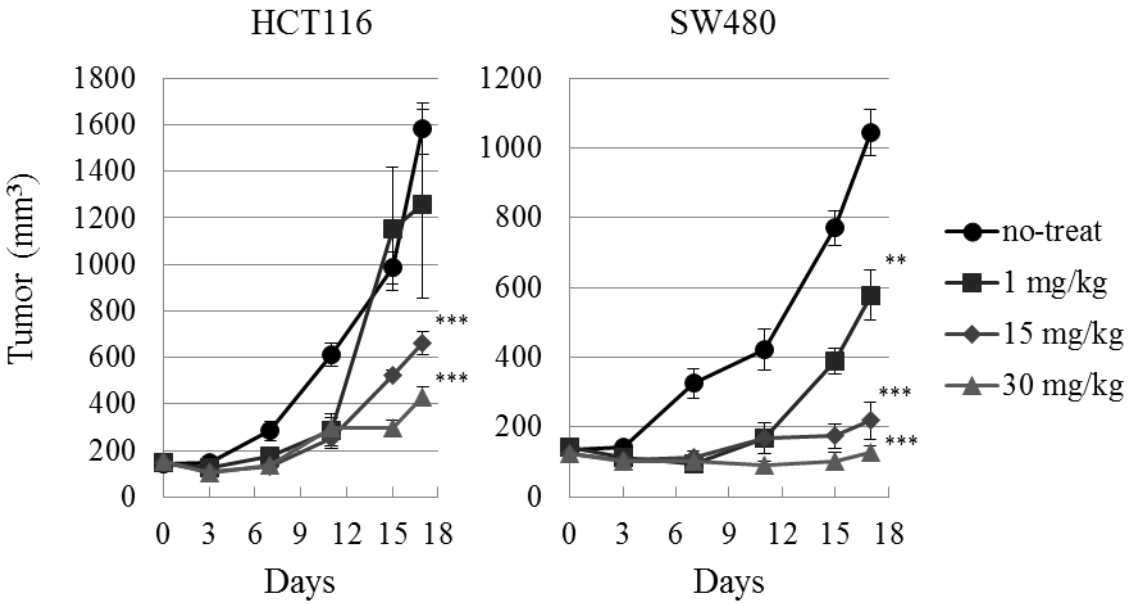

Figure 2-4. The antitumor effects of XN *in vivo*

Human colorectal tumor HCT116 and SW480 cells, the XN-sensitive cells, were injected subcutaneously into nude mice to establish xenograft models. After the tumors developed over a period of one week, reaching sizes of approximately 150 mm^3, mice were randomized into four groups of five, after which the vehicle or XN was administered daily by intraperitoneal injection for 17 days. Tumor size and body weight were measured and tumors were dissected and imaged with a digital camera. Values are the means of five tumors showed in Figure 2-5, bars, SD. ** P<0.01, *** P<0.001, compared with no-treat group mice at day 17.

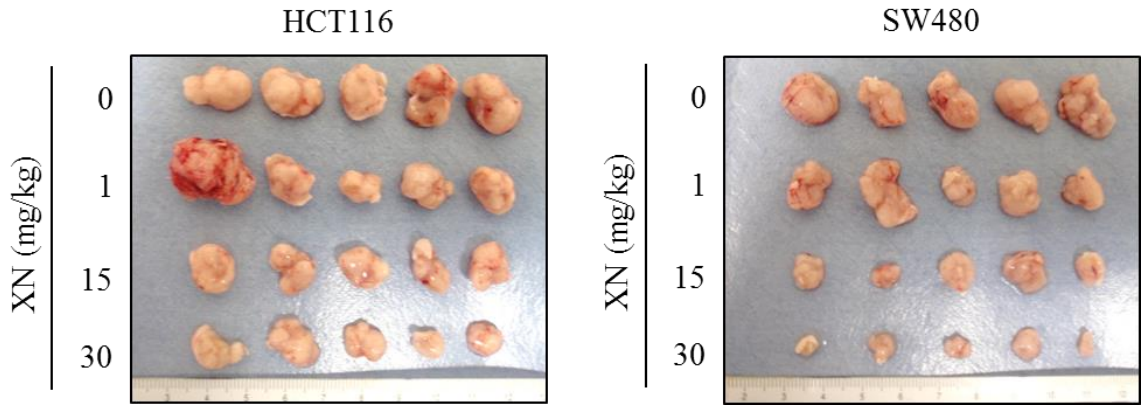

Figure 2-5. The picture of tumors

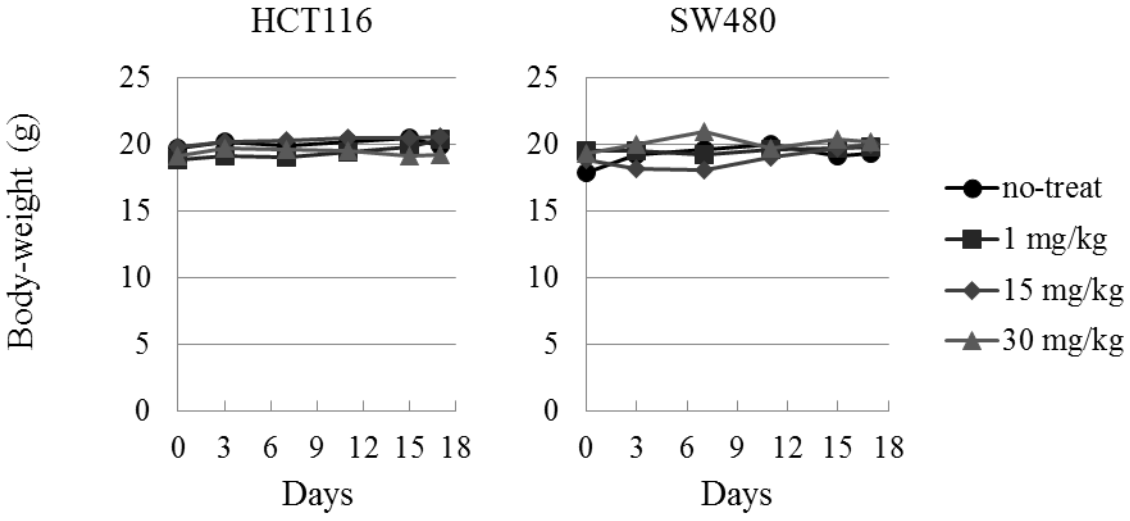

Figure 2-6. The body-weight of mice

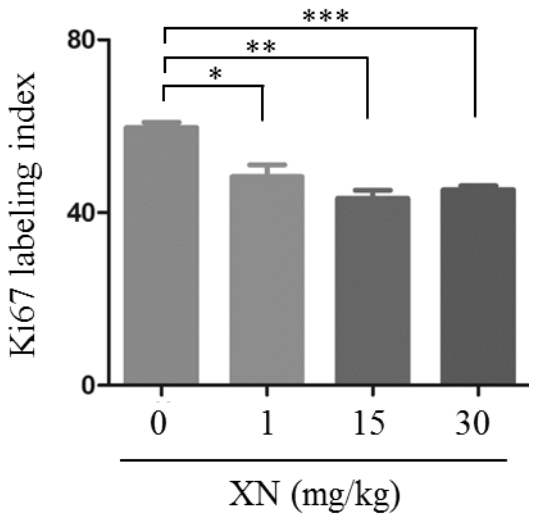

Figure 2-7. Ki67 labeling index in HCT116 cells

Dose-dependent inhibition of Ki67 labeling index by XN treatment in tumor xenografts *in vivo*. Nuclear Ki67 labeling index at indicated dose levels was determined in HCT116 tumors on study day 17. Bars, SD. * $P<0.05$, ** $P<0.01$, *** $P<0.001$, compared with no-treat group mice.

2.2.2 shRNA screening reveals the adenylate cyclase pathway is correlated with xanthohumol-induced cell death

To identify the key genes playing a critical role in XN-induced cell death, I generated a lentiviral-based shRNA screening system and screened for genes related to the antitumor activity of XN using HCT116 cells. Before the screening, I determined the drug concentration to be somewhat lower than IC_{50} value because at the concentration of IC_{50}, the shRNA-infected cells exhibit too many "random deaths" due only to the drug function without the synthetic shRNA effects. In our study, to decide the concentration of XN for the shRNA screening, I performed growth inhibition assay and IC_{50} value was calculated. A dose response curve of XN for HCT116 is shown in Figure 2-8, and the IC_{50} value was approximately 8.1 μM. Then, I decided to conduct the shRNA screening at the concentration of 7.0 μM XN, at a lower concentration compared to the IC_{50}, based on the above mentioned theoretical background.

Next, HCT116 cells were infected with a mixture of approximately 27,500 barcoded shRNAs and cultured in the presence of either 7.0 μM XN or DMSO. After three days, genomic DNA was isolated from the cells and the shRNA-specific barcode regions were amplified by PCR with the Lentivirus vector-specific primers. The abundance of each shRNA was then quantified by high-throughput sequencing (Figure 2-9). As a result, 138 shRNAs, which exhibited more than 5-fold high frequencies in DMSO treated cells compared to XN treated cells, were selected as the hit genes (Table 2-1). This suggests that knockdown of these genes enhances the antitumor activity of XN, since HCT116 cells infected with these 138 shRNAs showed growth inhibitions specifically under the synergic XN culture condition. Subsequently, Gene Ontology (GO) based bioinformatics analysis was performed on the hits using the DAVID bioinformatics

database[95,96]. As a result, GO-term enrichment analysis of the hit genes, focusing on molecular functions and biological processes, showed strong enrichment of genes involved in adenylate cyclase activity (Tables 2-2 and 2-3). These results raised the possibility that the adenylate cyclase pathway may play a crucial role in XN-induced cell death.

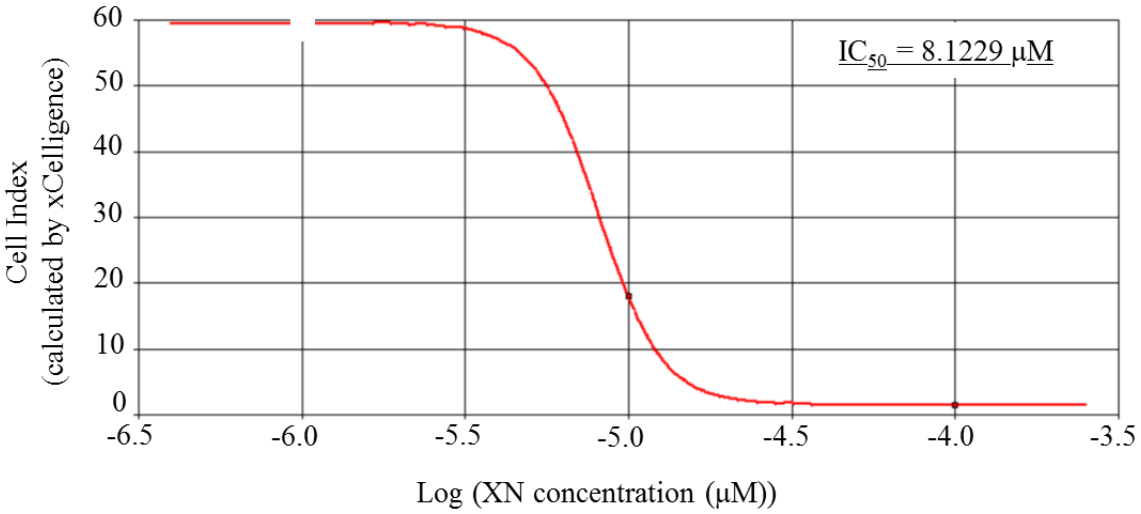

Figure 2-8. A dose response curve of XN on HCT116 cells for a global shRNA screening

A dose response curve of XN was calculated using xCelligence, an automated cell growth analyzer. HCT116 cells were cultured at a variety of XN concentrations for 48 h and the real-time cell growth rates were recorded by the xCelligence. The x- and y-axis represent log10 concentration of XN (μM) and cell index that represents live cell numbers, respectively. The IC_{50} of XN for HCT116 was revealed to be 8.1 μM.

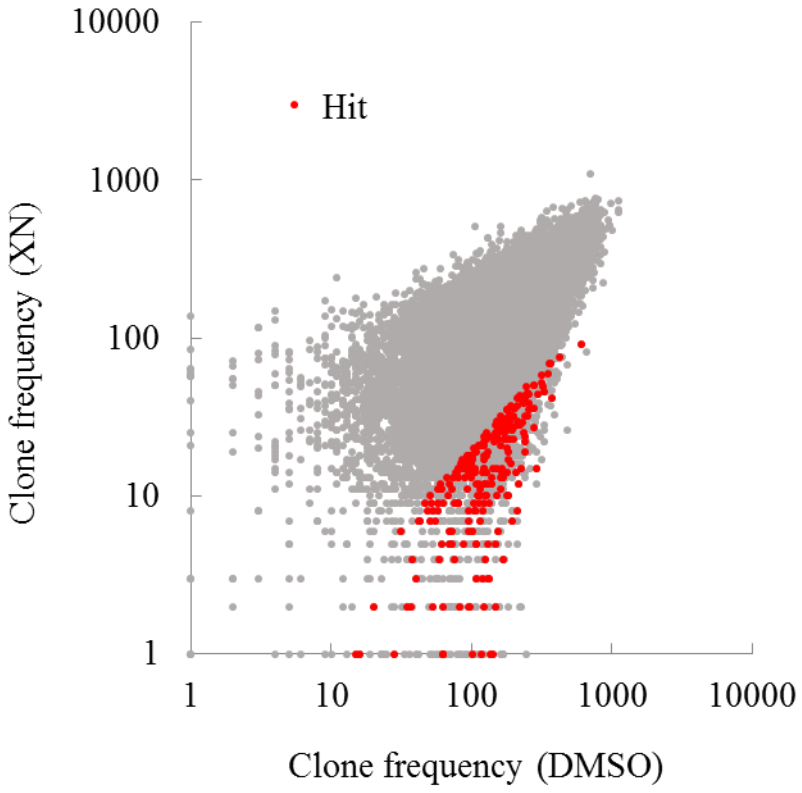

Figure 2-9. shRNA screening for genes related to the antitumor activity of XN

A lentiviral-based shRNA screening was performed for screening genes related to the antitumor activity of xanthohumol (XN). HCT116 cells were infected with an shRNA Lentivirus library containing approximately 27,500 shRNAs and then cultured in the presence or absence of 7.0 μM XN for three days. Genomic DNA was isolated and amplified by PCR targeting shRNA-specific barcode regions. Each shRNA was then quantified by high-throughput sequencing. The x- and y-axis represent clone frequency of each shRNA from the cells cultured with DMSO and XN. The hit genes that exhibited more than 5-fold high frequencies in DMSO treated cells compared to the XN treated cells were represented in red dots.

Table 2-1. Hit genes identified by shRNA screening

A lentiviral-based shRNA screening were performed to identify the genes related to the antitumor activity of xanthohumol (XN). All hit genes, clone frequencies and the ratio (XN/DMSO) are listed.

Hit gene	DMSO	XN	Ratio
ADCY3	45	0	0
ADCY8	41	0	0
ATG2A	77	0	0
ATP5L	24	0	0
CACNA2D3	65	0	0
CD40LG	46	0	0
CELA3B	6	0	0
DLAT	101	0	0
ECSIT	55	0	0
GAA	38	0	0
GAPDH	23	0	0
GPX6	62	0	0
GSTA1	68	0	0
HIP2	63	0	0
HPSE	117	0	0
IFNA8	117	0	0
ITPA	16	0	0
KDSR	30	0	0
MTNR1B	96	0	0
NODAL	12	0	0
POLR2B	3	0	0
POLR2F	29	0	0
PSMB6	2	0	0
PSMD12	72	0	0
RPN2	40	0	0
SCN2A	19	0	0
XRCC6	128	0	0
CDC25C	142	1	0.00704
IL2	137	1	0.00730
JAG1	101	1	0.00990
MCM2	147	2	0.0136
RPL8	63	1	0.0159
PDGFB	62	1	0.0161
E2F2	122	2	0.0164
ABCB11	97	2	0.0206
Luc	95	2	0.0211
CSTF3	134	3	0.0224
MERTK	169	4	0.0237
PDZK1	108	3	0.0278
MRE11A	63	2	0.0317
OCRL	124	4	0.0323
ENTPD3	53	2	0.0377
GTF2A1	130	5	0.0385
PIK3R3	76	4	0.0526
PTGER1	37	2	0.0541
RETNLB	178	10	0.0562

Hit gene	DMSO	XN	Ratio
ADORA2A	35	2	0.0571
RANBP2	102	6	0.0588
GPRC5A	150	10	0.0667
SPIB	120	8	0.0667
SSTR2	15	1	0.0667
ZCCHC11	59	4	0.0678
CD8B	160	11	0.0688
PNPO	71	5	0.0704
EIF3A	95	7	0.0737
ACOX2	106	8	0.0755
KCNH2	106	8	0.0755
EMR1	129	10	0.0775
VSNL1	179	14	0.0782
CLTA	162	13	0.0802
DAD1	61	5	0.0820
KCNA7	72	6	0.0833
GPAM	116	10	0.0862
SREBF2	69	6	0.0870
COL5A2	166	15	0.0904
ATP6V0D1	110	10	0.0909
MEFV	130	12	0.0923
UBE2D2	126	12	0.0952
CD86	279	27	0.0968
FOXA2	20	2	0.1000
ARHGEF11	239	24	0.1004
NDE1	113	12	0.1062
GRM5	180	20	0.1111
NEK2	200	23	0.1150
CFLAR	93	11	0.1183
ACTB	76	9	0.1184
OPRM1	122	15	0.1230
SERPINI1	230	29	0.1261
ATP6V0E1	99	13	0.1313
STAT4	196	26	0.1327
CDKN2D	173	23	0.1329
KPNA2	238	32	0.1345
ACTA1	333	46	0.1381
PECR	106	15	0.1415
TRAF5	127	18	0.1417
ABCA7	210	30	0.1429
PTGFR	181	26	0.1436
RPL30	62	9	0.1452
SOS2	89	13	0.1461
CGN	170	25	0.1471
CHAD	68	10	0.1471
TOB1	95	14	0.1474

Hit gene	DMSO	XN	Ratio
PRODH	122	18	0.148
CERK	296	44	0.149
BUB1B	186	28	0.151
CALCR	73	11	0.151
SUFU	321	49	0.153
RAC2	144	22	0.153
HNF4G	155	25	0.161
STAT6	99	16	0.162
KLK1	197	32	0.162
NBN	49	8	0.163
EIF4G1	171	28	0.164
PHKB	315	52	0.165
SRPR	88	15	0.170
GNAL	164	28	0.171
APOD	122	21	0.172
WIPI1	52	9	0.173
RFC5	231	40	0.173
ALPL	69	12	0.174
COX5A	161	28	0.174
ADARB1	240	42	0.175
HDAC11	74	13	0.176
NPM1	135	24	0.178
KIF11	123	22	0.179
HDAC3	279	50	0.179
PPP2R5D	128	23	0.180
SLC22A12	250	45	0.180
AASDH	105	19	0.181
PIGA	88	16	0.182
HPX	197	36	0.183
EIF2B1	98	18	0.184
PLK1	98	18	0.184
CDKN3	125	23	0.184
PICALM	168	31	0.185
ISG15	162	30	0.185
LIAS	81	15	0.185
HRH1	370	69	0.186
BCAR1	112	21	0.188
CASR	84	16	0.190
GTF2H3	147	28	0.190
IKBKG	94	18	0.191
ADCY6	31	6	0.194
SAT1	356	69	0.194
SYNJ2	178	35	0.197
AANAT	213	42	0.197
AADAC	150	30	0.200
SLC25A20	85	17	0.200

Table 2-2. Gene Ontology analysis focusing on molecular functions

Gene Ontology (GO) based bioinformatics analysis was performed on the hits using the DAVID bioinformatics database. GO terms focusing on molecular functions are listed. Count: number of genes that were categorized into each functional category. %: percentage of genes that were categorized into each functional category out of all 138 genes identified in our shRNA screening. Benjamini: False Discovery Rate value calculated by Benjamini-Hochberg method.

Category	Term	Count	%	PValue	Benjamini
GOTERM_MF_FAT	adenylate cyclase activity	4	0.265	3.47E-03	0.761
GOTERM_MF_FAT	cyclase activity	4	0.265	1.06E-02	0.888
GOTERM_MF_FAT	phosphorus-oxygen lyase activity	4	0.265	1.26E-02	0.824
GOTERM_MF_FAT	PDZ domain binding	4	0.265	0.0437	0.990
GOTERM_MF_FAT	monovalent inorganic cation transmembrane transporter activity	5	0.331	0.0736	0.998
GOTERM_MF_FAT	calcium- and calmodulin-responsive adenylate cyclase activity	2	0.132	0.0859	0.998
GOTERM_MF_FAT	deacetylase activity	3	0.199	0.0879	0.996
GOTERM_MF_FAT	translation factor activity, nucleic acid binding	4	0.265	0.0941	0.994

Table 2-3. Gene Ontology analysis focusing on biological processes

Gene Ontology (GO) based bioinformatics analysis was performed on the hits using the DAVID bioinformatics database. GO terms focusing on biological processes are listed. Count: number of genes that were categorized into each functional category. %: percentage of genes that were categorized into each functional category out of all 138 genes identified in our shRNA screening. Benjamini: False Discovery Rate value calculated by Benjamini-Hochberg method.

Category	Term	Count	%	PValue	Benjamini
GOTERM_BP_FAT	activation of adenylate cyclase activity by G-protein signaling pathway	7	0.464	1.77E-04	0.230
GOTERM_BP_FAT	regulation of adenylate cyclase activity involved in G-protein signaling	7	0.464	1.77E-04	0.230
GOTERM_BP_FAT	positive regulation of adenylate cyclase activity by G-protein signaling pathway	7	0.464	1.77E-04	0.230
GOTERM_BP_FAT	activation of adenylate cyclase activity	7	0.464	0.00106	0.543
GOTERM_BP_FAT	positive regulation of adenylate cyclase activity	7	0.464	0.00120	0.445
GOTERM_BP_FAT	positive regulation of cyclase activity	7	0.464	0.00135	0.391
GOTERM_BP_FAT	positive regulation of lyase activity	7	0.464	0.00151	0.360
GOTERM_BP_FAT	centrosome cycle	4	0.265	0.00202	0.392
GOTERM_BP_FAT	inhibition of adenylate cyclase activity by G-protein signaling	6	0.397	0.00227	0.381
GOTERM_BP_FAT	G-protein coupled receptor protein signaling pathway	20	1.325	0.00298	0.424
GOTERM_BP_FAT	cAMP biosynthetic process	4	0.265	0.00356	0.443
GOTERM_BP_FAT	G-protein signaling, coupled to cAMP nucleotide second messenger	8	0.530	0.00360	0.412
GOTERM_BP_FAT	M phase	11	0.728	0.00389	0.407
GOTERM_BP_FAT	centrosome organization	4	0.265	0.00454	0.428
GOTERM_BP_FAT	second-messenger-mediated signaling	13	0.861	0.00455	0.404
GOTERM_BP_FAT	regulation of adenylate cyclase activity	8	0.530	0.00518	0.422
GOTERM_BP_FAT	cAMP-mediated signaling	8	0.530	0.00556	0.422
GOTERM_BP_FAT	microtubule organizing center organization	4	0.265	0.00567	0.408
GOTERM_BP_FAT	regulation of cyclase activity	8	0.530	0.00636	0.425
GOTERM_BP_FAT	G-protein signaling, coupled to cyclic nucleotide second messenger	9	0.596	0.00637	0.408
GOTERM_BP_FAT	regulation of lyase activity	8	0.530	0.00679	0.411
GOTERM_BP_FAT	regulation of cAMP biosynthetic process	8	0.530	0.00679	0.411
GOTERM_BP_FAT	regulation of cAMP metabolic process	8	0.530	0.00725	0.415
GOTERM_BP_FAT	cell cycle phase	13	0.861	0.00742	0.407
GOTERM_BP_FAT	negative regulation of lyase activity	6	0.397	0.00756	0.399
GOTERM_BP_FAT	negative regulation of adenylate cyclase activity	6	0.397	0.00756	0.399
GOTERM_BP_FAT	negative regulation of cyclase activity	6	0.397	0.00756	0.399
GOTERM_BP_FAT	regulation of nucleotide biosynthetic process	8	0.530	0.00987	0.471
GOTERM_BP_FAT	regulation of cyclic nucleotide biosynthetic process	8	0.530	0.00987	0.471
GOTERM_BP_FAT	cAMP metabolic process	4	0.265	0.00998	0.460

2.2.3 PKA inhibitors enhanced the antitumor activity of VCP inhibitors

The Adenylate Cyclase (AC) pathway, also known as the cyclic AMP (cAMP)-dependent pathway, is a well-known G protein-coupled receptor-regulated signaling cascade. The G protein families, including G_i and G_s, regulate AC activity. AC catalyzes the conversion of ATP to cAMP, which in turn regulates cellular function *via* activating protein kinase A (PKA)-dependent phosphorylation[94]. Therefore, to examine whether the suppression of the AC/PKA pathway could synergistically enhance the antitumor activity of XN, I performed an MTT assay using the PKA inhibitor H-89[97] and graphically plotted the results on isobolograms[98,99]. HCT116 cells were treated with various concentrations of XN in the presence or absence of H-89 for 72 h and cell viability was measured by MTT assay. IC_{50} values of each combination of two agents and the combination indexes (CI) were then calculated and plotted on an isobologram. The combination of H-89 with XN produced a concave line, indicating a synergistic interaction (Figure 2-10). Similar results were obtained when another PKA inhibitor, KT5720[100], was used instead of H-89 (Figure 2-11). Conversely, when using the non-specific cytotoxic agent paclitaxel (PTX) instead of XN, H-89 plus PTX produced a straight line, indicating an additive interaction in the HCT116 cells (Figure 2-12). Thus, PKA inhibition is responsible for synergistically enhancing the antitumor activity of XN. I then performed similar tests using another VCP inhibitor, eeyarestatin I (ESI)[48]. As shown in Figure 2-13, the combinations of H-89 with ESI produced a concave line, indicating a synergistic interaction in HCT116 cells. Furthermore, the synergistic effect of H-89 and XN was confirmed in the other human tumor cell lines, XN-sensitive SW480 and XN-insensitive HT29 cells (Figures 2-14 and 2-15). These results suggest that the inhibition of AC/PKA pathway synergistically

enhances the antitumor activity of VCP inhibitors, including XN and ESI, in various types of human tumor cell lines.

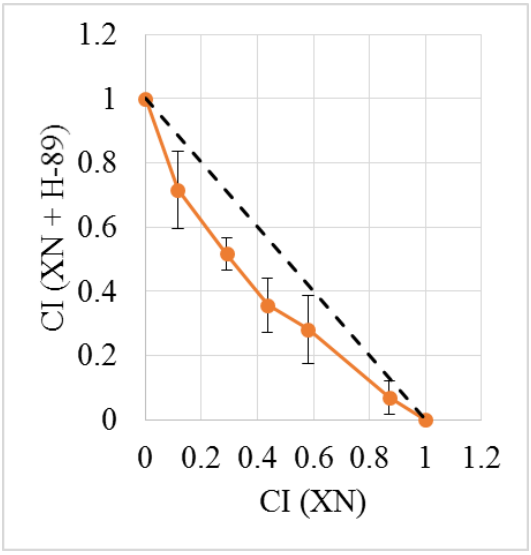

Figure 2-10. Isobologram (XN vs H-89 in HCT116 cells)

HCT116 cells were treated with various concentrations of xanthohumol (XN) in the presence or absence of H-89 for 72 h and the cell viability was measured by MTT assay. The combination index (CI) for each combination of two agents was calculated using the IC_{50} value and plotted on the isobologram. Values are the means of three independent experiments, bars, SD.

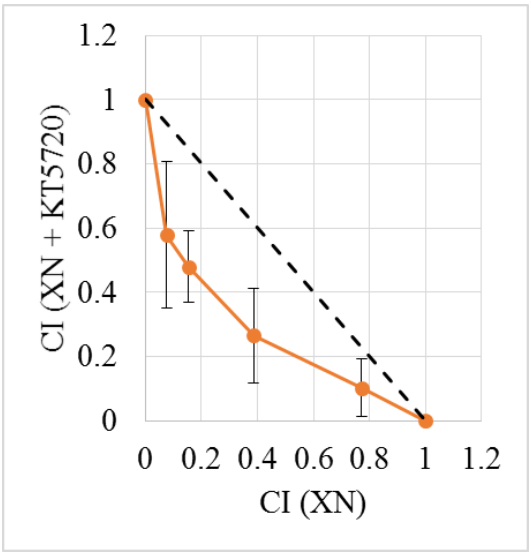

Figure 2-11. Isobologram (XN vs KT5720 in HCT116 cells)

HCT116 cells were treated with various concentrations of XN in the presence or absence of KT5720 for 72 h and the cell viability was measured by MTT assay. The CI for each combination of two agents was calculated using the IC_{50} value and plotted on the isobologram. Values are the means of three independent experiments, bars, SD.

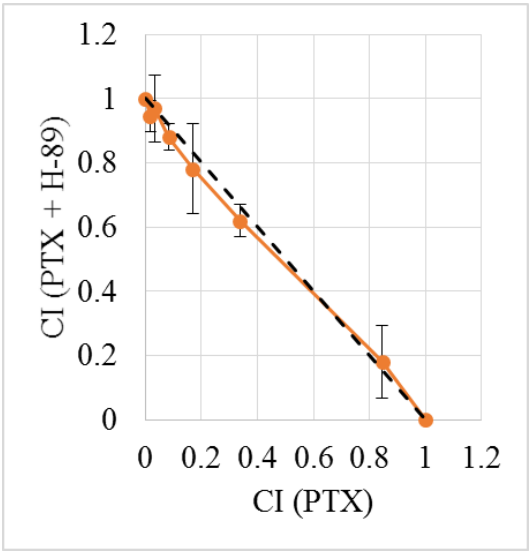

Figure 2-12. Isobologram (PTX vs H-89 in HCT116 cells)

HCT116 cells were treated with various concentrations of paclitaxel (PTX) in the presence or absence of H-89 for 72 h and the cell viability was measured by MTT assay. The CI for each combination of two agents was calculated using the IC_{50} value and plotted on the isobologram. Values are the means of three independent experiments, bars, SD.

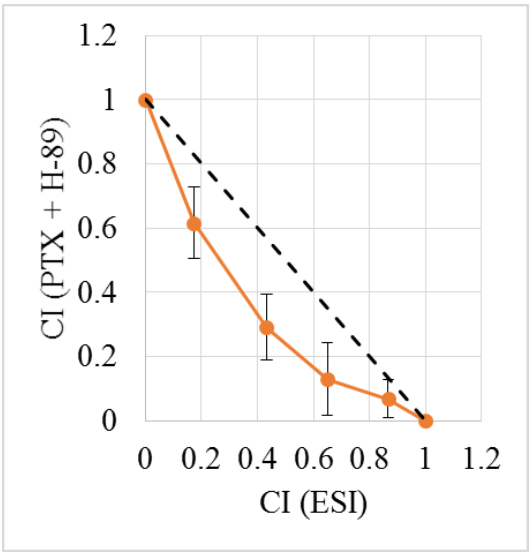

Figure 2-13. Isobologram (ESI vs H-89 in HCT116 cells)

HCT116 cells were treated with various concentrations of eeyarestatin I (ESI) in the presence or absence of H-89 for 72 h and the cell viability was measured by MTT assay. The CI for each combination of two agents was calculated using the IC_{50} value and plotted on the isobologram. Values are the means of three independent experiments, bars, SD.

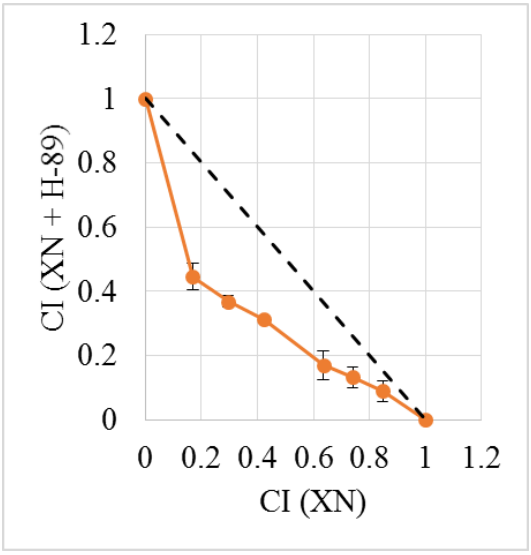

Figure 2-14. Isobologram (XN vs H-89 in SW480 cells)

SW480 cells were treated with various concentrations of XN in the presence or absence of H-89 for 72 h and the cell viability was measured by MTT assay. The CI for each combination of two agents was calculated using the IC_{50} value and plotted on the isobologram. Values are the means of three independent experiments, bars, SD.

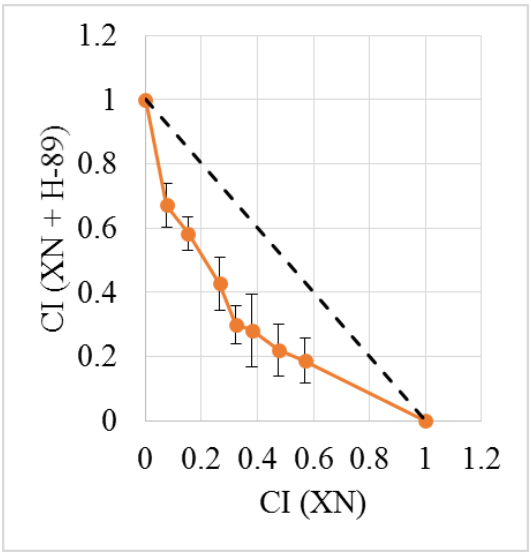

Figure 2-15. Isobologram (ESI vs H-89 in HT29 cells)

HT29 cells were treated with various concentrations of XN in the presence or absence of H-89 for 72 h and the cell viability was measured by MTT assay. The CI for each combination of two agents was calculated using the IC_{50} value and plotted on the isobologram. Values are the means of three independent experiments, bars, SD.

2.2.4 The synergistic effect of PKA inhibition and XN on apoptosis induction

I next investigated whether the combination of PKA inhibitors with XN exhibited a synergistic interaction on apoptosis induction. HCT116 cells were treated with the indicated concentrations of XN in the presence or absence of 10 μM H-89 or KT5720 for 48 h, after which sub-G_1 populations were measured by PI-stain and flow cytometry. As shown in Figures 2-16 and 2-17, co-treatment of PKA inhibitors and XN synergistically increased sub-G_1 populations compared to XN alone, indicating that PKA inhibitors affected apoptosis-inducing activity of XN. Interestingly, XN or H-89 alone did not increase the sub-G_1 population in HT29, A549, and LoVo cells. However, combinations with H-89 could increase the sub-G_1 population in these cell lines, indicating that H-89 treatment might facilitate XN-induced apoptosis also in XN-insensitive cells (Figures 2-18, 2-19, 2-20).

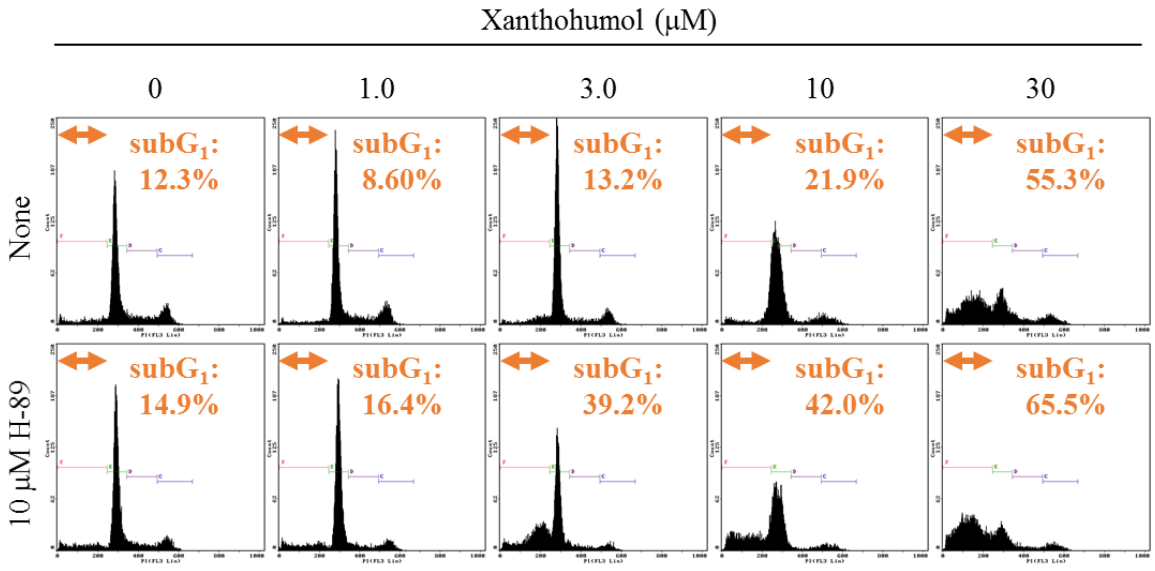

Figure 2-16. Synergistic effect on apoptosis induced by XN plus H-89 in HCT116 cells

HCT116 cells were treated with various concentration of XN in the presence or absence of H-89 for 48 h and the sub-G_1 populations were measured *via* flow cytometry.

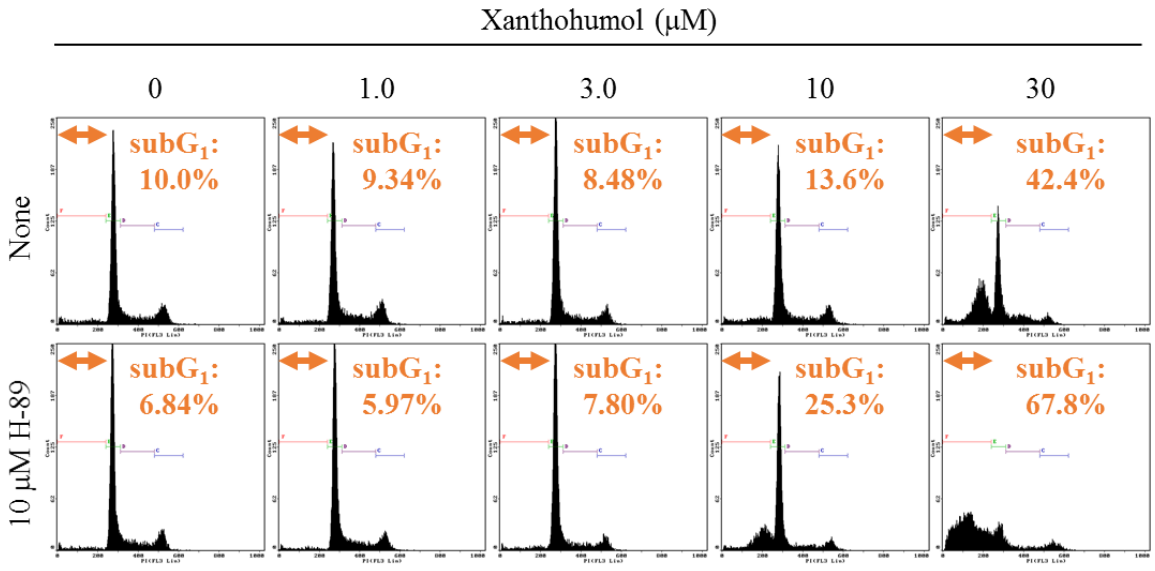

Figure 2-17. Synergistic effect on apoptosis induced by XN plus KT5720 in HCT116 cells

HCT116 cells were treated with various concentration of XN in the presence or absence of KT5720 for 48 h and the sub-G_1 populations were measured *via* flow cytometry.

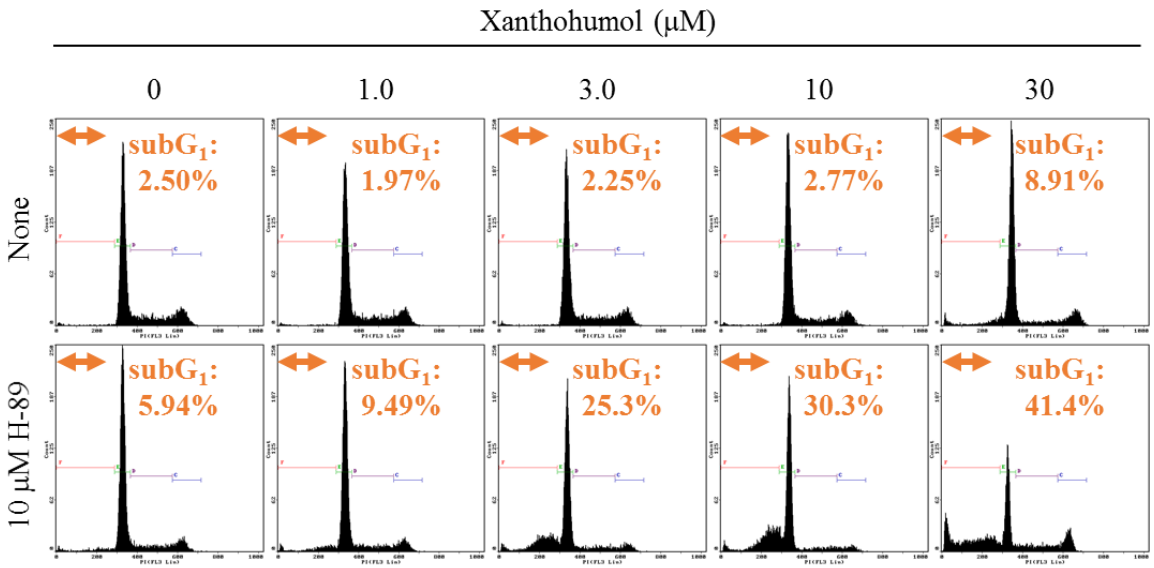

Figure 2-18. Synergistic effect on apoptosis induced by XN plus H-89 in HT29 cells
HT29 cells were treated with various concentration of XN in the presence or absence of H-89 for 48 h and the sub-G_1 populations were measured *via* flow cytometry.

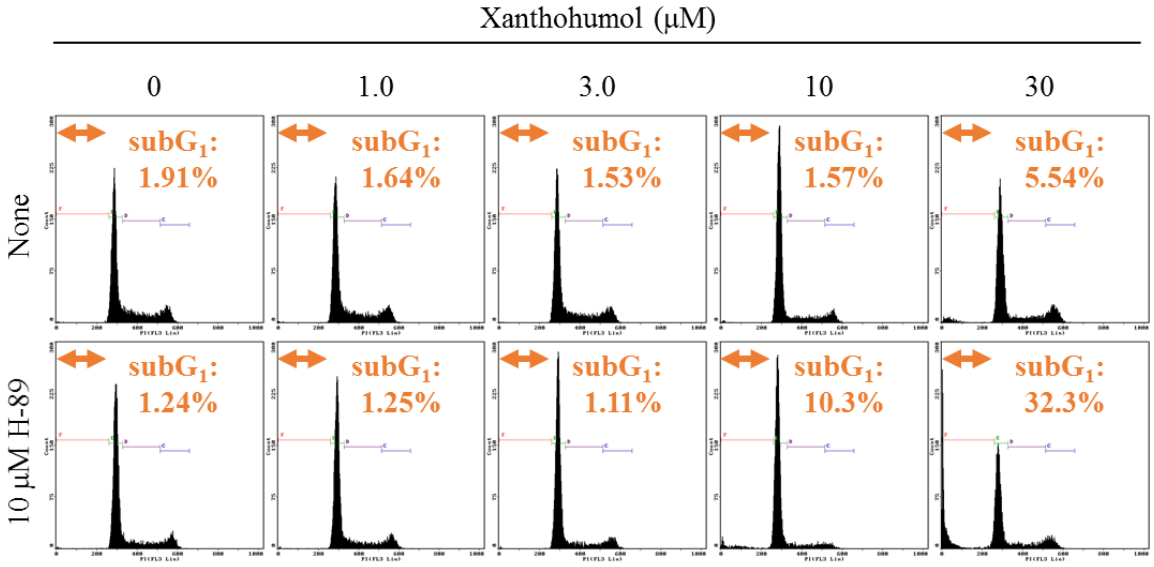

Figure 2-19. Synergistic effect on apoptosis induced by XN plus H-89 in A549 cells
A549 cells were treated with various concentration of XN in the presence or absence of H-89 for 48 h and the sub-G_1 populations were measured *via* flow cytometry.

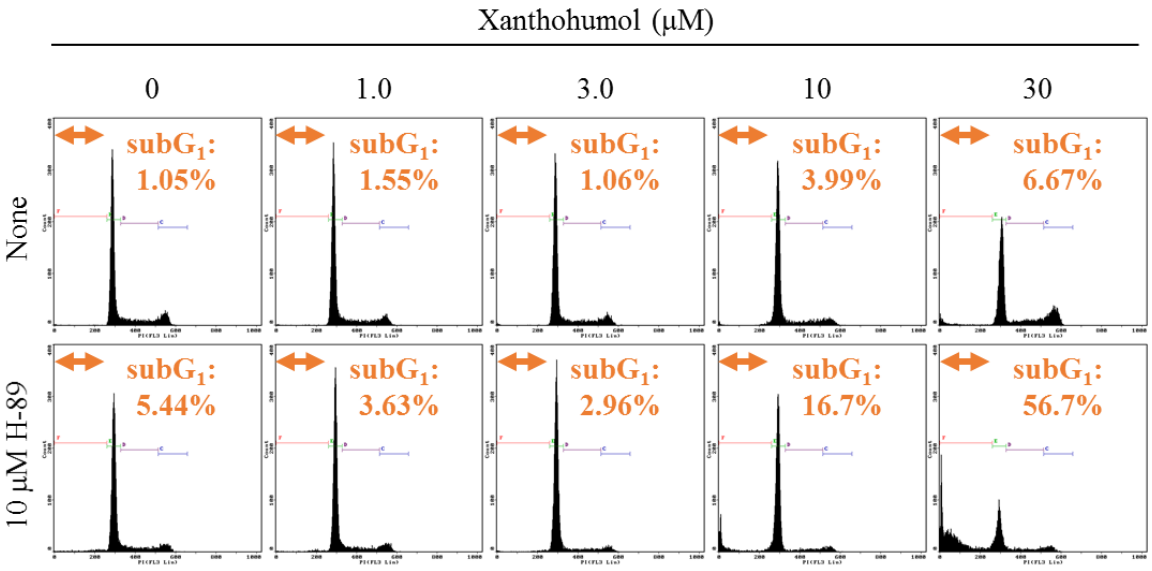

Figure 2-20. Synergistic effect on apoptosis induced by XN plus H-89 in LoVo cells
LoVo cells were treated with various concentration of XN in the presence or absence of H-89 for 48 h and the sub-G_1 populations were measured *via* flow cytometry.

2.3 Discussion

Xanthohumol (XN), a simple prenylated chalcone, is the most well studied compound isolated from hops because of its potential as a cancer chemopreventive agent against several human tumor cell lines[101-103]. Therefore, many researchers have proposed various molecular mechanisms explaining how XN exhibits antitumor activity. However, until now, there have been no reports of the contribution of valosin-containing protein (VCP) inhibition to XN's antitumor activity. VCP may play crucial roles in cancer progression, prognosis, and recurrence[45-47], and I previously reported that XN directly binds to VCP and inhibits its functions[54]. Therefore, in the current work, I examined the antitumor activity of XN targeting VCP.

I first investigated which human tumor cell lines were sensitive to XN, revealing several cell lines highly sensitive to XN *in vitro*. Overexpression of VCP occurs in many cancers and clinical studies have reported a correlation between elevated VCP expression and its progression[104]. However, because significant differences in the expression levels of VCP were not found among the cell lines I tested, XN-sensitivity is not dependent on VCP expression levels. Conversely, another VCP inhibitor, eeyarestatin I (ESI), showed antitumor effects in tumor cells with a similar waterfall profile to XN (Figure 2-21), indicating that inhibition of VCP function is responsible for cell viability in XN-sensitive tumor cells. VCP functions as a critical mediator of protein homeostasis. VCP is essential to some aspects of ubiquitin-dependent proteasomal degradation, including endoplasmic reticulum-associated degradation (ERAD), which degrades misfolded proteins. VCP is also involved in the aggresome-autophagy pathway, which is required for clearing misfolded proteins that form aggregates in the cytosol. The malignant transformation may result in cell deregulation often associated with cellular stress, such as accumulation of

misfolded proteins; adaptation to this stress phenotype is required for tumor cells to survive. Therefore, although the detailed function of VCP in XN-sensitive tumor cells remains unclear, subsets of tumor cells (XN-sensitive tumor cells) may in turn depend on VCP function.

Previously, Yoshimaru *et al.* reported that XN treatment (0.3-1.0 mg/kg) significantly inhibited estrogen (E2)-induced tumor growth *via* specific disruption of the BIG3-PHB2 interaction, regardless of VCP function *in vivo*[60]. Conversely, the lower dose range of XN did not show significant antitumor effects on the human colorectal tumor HCT116 and SW480 cells *in vivo*, but significant tumor growth inhibition was observed in these cells in response to daily intraperitoneal injection of higher doses of XN (15-30 mg/kg), possibly through VCP inhibition. Notably, no morphological changes were observed in the heart, lung, liver, kidney, spleen, and pancreas of mice despite receiving high dose of XN (30 mg/kg) daily for 17 days (Figure 2-22). However, what determines the sensitivity to XN still remained elusive. When I compared the effect of XN on the expression levels of several pro- and anti-apoptosis proteins in XN-sensitive cells, only expression levels of survivin was found to be affected by XN. XN induced in a decrease in the expression levels of survivin in XN-sensitive cells (HCT116 and SW480 cells) in a dose-dependent manner, however, XN weakly suppressed the expression levels of survivin in XN-insensitive tumor cells (A549 and HT29 cells), as shown in Figure 2-23. Therefore, it is likely that effect of XN on survivin expression may be related to the sensitivity of tumor cells to XN.

I also determined which key factors modulate the apoptosis-inducing activity of XN. For this, I performed shRNA screening and bioinformatics analysis. Interestingly, the adenylate cyclase (AC) pathway related genes were hits, indicating the AC pathway

plays a crucial role on XN-inducing apoptosis. The AC pathway is known to activate protein kinase A (PKA) phosphorylation *via* converting ATP to cyclic AMP (cAMP) and regulating target genes[94]. I found in this study that in the tumor cell lines I tested, the inhibition of PKA, a downstream kinase of AC and cAMP, enhanced the apoptosis-inducing activity of XN. These results raised the possibility that the AC/PKA pathway could contribute to preventing apoptosis induced by VCP inhibition and that the activity of AC/PKA pathway in tumor cells could determine sensitivity to XN. Recently, it has been reported that XN acts at GABAA receptors present in the hippocampal nerve terminals to decrease the Ca^{2+} influx through N- and P/Q-type Ca^{2+} channels, which subsequently suppresses the Ca^{2+}-calmodulin/PKA cascade to decrease the evoked glutamate release[105]. These results indicated that XN-mediated decrease in the Ca^{2+} influx caused the suppression of the PKA cascade in the rat hippocampus, and therefore, H-89 has been shown to largely prevent the inhibition of glutamate release by XN. On the other hand, I found that H-89 did not prevent apoptosis by XN, rather it synergistically enhanced antitumor activity of XN. Therefore, XN did not induce the suppression of PKA in tumor cells, and the target of XN to induce apoptosis was difference from that of PKA inhibitors.

The next question was how the AC/PKA pathway prevented apoptosis signals induced by VCP inhibition. Several previous studies have reported the anti-apoptotic role of AC/PKA in various types of cells; however, the mechanisms through which PKA works are often not known. One well-described anti-apoptotic role of PKA is that PKA inhibition induces a decrease in expression levels of survivin, an anti-apoptotic protein, in human colorectal tumor SW480 cells[106]. I also found that H-89 at 10 μM suppressed the expression levels of survivin in XN-sensitive and XN-insensitive tumor cells. In addition,

suppressed expression of survivin by H-89 was further enhanced in the presence of XN (Figure 2-23). Therefore, decreased expression of survivin by both PKA inhibition and VCP inhibition may be responsible for the synergistically enhancement of apoptosis by VCP inhibition and PKA inhibition. Further studies will be necessary to exactly delineate the factors contributing to the suppression of survivin expression by XN or PKA inhibitor.

In conclusion, our findings suggest that several human tumor cell lines require VCP function for their survival, and that targeting both VCP and the AC/PKA pathway is a potential chemotherapeutic strategy for the subset of tumor cells.

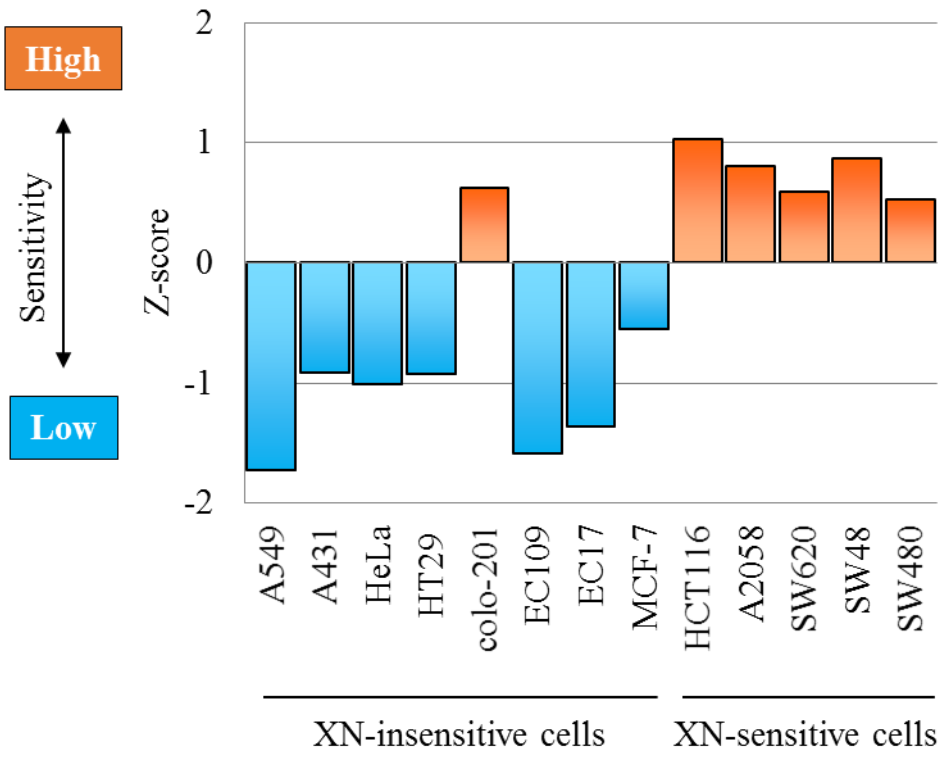

Figure 2-21. Antitumor activities of eeyarestatin I in vitro and a waterfall plot

The effects of eeyarestatin I (ESI), another VCP inhibitor, on several types of human tumor cell lines were examined for whether ESI shows a similar waterfall profile to xanthohumol. The sub-G_1 populations were determined 48 h after ESI treatment *via* flow cytometry. Z-score values were calculated as described in the Materials and Methods and plotted on a waterfall plot.

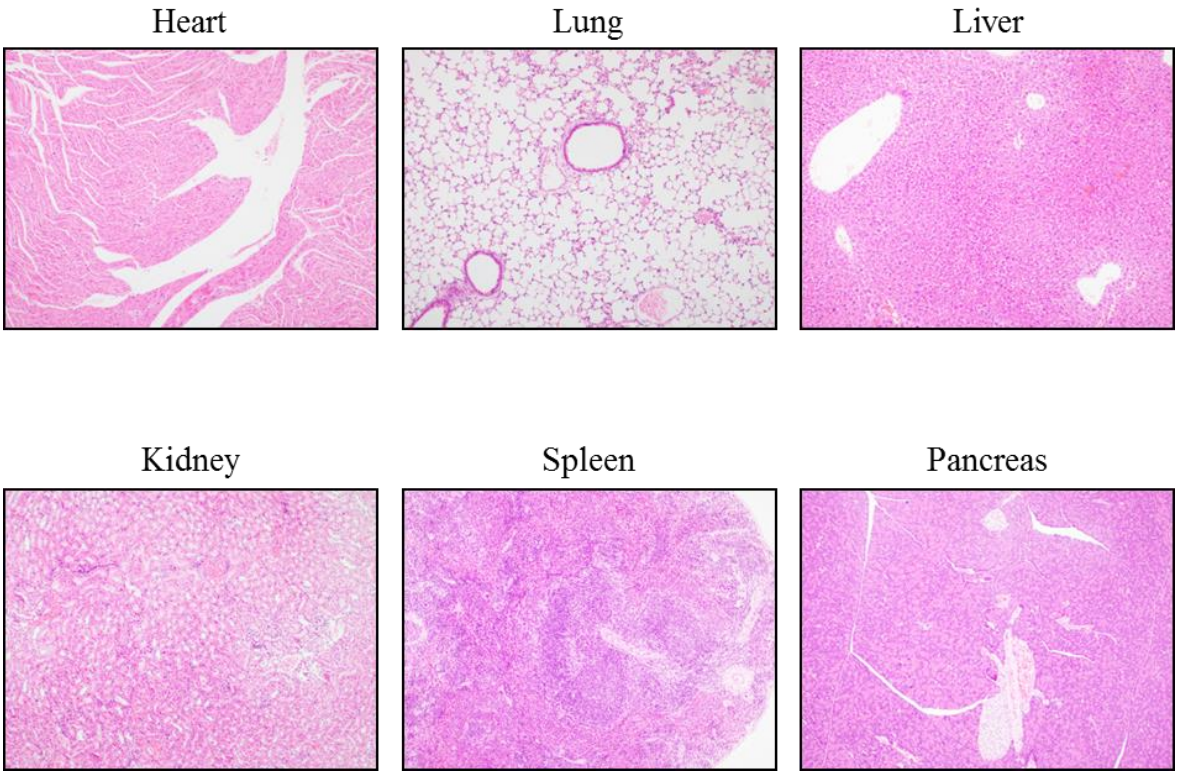

Figure 2-22. Representative morphological observations of dissected heart, lung, liver, kidney, spleen, and pancreas from mice

No morphological changes were observed in the heart, lung, liver, kidney, spleen, and pancreas of mice receiving XN (30 mg/kg) daily for 17 days.

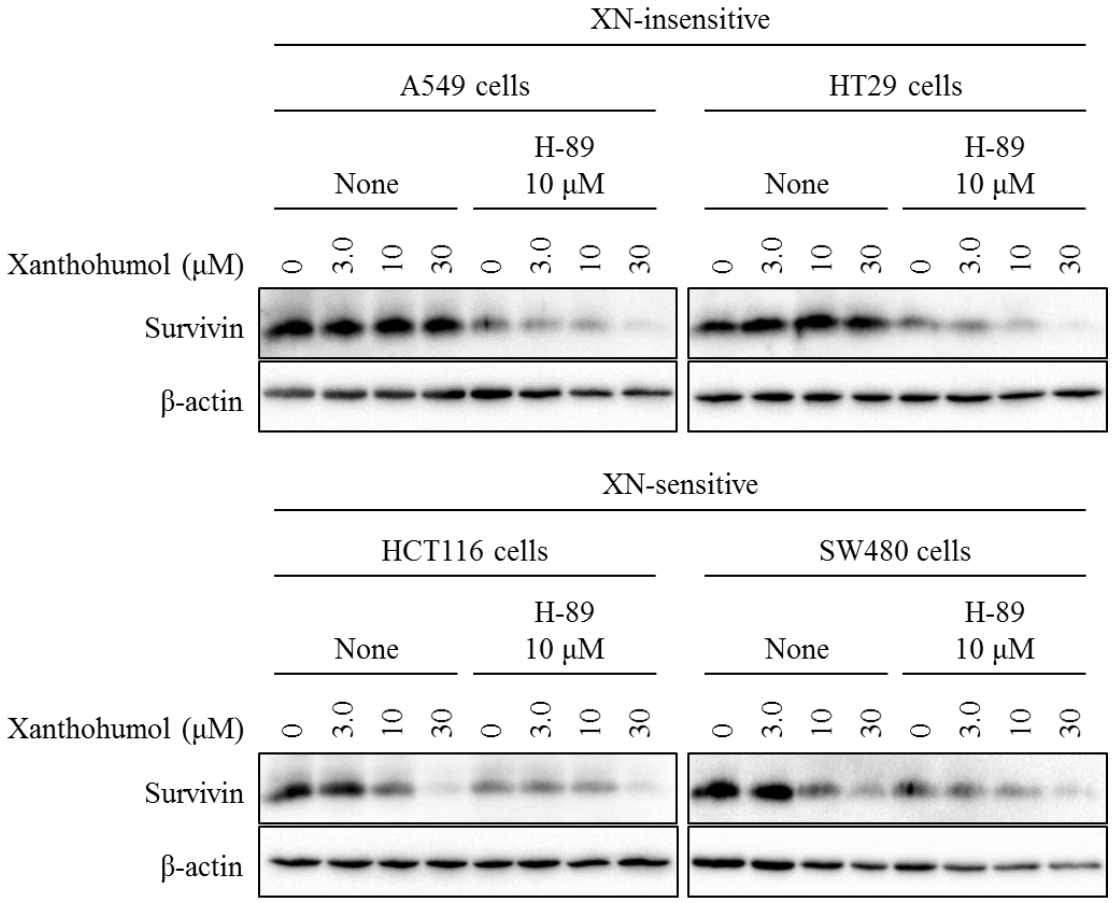

Figure 2-23. Involvement of survivin in xanthohumol-induced apoptosis

To investigate how the inhibition of protein kinase A (PKA) contributes to the enhanced apoptosis induction by xanthohumol (XN), the expression level of survivin was detected by western blot. XN-insensitive A549 and HT29 cells and XN-sensitive HCT116 and SW480 cells were treated with indicated concentrations of XN in the presence or absence of H-89 for 24 h, and the expression levels of survivin were determined.

2.4 Materials and Methods

2.4.1 Compounds

H-89 was purchased from Cayman Chemical (Ann Arbor, MI). Paclitaxel (PTX) was purchased from Wako Pure Chemical Industries (Osaka, Japan). KT5720 was purchased from Tocris Bioscience (Bristol, UK). Eeyarestatin I (ESI) was purchased from Santa Cruz Biotechnology (Santa Cruz, CA).

2.4.2 Isolation of xanthohumol from Hop

Xanthohumol (XN) was isolated and purified from Xantho-Flav Pure (Hopsteiner, Germany). The extract was purified by using HPLC (UG 80, 20 mm × 250 mm; Shiseido, Tokyo, Japan) with 70% aqueous MeOH to obtain pure XN as previously described[54].

2.4.3 Cell lines

A431 cells, human esophageal cancer EC17 cells, and human prostate cancer PC-3 cells were provided by M. Kawada (Institute of Microbial Chemistry, Japan). Human esophageal cancer EC109 cells were provided by Columbia University (New York, NY). Human cervical cancer HeLa cells were provided by M. Yoshida (RIKEN, Japan). Human embryonic kidney HEK293T cells were provided by S. Saiki (Juntendo University, Japan). Human colorectal tumor LoVo, HT29, Colo-201, HCT116, LS-174T, SW620, DLD-1, SW48 and SW480 cells, human lung cancer A549 cells, human breast cancer MCF-7 cells, and human melanoma A2058 cells were obtained from the American Type Culture Collection (ATCC, Rockville, MD).

A431 cells were maintained in Dulbecco's Modified Eagle's Medium (DMEM) supplemented with 5% Calf Serum (CS), 100 U/mL penicillin G (Sigma-Aldrich, St. Louis, MO), and 0.1 mg/mL kanamycin (Sigma-Aldrich) at 37°C in a humidified atmosphere containing 5% CO_2. EC17, HEK293T, HeLa, and MCF-7 cells were maintained in DMEM supplemented with 10% fetal bovine serum (FBS), 100 U/mL penicillin G, and 0.1 mg/mL kanamycin in the same conditions described above. The other cells were maintained in RPMI-1640 medium supplemented with 10% FBS, 100 U/mL penicillin G, and 0.1 mg/mL kanamycin, also in the above-mentioned conditions.

2.4.4 Cell cycle and apoptosis analysis by flow cytometry

The percentage of cells in different phases of the cell cycle, including the sub-G_1 population, was analyzed by flow cytometry following staining with propidium iodide (PI; Wako Pure Chemical Industries). In brief, cells were seeded in 6-well plates and, following overnight culture, were treated with XN for 48 h. In the co-treatment test for the PKA inhibitor and XN, the cells were pre-treated with PKA inhibitor for 1 h before being treated with XN. Following treatment, cells were harvested and fixed with ice-cold 70% EtOH at 4°C, followed by treatment with 10 μg/mL RNase A (Wako Pure Chemical Industries) for 20 min at 37°C. Subsequently, cells were stained with 50 μg/mL PI. PI fluorescence was measured by EPICS ALTRA (Beckman Coulter, Brea, CA).

To illustrate a waterfall plot, Z-score values were calculated using EC_{50} values of each cell viability (X_i), its mean (X_{mean}), and its standard derivation (S) using the following formula:

$$Z\text{-score} = (X_{mean} - X_i) / S$$

2.4.5 Western blot analysis

Anti-cleaved-PARP, anti-VCP, and anti-survivin were purchased from Cell Signaling Technology (Danvers, MA). Anti-β-actin, HRP-linked anti-mouse IgG, and HRP-linked anti-rabbit IgG were purchased from Sigma-Aldrich. Cells were immediately harvested and lysed with RIPA buffer (25 mM HEPES, 1.5% TX-100, 1% sodium deoxycholate, 0.1% SDS, 500 mM NaCl, 5 mM EDTA, 50 mM NaF, 0.1 M Na_3VO_4, and cOmplete Protease Inhibitor Cocktail Tablets (Roche, Germany); pH 7.8). The lysates were centrifuged at 13,000 rpm for 15 min to remove the insoluble fraction. Equal amounts of total protein were subsequently separated by SDS-polyacrylamide gel electrophoresis before being transferred on to a PVDF membrane (Millipore, Billerica, MA). The membrane was probed with the indicated antibodies. The chemiluminescence signal was detected using an Immobilon Western kit (Millipore) and ChemiDoc XRS+ System (Bio-Rad, Hercules, CA).

2.4.6 Anti-tumor efficacy in the xenograft model

Nude mice were purchased 6-week-old female BALB/c nude mice from Charles River Laboratories (Tokyo, Japan). XN was suspended in dimethyl sulfoxide (DMSO) at a concentration of 100 mM, then diluted with phosphate-buffered saline (PBS) to the concentrations indicated and given daily to the mice. Conversely, control mice received a vehicle control of 0.85% DMSO corresponding to 30 mg/kg XN. Each suspension (1×10^7 cells/mouse) of HCT116 and SW480 cells was mixed with an equal volume of Matrigel (BD, Franklin Lakes, NJ) and injected subcutaneously into the mammary fat pads of mice. After the tumors developed over a period of 1 week, reaching sizes of approximately 150 mm^3 [calculated as $1/2 \times (\text{width} \times \text{length}^2)$], mice were randomized

into four groups of five and administered drugs by intraperitoneal injection for 17 days. Tumor volume was measured with callipers. Thereafter, mice were euthanized and tumors were dissected; images were captured with a digital camera.

After being killed, the organs (heart, lung, liver, kidney, spleen, and pancreas) were immediately removed. A portion of each tissue was fixed in 10% neutral formalin for histological examination, while the remaining tissue sample was frozen, and preserved at -80°C for subsequent immunohistochemistry. All experiments were performed in accordance with the guidelines of the animal facility at Tokushima University.

2.4.7 Immunohistochemical staining of xenografts

Anti-Ki67 antibody [Sp6], (ab16667) was purchased from abcam (Cambridge, USA). Anti-rabbit immunoglobulins/HRP antibody (P0448) and Liqud DAB+ (K3468) were purchased from DAKO (Carpinteria, CA, USA). To examine the Ki67 protein expression in HCT116 xenograft tumors, I stained the tissue sections of paraffin-embedded tumors. In brief, 4-μm sections were dewaxed in xylene and ethanol. The slides were subjected to high-temperature antigen retrieval in citric buffer (10 mM, pH 6.0). After antigen retrieval, the slides were dipped in methanol containing H_2O_2 [0.3 % (v/v)] for 30 min. After washing with 10 mM PBS at pH 7.4, the slides were incubated with anti-Ki67 (dilution 1: 1600) antibody with microwave irradiation. The slides were then washed with PBS three times for 5 minutes each time, anti-rabbit immunoglobulins/HRP antibody was applied to the slides. After washing with PBS three times, the expression of Ki67 was visualized as brown precipitates with liquid DAB+. After washing with distilled water, nuclear counterstaining was performed with hematoxylin. The nuclear labeling index of the Ki67 staining was determined under microscope (BX-50, Olympus) for regular

pathological diagnosis. In brief, 1,000 tumor cells were counted manually and the positive ratio was calculated in each xenograft. Statistical analysis was performed by Graphpad prism 5 (GraphPad Software, La Jolla, CA, USA)[107].

2.4.8 Lentiviral genome-wide shRNA screening

A dose response curve of XN for HCT116 was calculated using xCelligence (ACEA Biosciences, San Diego, CA), an automated cell growth analyzer. HCT116 cells were cultured at a variety of XN concentrations for 48 h and the real-time cell growth rates were recorded by the xCelligence.

Genome-wide Lentiviral shRNA screenings were performed using HCT116 cells. In brief, an shRNA Lentivirus library containing approximately 27,500 barcoded shRNAs (DECIPHER shRNA Library: Human Module #1, Cellecta Inc., Mountain View, CA) was produced according to the manufacturer's protocol, after which 2.0×10^7 HCT116 cells were infected by the Lentivirus and maintained for 48 h after infection. The shRNA Lentivirus-infected HCT116 cells were then selected by puromycin (1.0 μg/mL) for 72 h; the selected cells were then separated into two 15 cm culture dishes with an equal number of cells, one of which contained XN at a 7.0 μM concentration and the other cultured with DMSO as a control. At 72 h after the XN treatment, the HCT116 cells were harvested and their genomic DNA extracted using a QiaAmp DNA Mini Kit (Qiagen, Hilden, Germany). The shRNA-specific barcode regions were then amplified by PCR according to the manufacture's protocol with mild modifications for the PCR primers to make the PCR amplicons readable by an Ion PGM system (Thermo Scientific, Waltham, MA). Quantifications of the cellular clone sizes of each shRNA-infected HCT116 population within control or XN-treated culture conditions were calculated based on the sequence

read counts within each sample. shRNAs that suppress growth of infected cells in synergy with XN should show significant decreases in the sequence read counts specifically under the XN condition. Therefore, genes that exhibited more than 5-fold high frequencies in DMSO treated cells compared to the XN treated cells were selected as "hit genes". Thereafter, Gene Ontology based bioinformatics analysis was performed for the hit genes using the DAVID bioinformatics database focusing on molecular functions and biological processes[95,96].

2.4.9 Growth inhibition assay and isobologram test

Cell growth was measured by using an MTT assay. In brief, cells were seeded in 96-well plates and, after overnight culture, were treated with H-89 or KT5720 for 1 h. Thereafter, cells were treated with XN, ESI, or PTX for an additional 72 h. Following treatment, cells were treated with 0.5 mg/mL MTT (Sigma-Aldrich) for 4 h at 37°C, and lysed with DMSO. Absorbance at 595 nm was measured by a Multiskan FC (Thermo Scientific) and IC_{50} values of each combination of two agents were calculated and plotted on the graph. For each combination experiment, the combination indexes (CI) were calculated and normalized with IC_{50} values as reported[99] and plotted on an isobologram graph[98]. On the isobologram, a straight line connecting the x- and y-intercepts and the intervening points infers an additive effect between two agents. Conversely, a concave or convex line infers a synergism or an antagonism between the two agents, respectively.

Chapter 3 Mitochondrial uncoupler exerts a synthetic lethal effect against β-catenin mutant tumor cells

3.1 Introduction

The wingless/int-1 (Wnt) signal transduction pathway plays a central role in cell proliferation, survival, differentiation and apoptosis. Interaction of a Wnt ligand with its receptors: Frizzled and LRP5/6, allows β-catenin to accumulate in the cytosol and translocate to the nucleus[65,66], leading to the activation of Wnt target genes, including cyclin D1 and c-Myc[61,67,68]. Typically, this activity is tightly regulated by the "destruction complex" which consists of Axin, adenomatous polyposis coli (APC), casein kinase 1α (CK1α), glycogen synthase kinase 3β (GSK3β) and β-TrCP[62,63]. Most human cancer cell lines contain mutations in β-catenin at codons 33, 41, and 45[108]. CK1 initially phosphorylates Ser45 of β-catenin, and phosphorylated Ser45 primes GSK-3-mediated phosphorylation of Thr41, which in turn primes successive phosphorylation of Ser37 and Ser33 by GSK-3[109]. Cancer cells in which these key phosphorylated serines or threonine are mutated have inappropriately high levels of β-catenin that activate Wnt target genes[108]. It has been reported that β-catenin is mutated in a wide variety of human tumor cells[70], including colon[69], liver[71], ovarian[72], and prostate cancer[73]. In addition, approximately 10% of all human tumors harbor activating mutations in β-catenin[74].

As described above, activation of β-catenin plays a critical role in the pathogenesis of human tumors. Therefore, this pathway has been considered a promising target for therapeutic intervention, and several molecularly targeted agents have been developed. Some have already entered Phase I studies for solid tumors[81,82], such as a Porcupine inhibitor LGK974[83,84], a pan-Frizzled antibody OMP-18R5[85], a Wnt ligand antibody OMP-54F28[87], and a CBP inhibitor PRI-724[88,89]. However, no approved drugs are clinically available for treatments that target the Wnt signaling pathway. In addition, most of these agents induce growth arrest in tumor cells by targeting the Wnt signaling

pathway. Thus, the tumor cells do not die and can acquire resistance.

I have previously reported that MEK1/2 inhibitors induce cell growth arrest in β-catenin wild type tumor cell lines, whereas they induce apoptosis in β-catenin mutant tumor cell lines *in vitro*. Furthermore, I have reported that a MEK inhibitor alone could induce significant tumor regression in β-catenin-mutant xenograft models[90]. These findings support the clinical use of MEK inhibitors as single agents for patients with colorectal carcinoma who carry active β-catenin mutations. To find another effective compound that is effective for patients with tumors who carry active β-catenin mutations, I screened for compounds that exhibited synthetic lethality with β-catenin mutations, other than MEK1/2, from an in-house natural product library. In addition, I also found that V-ATPase inhibitors induced apoptosis preferentially in β-catenin mutant tumor cells[110]. In our continued screening, I have now identified nonactin as a hit compound. Nonactin is a member of a family of naturally occurring cyclic ionophores known as macrotetrolide antibiotics. In this study, I show that nonactin exhibits high selectivity against β-catenin mutant tumor cell lines with apoptosis induction *in vitro* and *in vivo*. I also demonstrate the mechanism by which nonactin selectively induces apoptosis in cell lines harboring active mutant β-catenin.

3.2 Results

3.2.1 Nonactin was identified as inducing apoptosis in β-catenin mutant HCT116 cells

I screened more than 3,000 microbial extracts for compounds that induced apoptosis in β-catenin mutated HCT116 cells, but not in A375 cells harboring wild type β-catenin. One culture broth extract of *streptomyces* gave a positive result in the screening, and subsequently the active compound produced by this strain was isolated and identified as nonactin (Figure 3-1). Nonactin is well-known as a macrotetrolide antibiotic ionophore[111,112]. Western blot analysis using anti-cleaved-PARP antibody revealed that the expression levels of cleaved-PARP in β-catenin mutant HCT116 cells significantly increased upon treatment with concentrations above 0.1 μM nonactin for 24 h. The apoptosis-inducing ability of nonactin in HCT116 cells was further confirmed by measuring sub-G_1 populations of tumor cells *via* flow cytometry, and nonactin-induced apoptosis was significantly suppressed by Z-VAD-FMK, a pan-caspase inhibitor (Figure 3-2). On the other hand, cleaved-PARP was not detected at nonactin concentrations of up to 10 μM in A375 cells expressing wild type β-catenin. This outcome indicates that nonactin induced apoptosis in HCT116 cells at least 100 times more effectively than in A375 cells. I have previously reported that MEK1/2 inhibitors induced apoptosis selectively in β-catenin mutant tumor cell lines[90]. However, nonactin did not inhibit ERK1/2 phosphorylation in either cell line (Figure 3-3), indicating that nonactin induced apoptosis in HCT116 cells but not in A375 cells with a mechanism other than MEK inhibition.

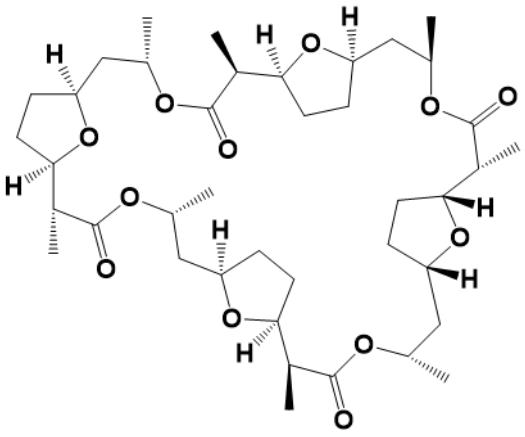

Figure 3-1. Structure of nonactin

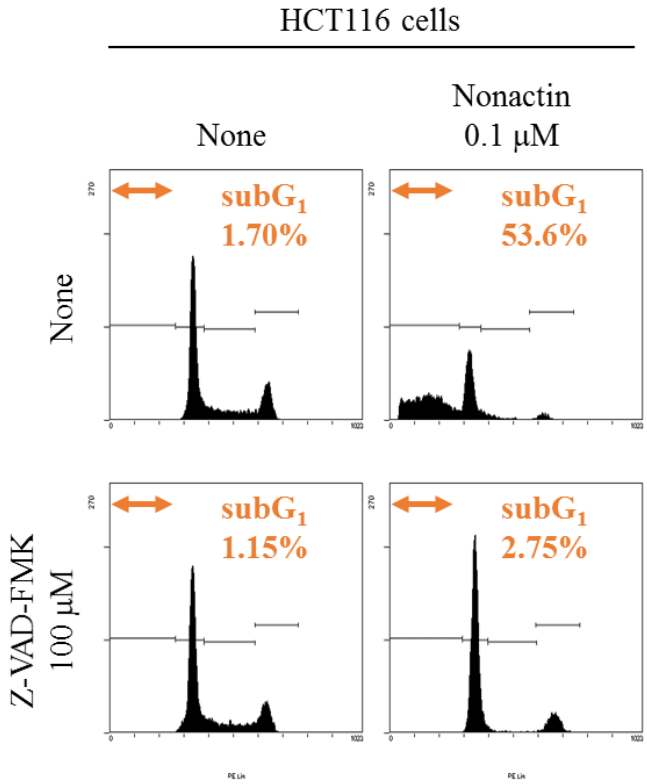

Figure 3-2. Z-VAD-FMK, a pan-caspase inhibitor, significantly suppressed nonactin-induced dell death

β-catenin mutant HCT116 cells were treated with 0.1 μM of nonactin in the presence or absence of 100 μM of Z-VAD-FMK for 48 h, after which the sub-G_1 populations of each cell line were detected by flow cytometry.

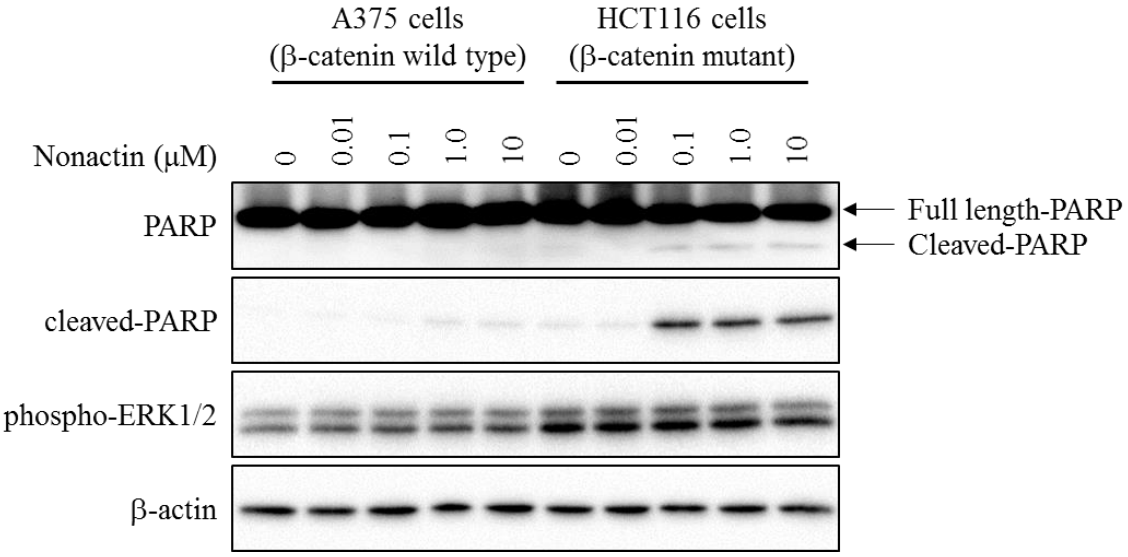

Figure 3-3. Nonactin induced apoptosis in HCT116 cells without ERK phosphorylation

A375 and HCT116 cells were treated with nonactin, and the PARP-cleavage and ERK1/2-phosphorylation were detected by western blot.

3.2.2 Nonactin induced apoptosis preferentially in β-catenin mutant tumor cells

To further confirm the selectivity of nonactin-induced apoptosis against the β-catenin mutant tumor cell lines, I examined the effects of nonactin on cell viability in various types of human tumor cell lines. For this, I selected 11 tumor cells including four β-catenin mutant tumor cells harboring mutations in key β-catenin N-terminal phosphorylation sites: A427 cells (T41A); HCT116 cells (S45 deletion); LS-174T cells (S45F); and SW48 cells (S33Y). These tumor cells were treated with 0.1, 0.3, 1.0, 3.0, or 10 μM nonactin for 48 h and the number of cells was recorded. As shown in Figure 3-4, nonactin induced cell death at 0.1 μM in tumor cells harboring mutant β-catenin (growth ratio<0). By contrast, nonactin induced cell growth inhibition but not cell death in concentrations of up to 10 μM in tumor cells harboring wild type β-catenin, including APC mutant tumor cells (growth ratio>0). This indicates that nonactin induced cell death in β-catenin mutant cells at least 100 times more effectively than in β-catenin wild type cells.

Furthermore, nonactin-induced cell death was detected by western blot using anti-cleaved-PARP antibody. As shown in Figures 3-5 and 3-6, the expression levels of cleaved-PARP increased upon treatment with nonactin concentrations above 0.1 μM in four β-catenin mutant tumor cell lines, but nonactin did not induce PARP-cleavage in tumor cells expressing wild type β-catenin (including APC mutant tumor cells) at concentrations of up to 1 μM. Effects of nonactin on tumor cell death were further confirmed by the measurement of the sub-G_1 populations using flow cytometry. As shown in Table 3-1 and Figure 3-7, correlating with the western blot analysis, 0.1 μM nonactin induced an increase in the sub-G_1 population in four β-catenin mutant tumor cell lines. However, nonactin did not significantly affect the sub-G_1 population in any other β-

catenin wild type tumor cell lines. Taken together, nonactin induced apoptosis selectively in tumor cell lines harboring active mutations of β-catenin.

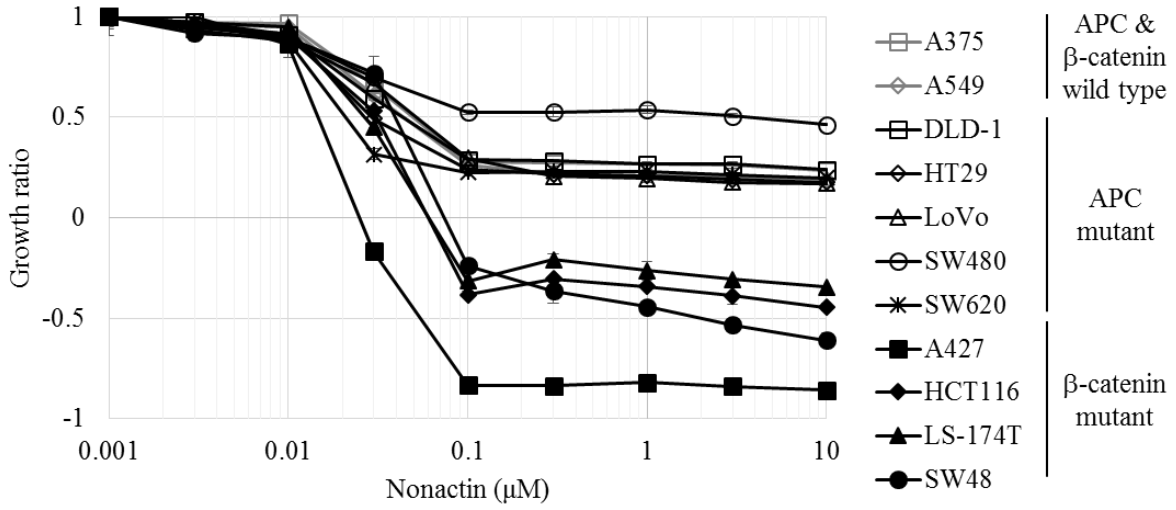

Figure 3-4. Nonactin potently suppressed cell growth in β-catenin mutant cells
Cells were treated with nonactin, and cell growth was measured by a CellTiter-Glo Luminescent Cell Viability Assay. Values are the means of three independent experiments, bars, SD.

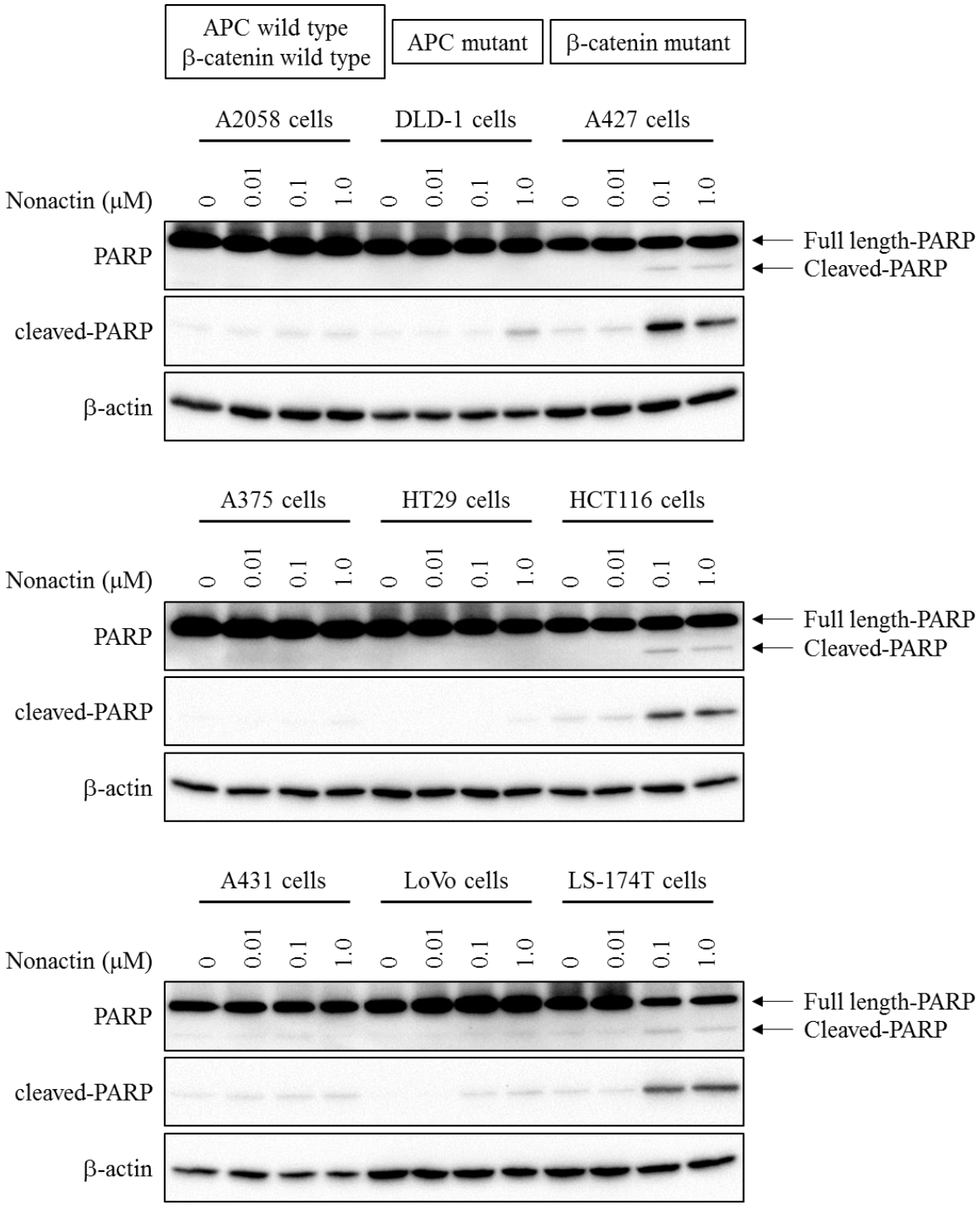

Figure 3-5. Nonactin induced apoptosis only in β-catenin mutant cells

Cells were treated with nonactin, and the PARP-cleavage was detected by western blot.

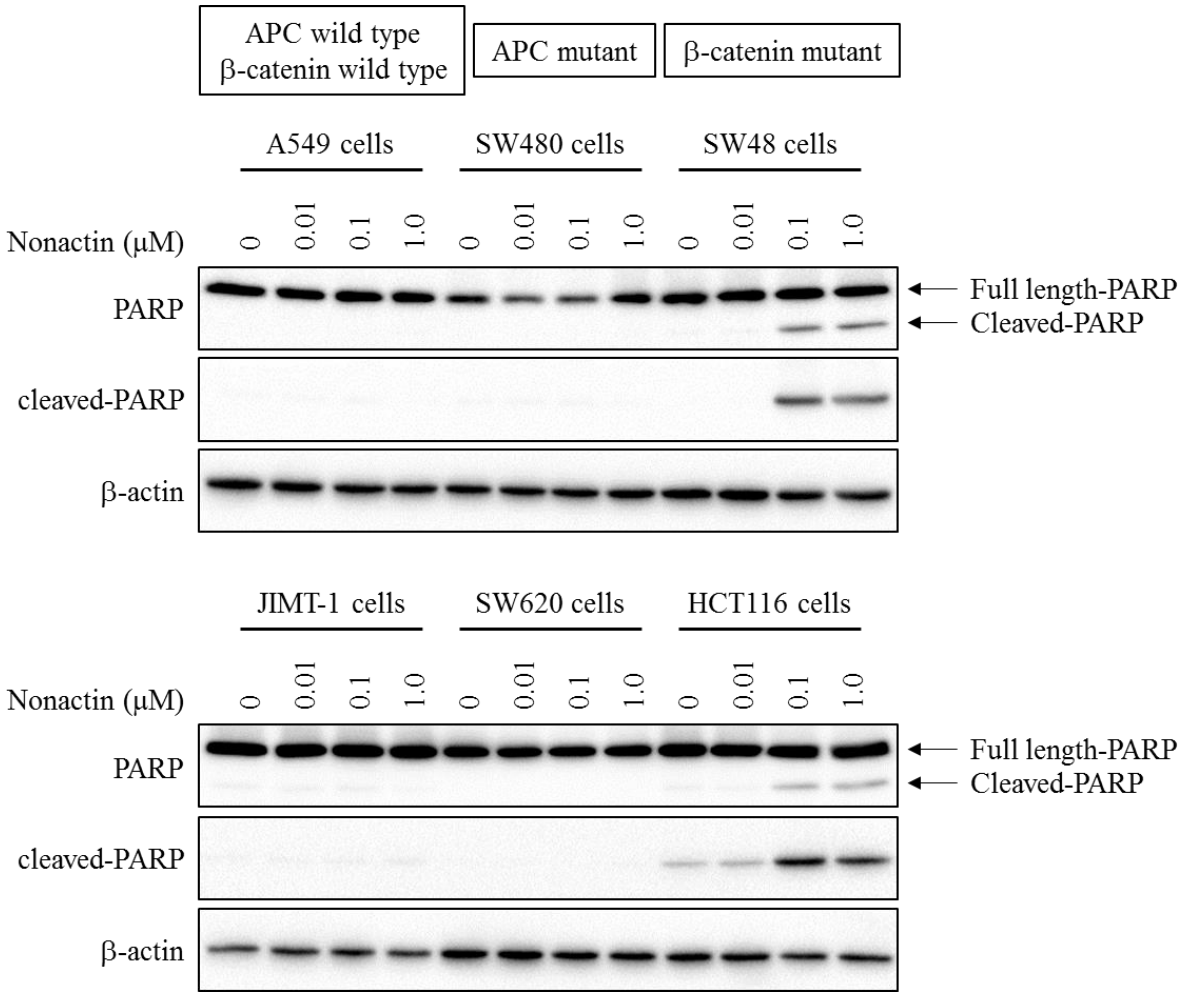

Figure 3-6. Nonactin induced apoptosis only in β-catenin mutant cells

Cells were treated with nonactin, and the PARP-cleavage was detected by western blot.

Table 3-1. The apoptosis-inducing ability of nonactin detected by flow cytometer
Cells were treated with nonactin, and the sub-G_1 populations were detected by flow cytometry.

	Cell line	sub-G_1 population (%)	
		None	Nonactin 0.1 μM
APC & β-catenin wild type	A2058	0.77	3.5
	A375	0.80	1.7
	A431	2.1	5.1
	A549	1.6	4.3
	JIMT-1	1.4	2.2
APC mutant	DLD-1	2.7	9.0
	HT29	1.2	2.6
	LoVo	0.55	6.6
	SW480	1.6	2.3
	SW620	3.5	6.7
β-catenin mutant	A427	12	42
	HCT116	3.0	48
	LS-174T	15	66
	SW48	1.5	43

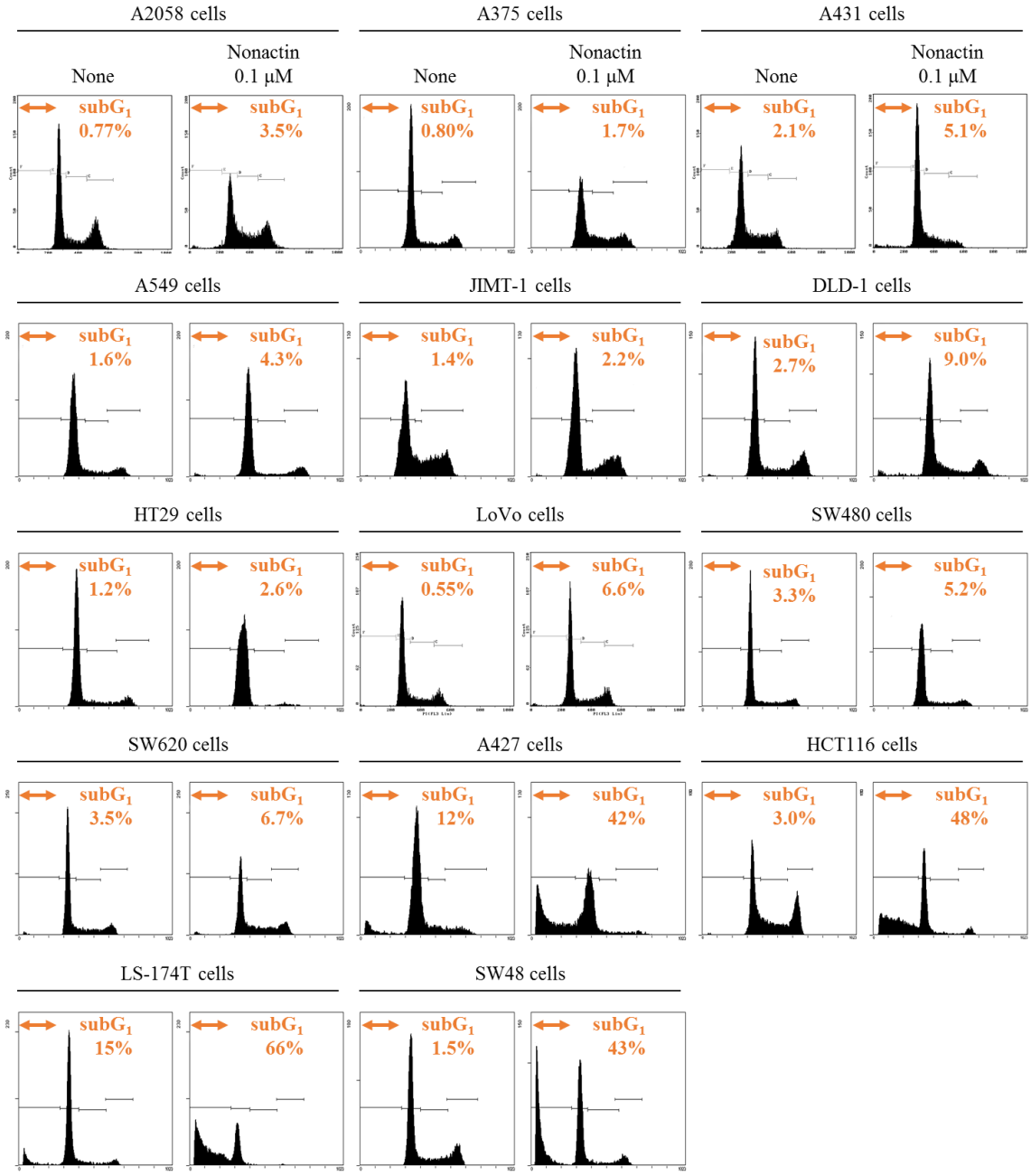

Figure 3-7. The selectivity of nonactin against β-catenin mutant tumor cells investigated by flow cytometry

Cells were treated with 0.1 μM of nonactin for 48 h, after which the sub-G_1 populations of each cell line were detected by flow cytometry.

3.2.3 Nonactin induced apoptosis in β-catenin mutant tumor cells *via* mitochondrial uncoupling activity

Nonactin is known for its ability to form complexes with alkali cations, most notably potassium and sodium. Therefore, I next investigated whether such ionophore activities are involved in nonactin-induced apoptosis against β-catenin mutated tumor cells by using salinomycin (a K^+ ionophore), valinomycin (a K^+ ionophore), and monensin (a Na^+ ionophore). As shown in Figure 3-8, valinomycin induced a dose-dependent increase in the expression levels of cleaved-PARP in β-catenin mutant HCT116 cells, but not in β-catenin wild type A375 cells. On the other hand, neither salinomycin: another K^+ ionophore, nor monensin exhibited significant selectivity against β-catenin mutated tumor cells. As nonactin and valinomycin are also able to uncouple the oxidative phosphorylation of mitochondria[113,114], I next examined whether another uncoupler: carbonyl cyanide m-chlorophenyl hydrazone (CCCP) could also induce apoptosis selectively in β-catenin mutant tumor cells. As shown in Figure 3-9, CCCP increased cleaved-PARP levels in β-catenin mutant HCT116 and SW48 cells in a dose-dependent manner, but not in β-catenin wild type A375 and HT29 cells. These outcomes indicate that mitochondrial uncoupling activity is, at least in part, responsible for selective apoptosis induction in β-catenin mutant tumor cells.

The apoptosis-inducing ability of uncoupler was further confirmed by measuring sub-G_1 populations of tumor cells *via* flow cytometry. As shown in Figure 3-10, correlating with the western blot analysis, 48 h treatment of tumor cells with uncouplers increased the sub-G_1 populations in β-catenin mutant HCT116 and SW48 cells, but not in β-catenin wild type A375 and HT29 cells. Therefore, these results suggest that the

mitochondrial uncoupling activity is closely related to the selective apoptosis induction in β-catenin mutated tumor cells.

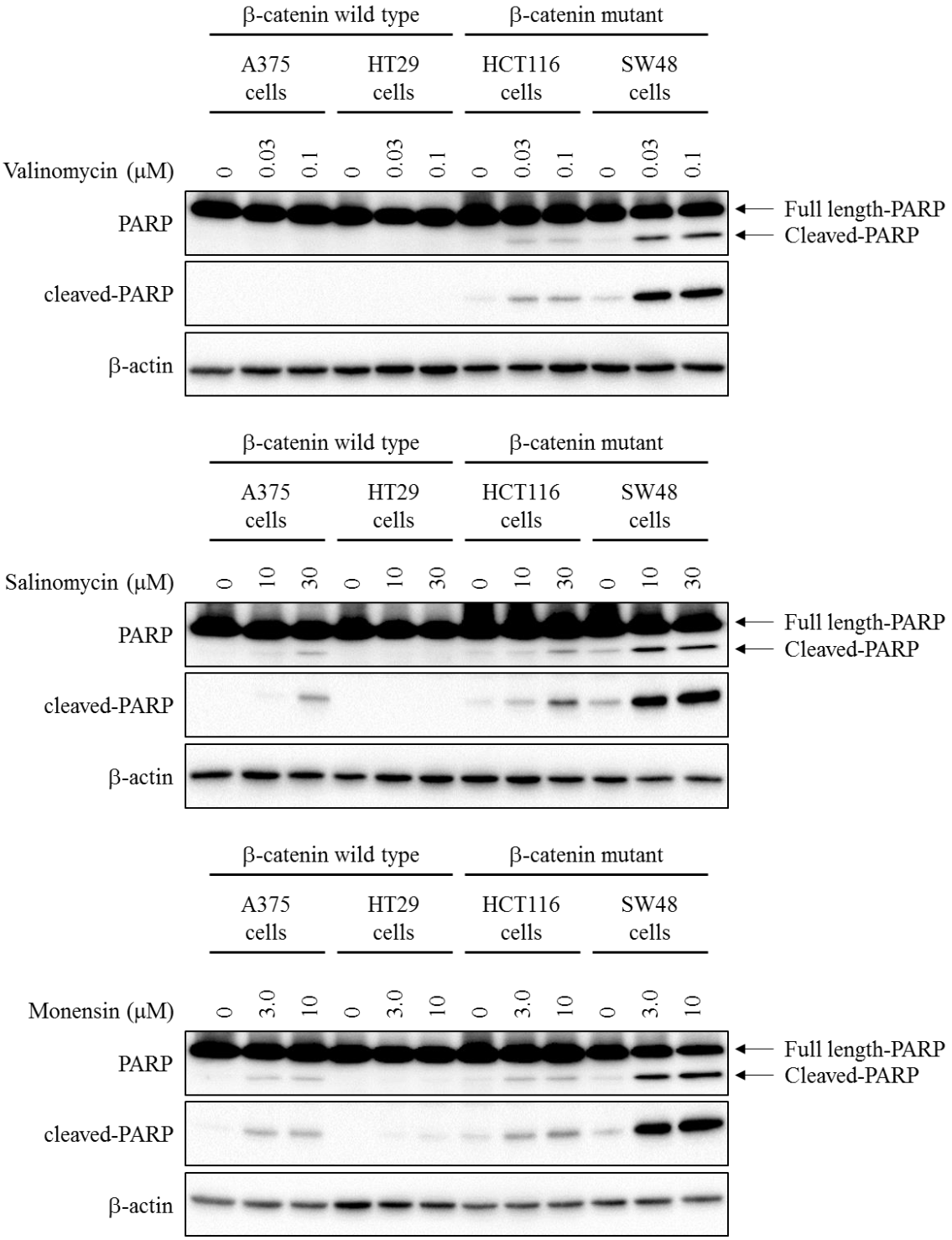

Figure 3-8. Mitochondrial uncoupling activity is required for nonactin-induced apoptosis

A375, HT29, HCT116, and SW48 cells were treated with indicated ionophores, after which the PARP-cleavage was detected by western blot.

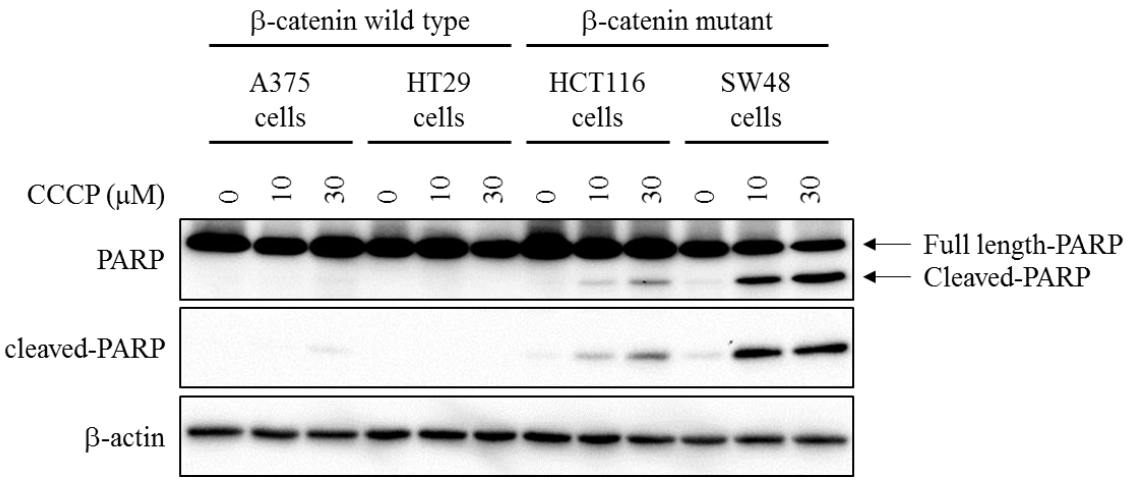

Figure 3-9. Mitochondrial uncoupling activity is required for nonactin-induced apoptosis

A375, HT29, HCT116, and SW48 cells were treated with CCCP, after which the PARP-cleavage was detected by western blot.

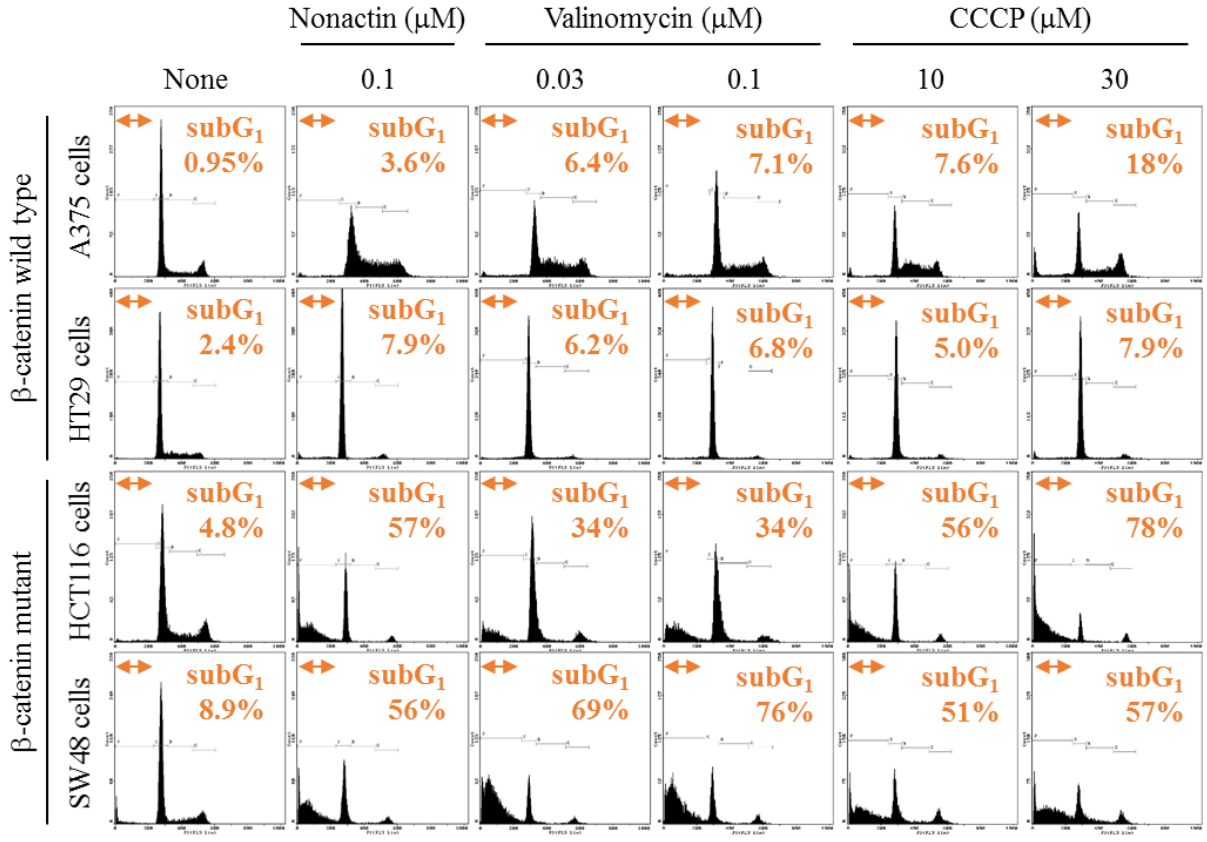

Figure 3-10. Uncouplers induced apoptosis selectively in β-catenin mutant cells
A375, HT29, HCT116, and SW48 cells were treated with indicated ionophores. The apoptosis-inducing ability of uncouplers was investigated by flow cytometry.

3.2.4 Expression of the active form of mutated β-catenin was required for uncoupler-induced apoptosis

To examine whether the expression of mutant β-catenin was a cause for apoptosis induction following treatment with uncouplers, a mutant active form of β-catenin (S37A, S45A) were transfected into A375 cells and A549 cells, which usually harbor only wild type β-catenin, and tested for the apoptosis-inducing activity of uncouplers. As shown in Figures 3-11, 3-12, and 3-13, nonactin or CCCP did not induce apoptosis in vector control-transfected A375 cells or wild type of β-catenin-transfected A375 cells; whereas they induced apoptosis in mutant β-catenin-transfected A375 cells, as judged from the sub-G_1 population. Similar results were obtained when A549 cells were used. These results suggest that active mutant β-catenin is the key factor in uncoupler-induced apoptosis.

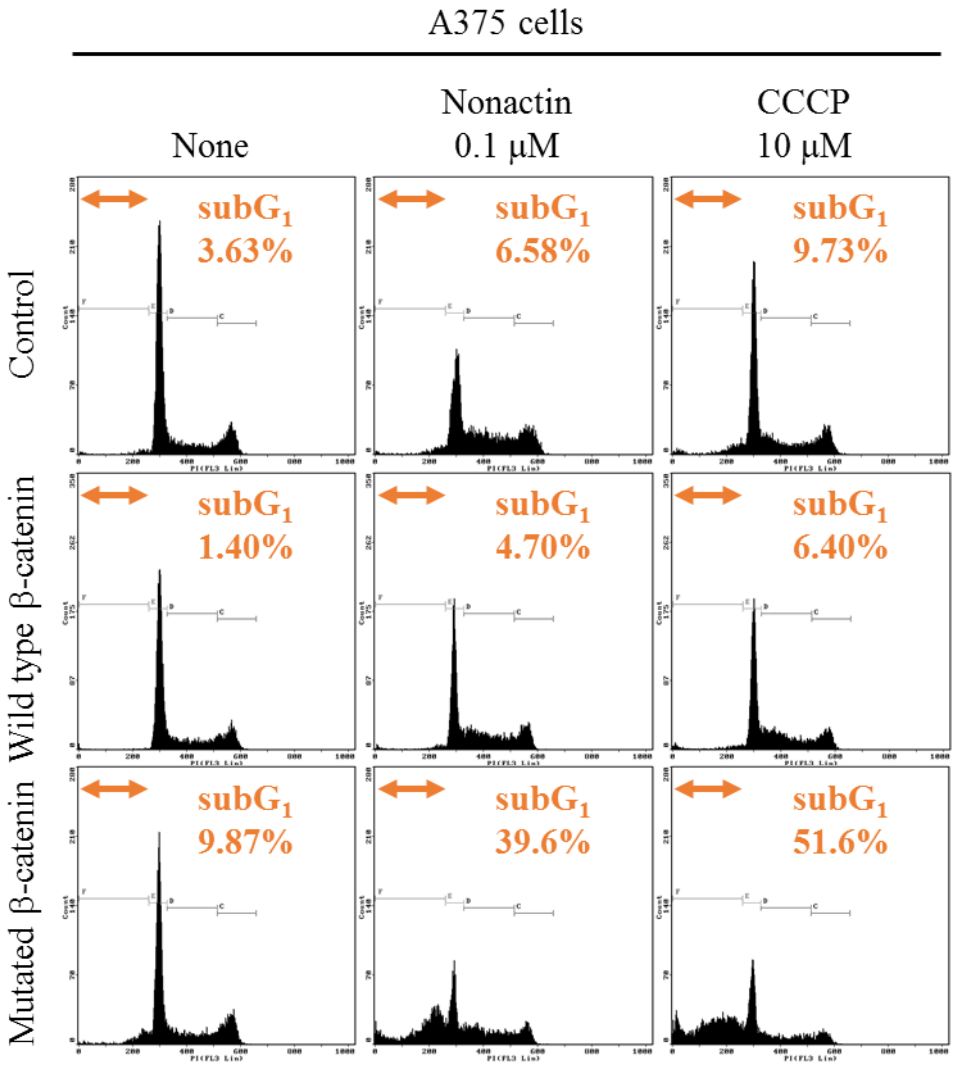

Figure 3-11. The expression of active mutant β-catenin is required for uncoupler-induced apoptosis.

A375 cells were transiently transfected with wild type and mutated β-catenin (S37A, S45A), and treated with indicated uncouplers, after which the sub-G_1 populations were detected by flow cytometry.

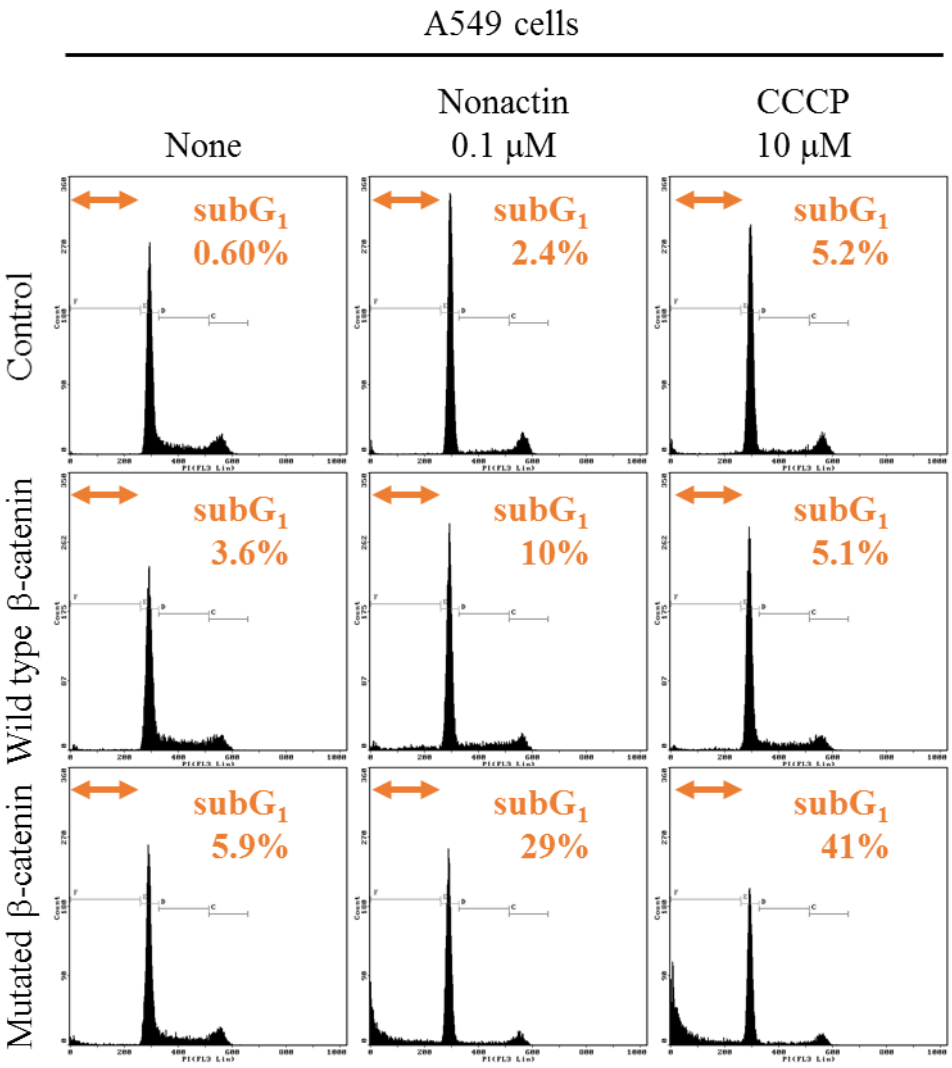

Figure 3-12. The expression of active mutant β-catenin is required for uncoupler-induced apoptosis.

A549 cells were transiently transfected with wild type and mutated β-catenin (S37A, S45A), and treated with indicated uncouplers, after which the sub-G_1 populations were detected by flow cytometry.

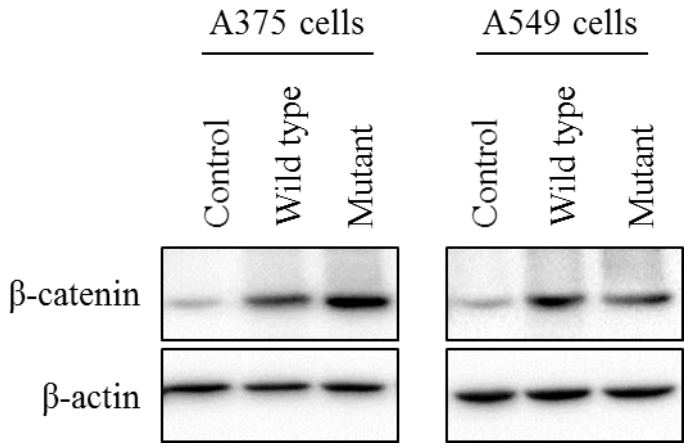

Figure 3-13. The expressions of transfected β-catenin

The expressions of transfected β-catenin in A375 and A549 cells were confirmed by western blot.

3.2.5 Dysfunction of the Warburg effect is involved in the apoptosis induced by uncouplers

As mitochondrial uncouplers induced apoptosis selectively in tumor cells harboring active mutant β-catenin, I hypothesized that these tumor cells may have a higher sensitivity to mitochondrial uncouplers than tumor cells harboring wild type β-catenin. To examine this possibility, I investigated the effect of nonactin on the mitochondrial membrane potential in both β-catenin wild type and mutant tumor cells. As shown in Figures 3-14, 3-15 and 3-16, nonactin, at the concentration which induced selective apoptosis in β-catenin mutant tumor cells, significantly reduced the red fluorescence (aggregate form) of JC-1 in both β-catenin wild type and mutant tumor cell lines to a similar extent, as judged from quantifying red and green fluorescence and calculating the red/green ratio. Similar results were obtained when CCCP was used instead of nonactin. Thus, contrary to expectations, mitochondrial uncouplers induced loss of mitochondrial membrane potential not only in β-catenin mutant tumor cells, but also in β-catenin wild type tumor cells that did not undergo apoptosis after treatment with mitochondrial uncouplers.

The mitochondrial membrane potential plays a crucial role in the function of the respiratory chain to produce ATP[115]; however, the mitochondrial uncouplers did not induce apoptosis in β-catenin wild type tumor cell lines. Therefore, I next examined the possibility that β-catenin wild type tumor cells, but not β-catenin mutant tumor cells, produced ATP by relying on aerobic glycolysis rather than mitochondrial oxidative phosphorylation for their proliferation[116], thereby surviving in the condition where mitochondrial function was damaged by uncouplers. For this, β-catenin wild type A375, A549, and HT29 cells were treated with a glycolysis inhibitor: 2-deoxyglucose (2-DG),

in the presence or absence of 0.1 μM nonactin or 10 μM CCCP for 24 h, and apoptosis status was analyzed by western blot. As shown in Figure 3-17, 2-DG alone did not affect the expression levels of cleaved-PARP in these cells, but co-treatment of cells with 2-DG and the uncouplers induced an increase in the expression levels of cleaved-PARP in a dose-dependent manner. These results indicated that glycolysis-dependent production of ATP is required for the survival of β-catenin wild type tumor cell lines when cells were treated with uncouplers. Furthermore, these results indicated that the glycolysis-dependent production of ATP was suppressed in β-catenin mutant tumor cell lines. Therefore, I next examined the possibility that active mutant β-catenin could suppress glycolysis. The active mutant form of β-catenin (S37A, S45A) was transiently transfected into β-catenin wild type A375 and A549 cells. The extracellular acidification rate (ECAR) in response to glucose was subsequently measured by an Extracellular Flux Analyzer. As shown in Figure 3-18 and 3-19, glucose-induced ECARs were significantly suppressed in active mutant β-catenin expressing cells, compared to control cells or wild type β-catenin expressing cells. These results suggested that the expression of active mutant β-catenin suppressed the ability to perform glycolysis and limited tumor cells to relying on mitochondrial oxidative phosphorylation to survive.

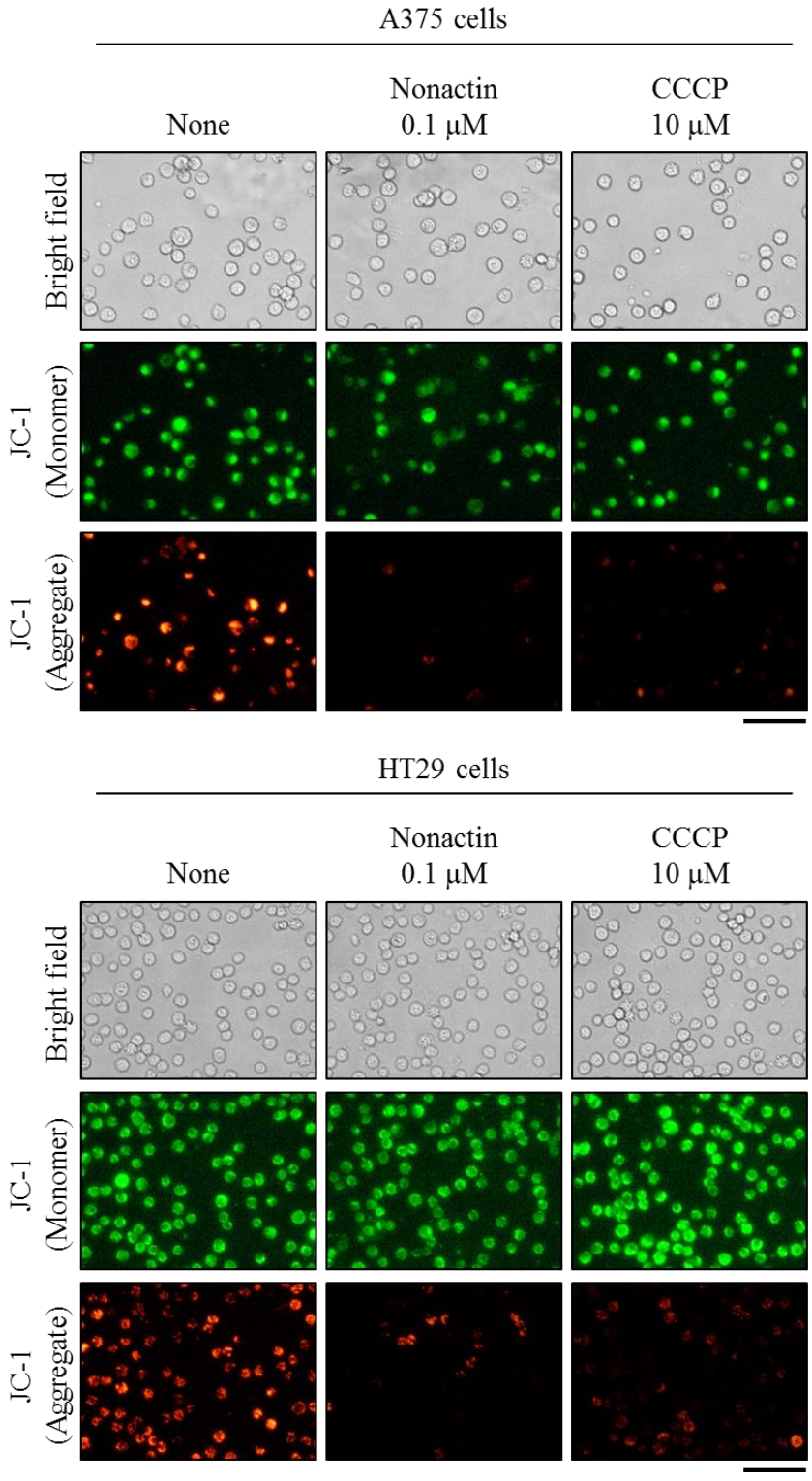

Figure 3-14. Mitochondrial membrane potential in β-catenin wild type cells

A375 and HT29 cells were treated with indicated uncouplers. Following treatment, cells were stained with 2.0 μM JC-1, after which cells were harvested and the red and green fluorescence was observed by fluorescence microscopy. Scale bar, 100 μm.

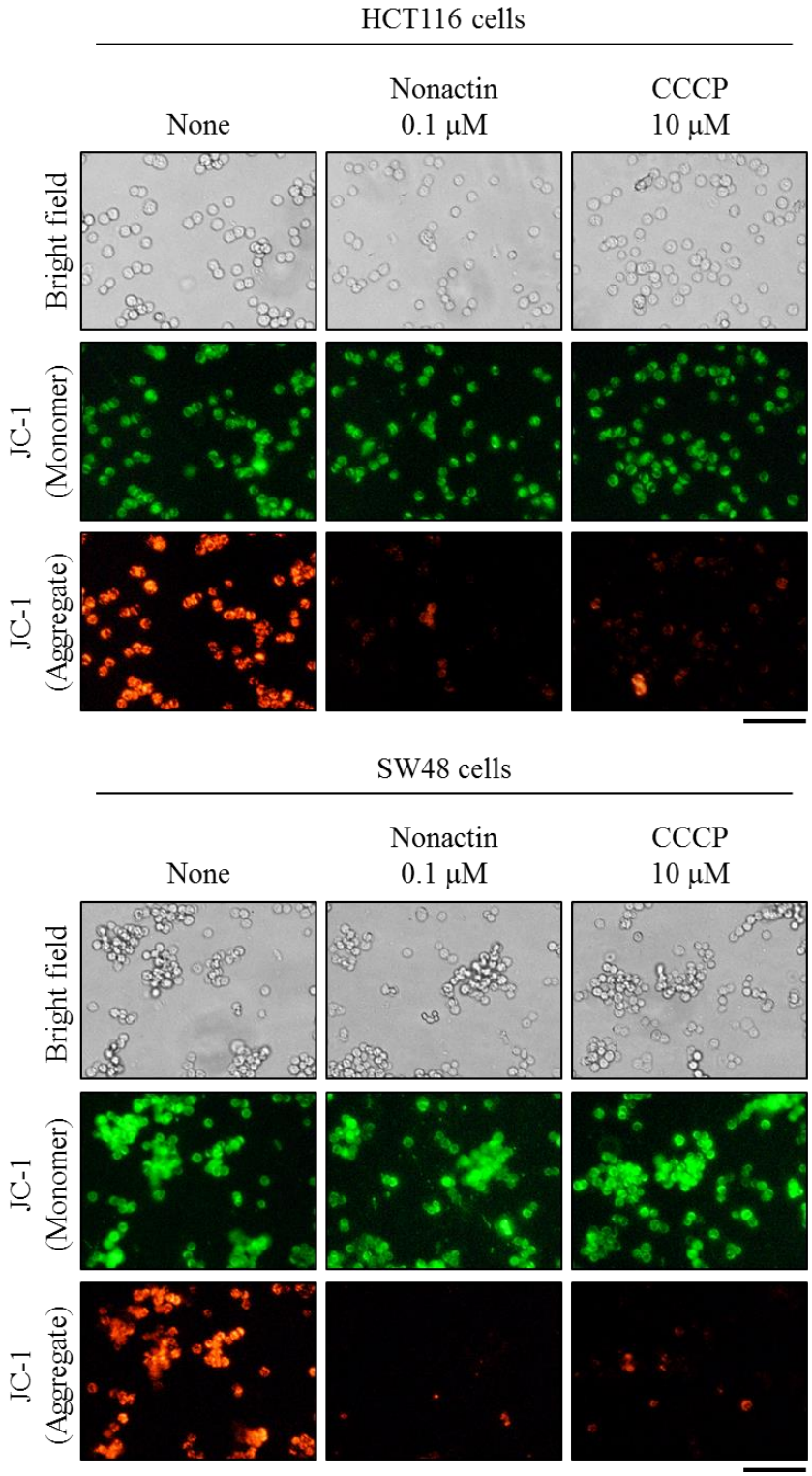

Figure 3-15. Mitochondrial membrane potential in β-catenin mutant cells

HCT116 and SW48 cells were treated with indicated uncouplers. Following treatment, cells were stained with 2.0 μM JC-1, after which cells were harvested and the red and green fluorescence was observed by fluorescence microscopy. Scale bar, 100 μm.

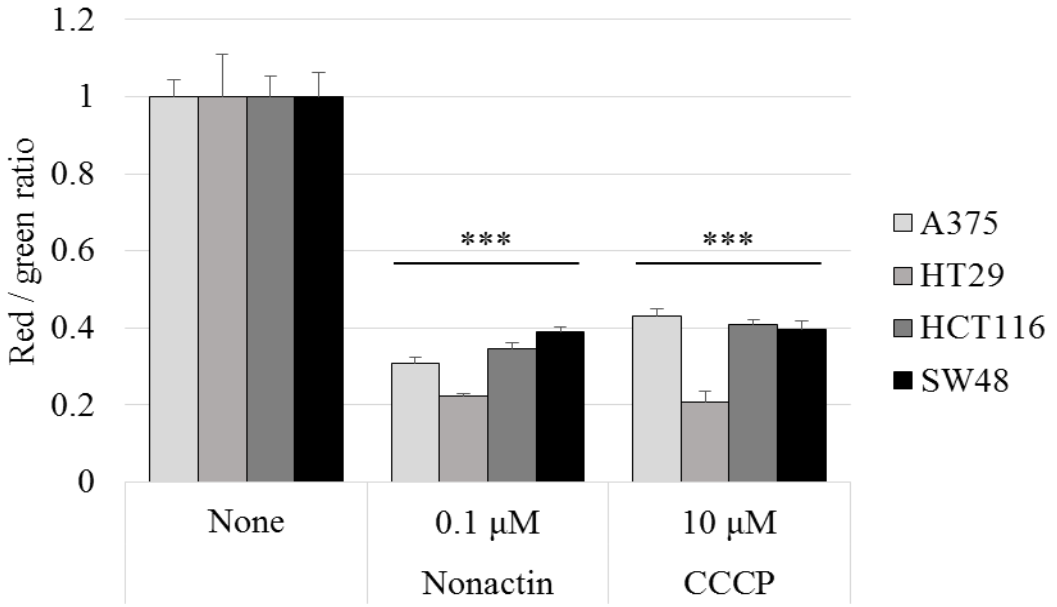

Figure 3-16. Uncouplers reduced mitochondrial membrane potential in all cell lines

Cells were treated with indicated uncouplers. Following treatment, cells were stained with 2.0 μM JC-1, after which cells were harvested and the red and green fluorescence was observed by fluorescence microscopy. Each level of fluorescence was quantified using ImageJ and the red/green ratios were calculated. Values are the means of three independent experiments, bars, SD. *** P<0.001, compared with non-treat group cells.

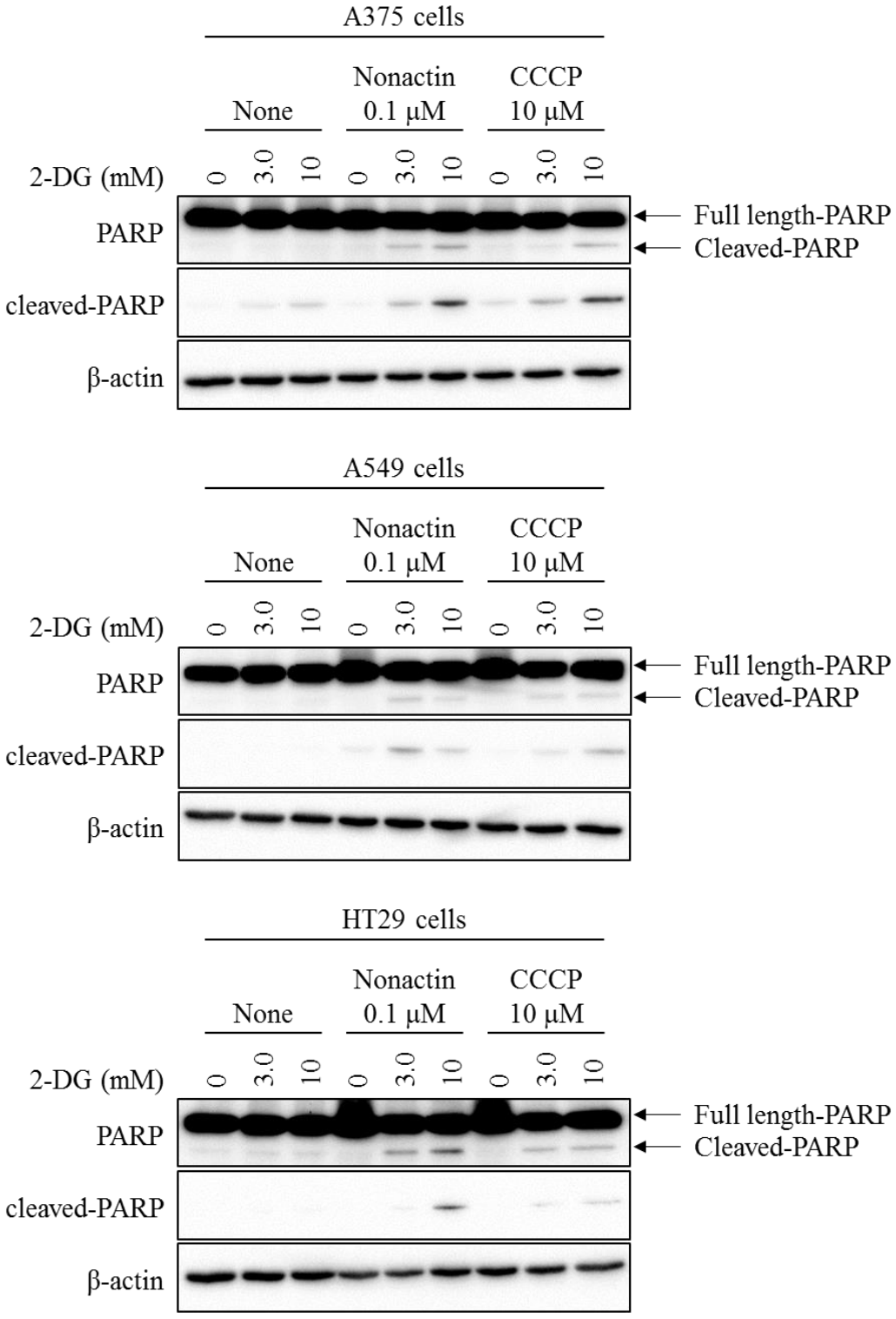

Figure 3-17. 2-DG facilitated uncoupler-induced apoptosis

A375, A549, and HT29 cells were treated with the indicated concentrations of 2-DG in the presence or absence of indicated uncouplers, and the PARP-cleavage was detected by western blot.

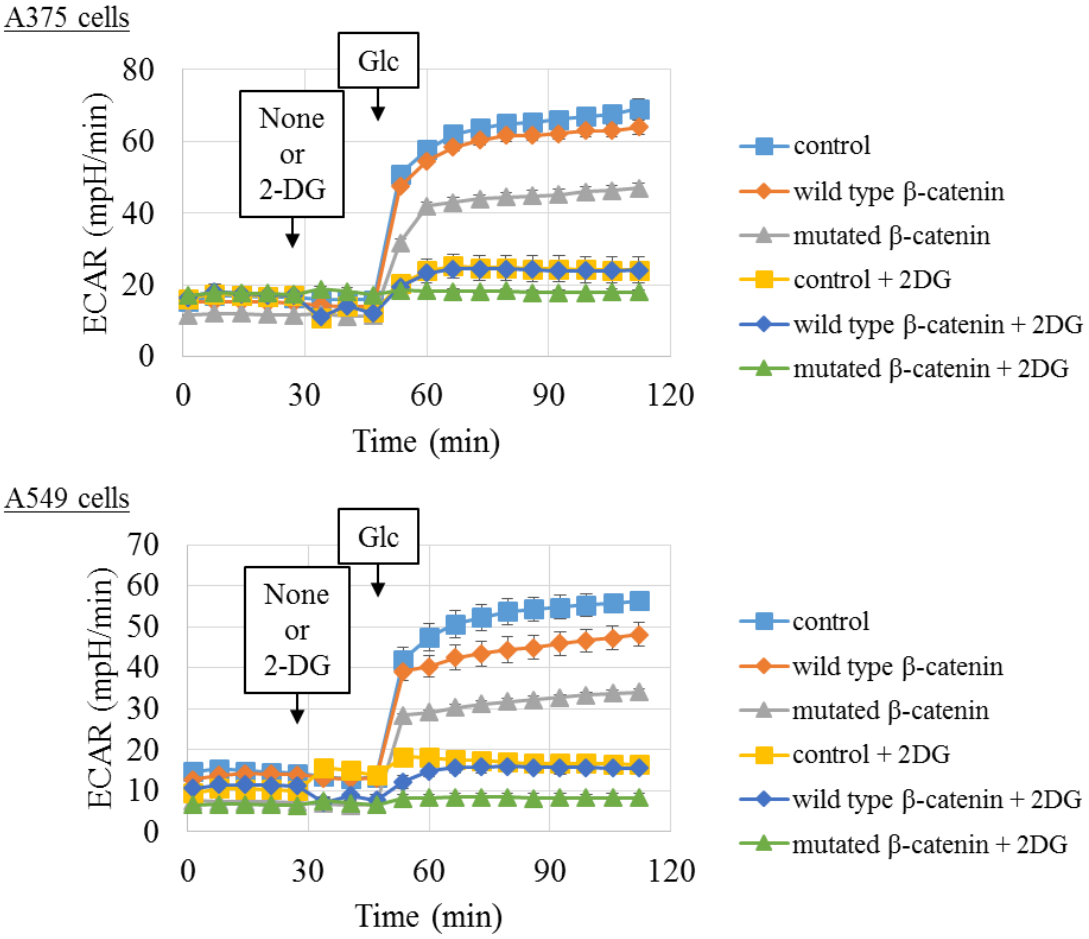

Figure 3-18. Assessment of glycolysis ability

A375 and A549 cells were transiently transfected with wild type β-catenin or mutated β-catenin, and the extracellular acidification rate (ECAR) in response to 11 mM D-glucose was measured in the presence or absence of 50 mM 2-DG. Values are the means of three independent experiments, bars, SD.

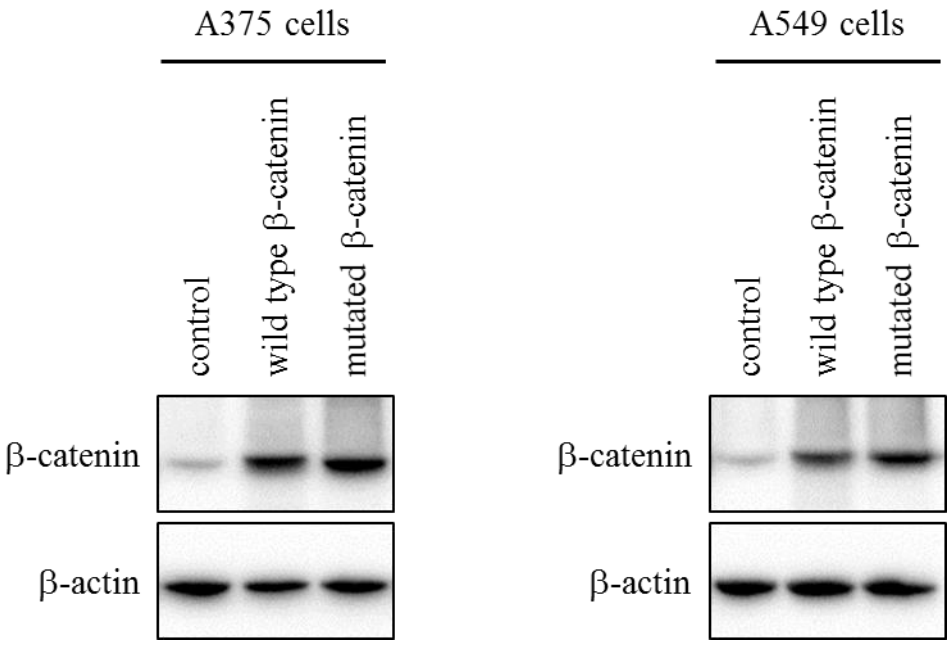

Figure 3-19. The expressions of transfected β-catenin

The expressions of transfected β-catenin in A375 and A549 cells were confirmed by western blot.

3.2.6 Antitumor effect of nonactin in xenograft models

As nonactin induced apoptosis selectively in β-catenin mutant cell lines *in vitro*, I examined the antitumor activity of nonactin *in vivo*. β-catenin wild type A375 cells and β-catenin mutant HCT116 cells were injected subcutaneously into nude mice. The mice were then intraperitoneally administered nonactin once-daily. As shown in Figure 3-20, the maximum effect of nonactin at MTD dosing (100 mg/kg) was growth inhibition of A375 tumors expressing wild type β-catenin. However, tumor regression in response to nonactin at 100 mg/kg was observed in a β-catenin mutant xenograft model without significant body weight loss. Furthermore, TUNEL staining revealed significant apoptosis induction in HCT116 tumor tissues from nonactin-treated mice, but not in HCT116 tumor tissues from control mice (Figure 3-21). These results suggested that nonactin induced apoptosis selectively in β-catenin mutant tumor cell lines also *in vivo*.

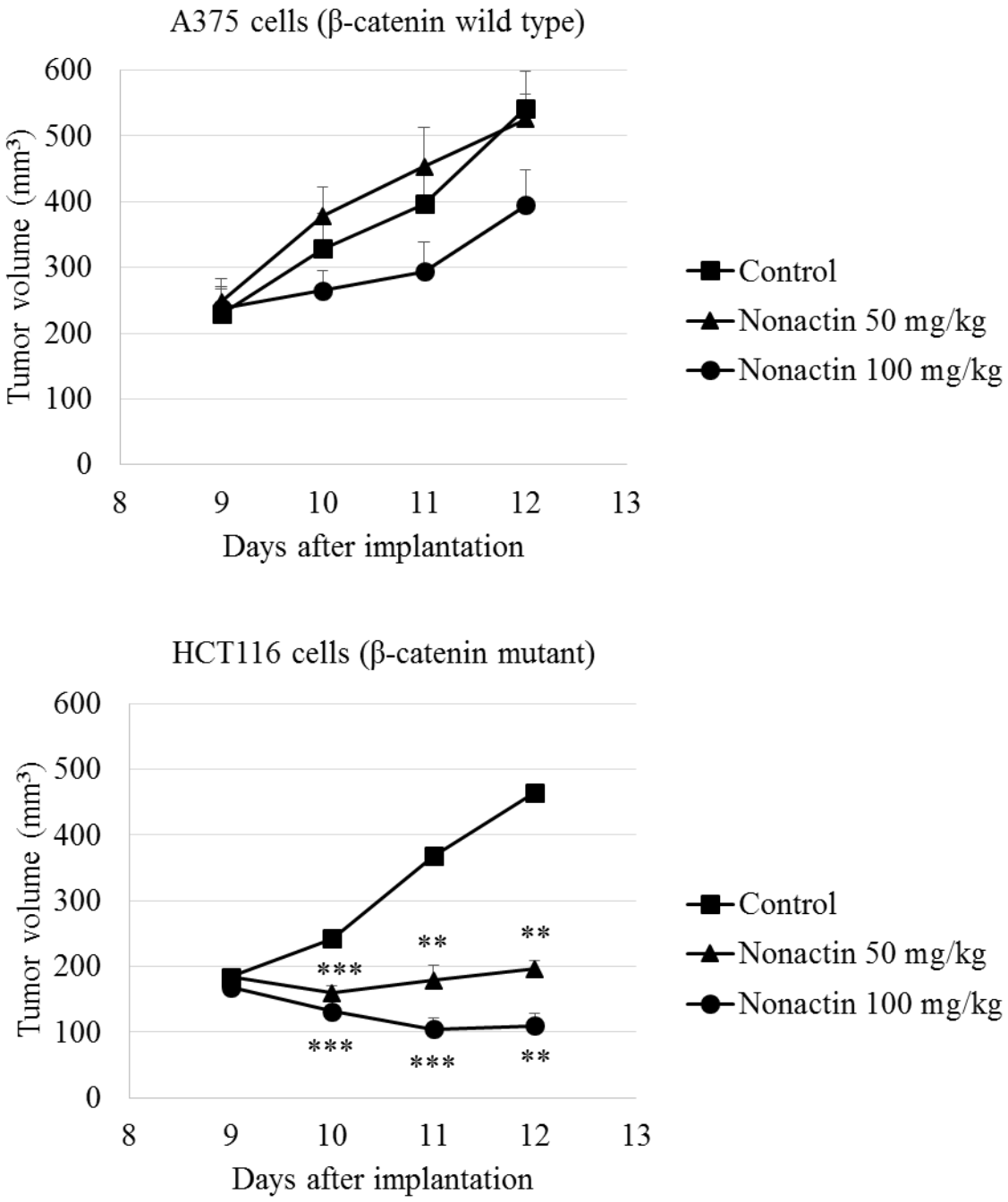

Figure 3-20. The antitumor effects of nonactin *in vivo*

A375 and HCT116 cells were injected subcutaneously into nude mice to establish xenograft models. Mice were then intraperitoneally administered a control vehicle or nonactin once-daily. Values are the means of six tumors, bars, SD. ** $P<0.01$, *** $P<0.001$, compared with control group mice.

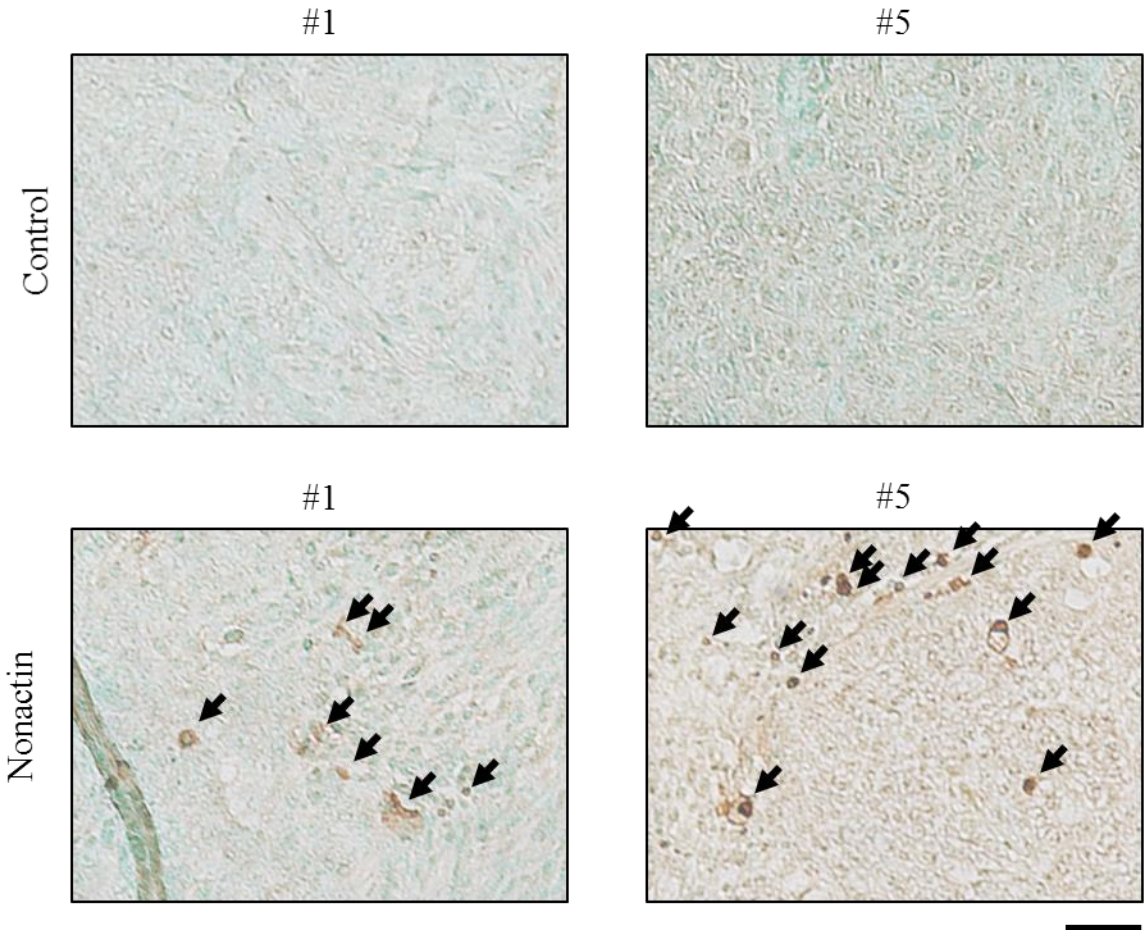

Figure 3-21. TUNEL staining

Tissue sections of HCT116 tumors were stained by TUNEL, and images were captured with a digital camera. Black arrows showed apoptotic cells (TUNEL-positive cells). Scale bar, 100 μm.

3.3 Discussion

β-Catenin is one of the main components of the Wnt signaling pathway, playing a central role in cell proliferation, survival, differentiation and apoptosis. β-Catenin is mutated in a wide variety of tumors[117,118], and mutations can be detected in up to 10% of all sporadic colon carcinomas and 20% of hepatocellular carcinomas[70]. The mutation in the N-terminus of β-catenin stabilizes β-catenin and allows it to escape from the destruction complex, after which the Wnt signaling pathway is hyperactive and drives oncogenesis[70,75,76]. Several small molecules targeting the Wnt signaling pathway have been identified; however, no approved drugs are clinically available for treatment *via* targeting of the Wnt signaling pathway. As the Wnt signaling pathway plays a crucial role in normal development and adult tissue homeostasis, interference with this pathway will not only target β-catenin mutant tumor cells, but also normal cells, resulting in significant toxicity. Therefore, to obtain compounds that act on targets other than the Wnt signaling pathway itself, I conducted a synthetic lethal chemical screen with a β-catenin mutation from our in-house natural product library. As a result, I found that nonactin induced apoptosis in β-catenin mutant tumor cells that harbor mutations in the N-terminus resulting from point mutations or in-frame deletions of the serine or threonine residues phosphorylated by CK1α or GSK3β (A427 cells: T41A, HCT116 cells: S45 deletion, LS-174T cells: S45F, and SW48 cells: S33Y). The selective apoptosis induction by nonactin was not found to simply correlate to nuclear accumulation of β-catenin.

A requirement for an active mutation in β-catenin for nonactin-induced apoptosis was confirmed by the finding that nonactin did not induce apoptosis in A375 or A549 cells harboring wild-type β-catenin, but it induced apoptosis in A375 or A549 cells by the expression of the active form of β-catenin (S37A, S45A) (Figures 3-11, 3-12, and 3-13).

These results demonstrate that nonactin exhibits synthetic lethality with an active mutant form of β-catenin. Interestingly, nonactin did not induce apoptosis in Colo-201 and Colo-205 cells harboring β-catenin N287S mutation[119] (Figure 3-22). Furthermore, at the concentration that induced apoptosis in β-catenin mutant tumor cells, nonactin did not induce apoptosis in adenomatous polyposis coli (APC) mutant tumor cell lines. APC is a negative regulator of the Wnt signaling pathway, and the truncated mutations of APC fail to form a scaffold for the destruction complex, leading to stabilized β-catenin and an aberrantly activated Wnt signaling pathway[120]. Moreover, stimulation of β-catenin wild type A375 cells with Wnt-3a enhanced the ability of SMK-17 to induce apoptosis in β-catenin wild type A375 cells, as previously reported[90]. However, nonactin failed to induce apoptosis in A375 cells even after stimulation with Wnt-3a (Figure 3-23). These results suggest that activation of the Wnt signaling pathway is not sufficient for nonactin-induced selective apoptosis in β-catenin mutant tumor cells.

Nonactin has been suggested to act as a K^+ ionophore, and another K^+ ionophore: valinomycin, showed similar selective apoptosis-inducing ability. Although salinomycin, which is also a K^+ ionophore, has been recently reported to induce programmed cell death in cancer stem cells (CSCs)[121], as well as in various other cancer cells[122-124], it did not show a significant selective induction of apoptosis in β-catenin mutant tumor cells. Thus, nonactin action is comparable to that of valinomycin while being distinct from the effects of salinomycin. This difference can be explained by the observations reported by the Szabò group, who found that salinomycin is also known to mediate K^+/H^+ exchange and induces rapid hyperpolarization of mitochondria. In contrast, the common mechanism of nonactin and valinomycin is one of mitochondrial uncoupling, causing depolarization[125]. As proton influx occurs in exchange for K^+ and is electroneutral, it does not by itself have

any effect on potential. Hyperpolarization derives from the collapse of ΔpH, which the mitochondrion compensates for by increasing mitochondrial membrane potential so as to keep the overall electrochemical potential nearly constant[125]. Indeed, the concentration of salinomycin that induced apoptosis in tumor cells did not induce a loss of mitochondrial membrane potential (Figure 3-24), while CCCP, acting as a protonophoric uncoupler, induced apoptosis selectively in the β-catenin mutant tumor cell lines (Figures 3-10 and 3-17). Further studies will be necessary to delineate the exact factors that contribute to the selective cell death in β-catenin mutant tumor cells by mitochondrial uncouplers.

Mitochondrial membrane potential plays a crucial role in the function of the respiratory chain to drive the synthesis of ATP by F_oF_1ATPase. A significant loss of mitochondrial membrane potential induces cytotoxicity resulting from ATP depletion[115]. Nonactin and CCCP induced loss of mitochondria membrane potential in both β-catenin wild type and mutant tumor cells at the same concentration of apoptosis induction. Nevertheless, nonactin, and CCCP did not induce apoptosis in β-catenin wild type tumor cells despite the loss of mitochondrial membrane potential. One possible explanation is that "the Warburg effect" may be responsible for the cell survival of β-catenin wild type tumor cells. This explanation can be confirmed by our findings that inhibition of glycolysis using 2-DG: a hexokinase 2 inhibitor, enables β-catenin wild type cells to undergo apoptosis following the treatment with uncouplers (Figure 3-17). On the other hand, because β-catenin mutant tumor cells underwent apoptosis following the treatment with the uncoupler alone, I hypothesized that the Warburg effect might be unable to function in β-catenin mutant tumor cell lines. Indeed, the expression of active mutant β-catenin (S37A, S45A), but not of wild type β-catenin, induced a decrease in glycolysis rate. This indicates that mutant β-catenin (S37A, S45A) might inhibit the Warburg effect.

At present, I do not know how mutant β-catenin (S37A, S45A) inhibited the Warburg effect. β-Catenin reportedly binds several proteins including cadherins[126], α-catenin[127], axin[76], the EGF receptor[128], APC, the actin-bundling protein fascin[129], the LEF/TCF transcription factors[130,131], the MUC-1 breast cancer antigen[132], the Alzheimer's-associated protein presenilin[133], protein phosphatases[134], and the regulator of small GTPases: IQ GAP[135]. In addition, it has been reported that c-Src-phosphorylated β-catenin at Tyr333 directly binds to nuclear Pyruvate kinase M2 (PKM2), leading to a regulation of the Warburg effect[136]. Therefore, this raises the possibility that mutant β-catenin could bind to and modulate binding proteins that regulate glycolysis, thereby inducing a dysfunction of the Warburg effect. The mechanism by which the mutation of N-terminus phosphorylation site in β-catenin inhibits glycolysis is currently under investigation.

To link these findings to a clinically relevant model, I conducted *in vivo* studies using active β-catenin mutant xenograft models. Significant tumor regression without any severe toxicity was observed in β-catenin mutant HCT116 cells in response to daily administration of nonactin (Figures 3-20 and 3-21).

In conclusion, our findings suggest that tumor cells harboring active mutant β-catenin showed a dysfunction of the Warburg effect, and produced ATP by relying on mitochondrial oxidative phosphorylation for survival. Therefore, mitochondrial uncouplers such as nonactin, valinomycin, and CCCP induced apoptosis selectively in β-catenin mutant tumor cells. Our results provide new insights into the development of potential chemotherapeutic strategies for tumor cells harboring β-catenin mutations.

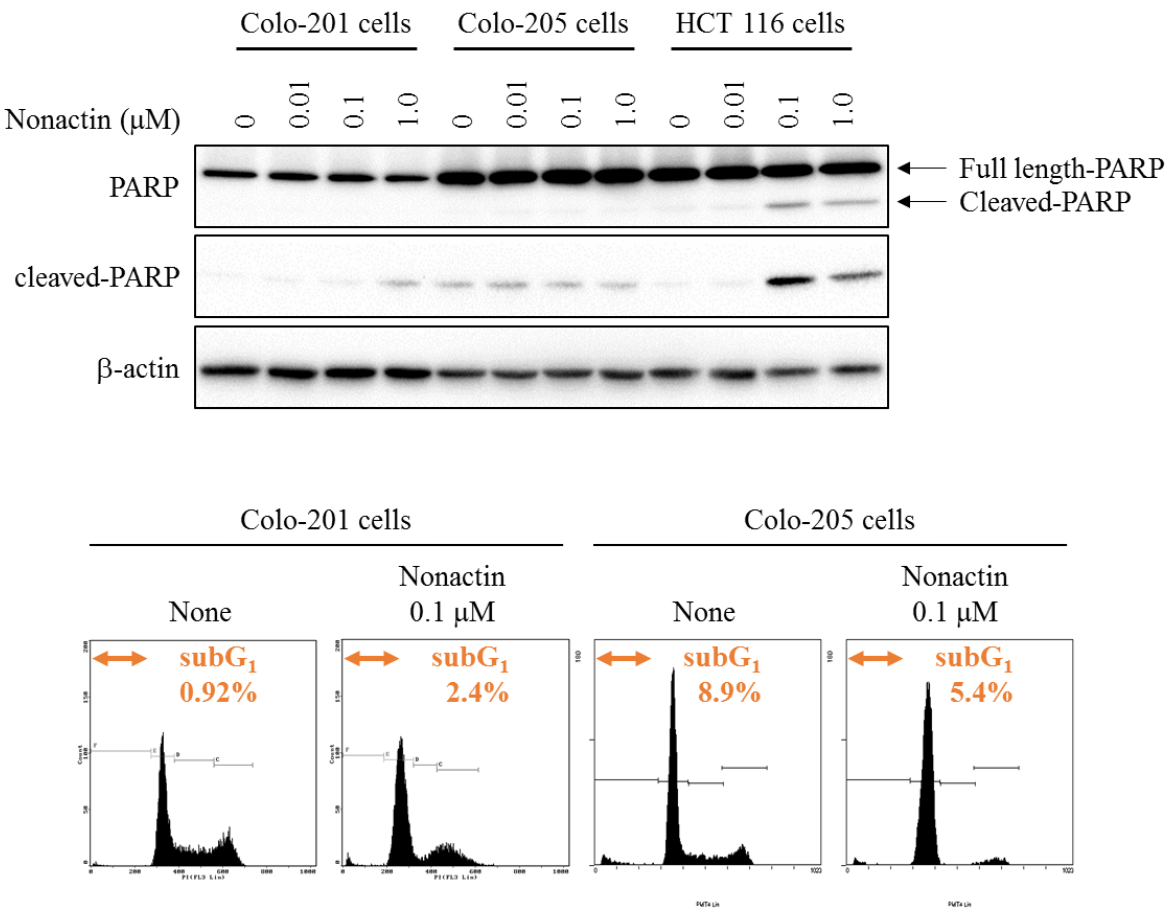

Figure 3-22. Colo-201 and colo-205 cells exhibited resistance to nonactin

Colo-201 and colo-205 cells were treated with the indicated concentrations of nonactin for 24 h, after which the expression levels of cleaved-PARP were detected by western blot. Furthermore, the cells were treated with 0.1 μM of nonactin for 48 h, after which the sub-G_1 populations were detected by flow cytometry.

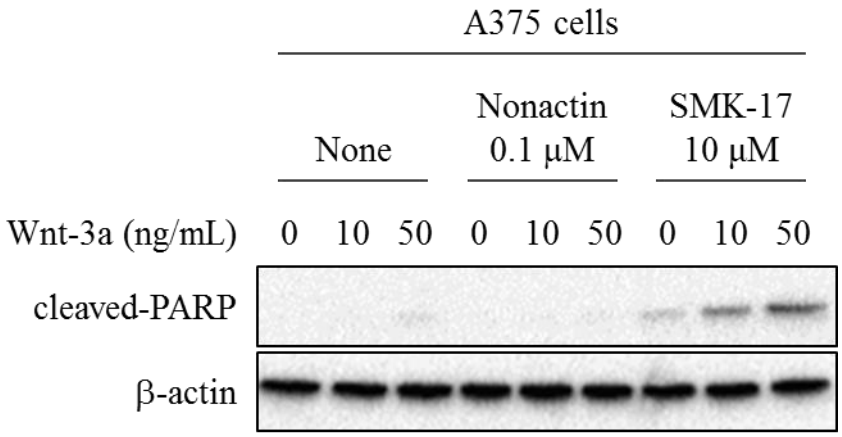

Figure 3-23. The effect of the Wnt pathway activation on the apoptosis-inducing ability of nonactin

β-Catenin wild type A375 cells were treated with the indicated concentrations of Wnt-3a in the presence or absence of 0.1 μM nonactin or 10 μM SMK-17 for 24 h, after which the expression levels of cleaved-PARP were detected by western blot.

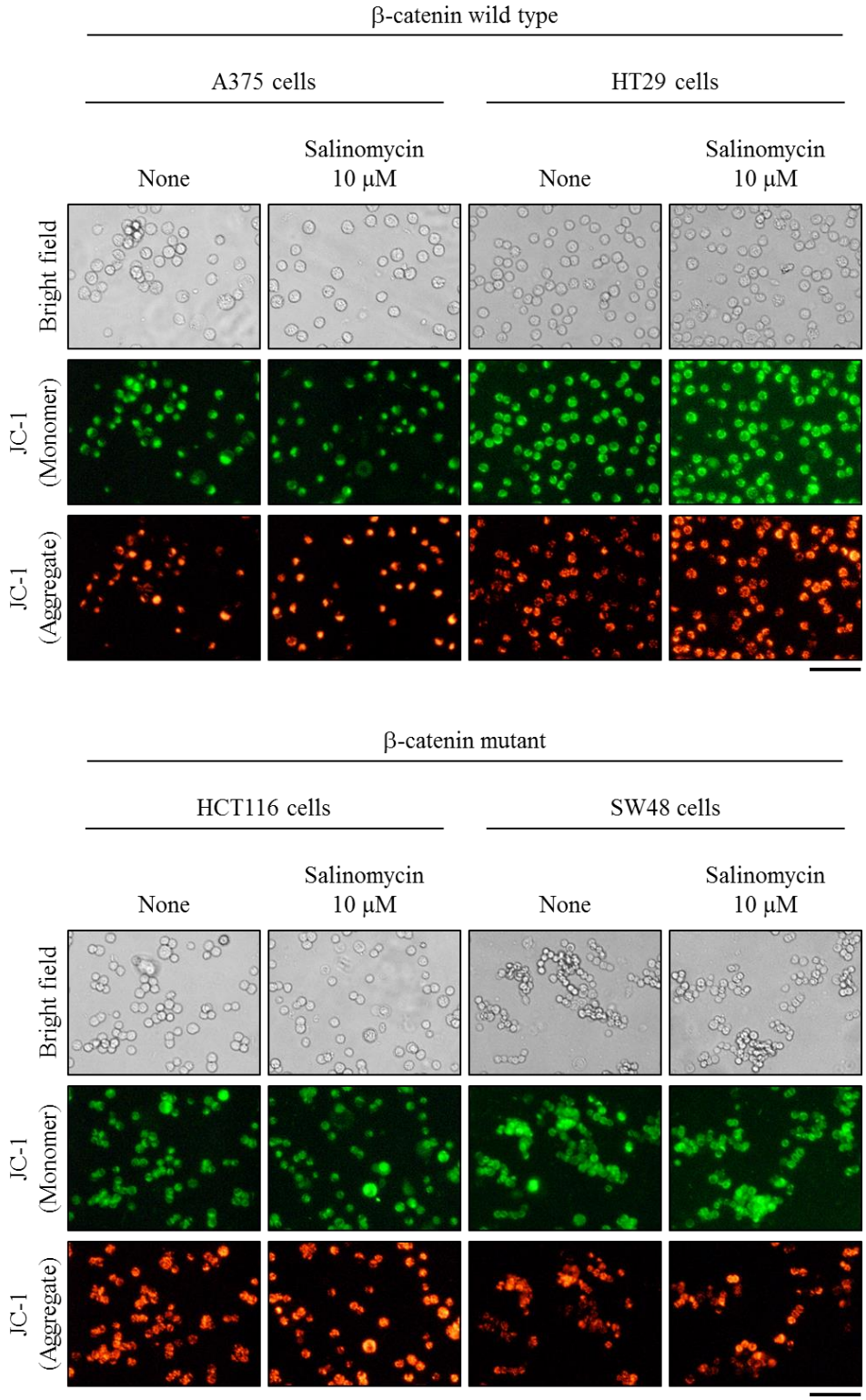

Figure 3-24. Salinomycin did not induce loss of mitochondrial membrane potential
Cells were treated with 10 μM of salinomycin for 30 min. Following treatment, cells were stained with 2.0 μM of JC-1 for 30 min, after which cells were harvested and the red and green fluorescence was observed by fluorescence microscopy. Scale bar, 100 μm.

3.4 Materials and Methods

3.4.1 Reagents and Compounds

Nonactin, valinomycin, carbonyl cyanide m-chlorophenyl hydrazone (CCCP), and 2-deoxyglucose (2-DG), Z-VAD-FMK were purchased from Sigma-Aldrich (St. Louis, MO). Salinomycin and monensin were purchased from Cayman Chemical (Ann Arbor, MI). SMK-17 was provided by M. Kiga (Keio University, Japan). Wnt-3a ligand was purchased from Wako Pure Chemical Industries (Osaka, Japan).

3.4.2 Isolation of nonactin from microbial extract

Nonactin was isolated from a culture broth extract of *streptomyces*. The broth was purified using HPLC (MG-II, ϕ4.6 mm × 250 mm; Shiseido, Tokyo, Japan) with 85% aqueous MeOH to obtain pure nonactin.

3.4.3 Cell lines

A431 cells were provided by M. Kawada (Institute of Microbial Chemistry, Japan). The other cell lines were obtained from the ATCC (Rockville, MD)[90]. A431 cells were maintained in DMEM supplemented with 5% Calf Serum (CS), 100 U/mL penicillin G (Sigma-Aldrich), and 0.1 mg/mL kanamycin (Sigma-Aldrich) at 37°C in a humidified atmosphere containing 5% CO_2. The other cells were maintained in RPMI-1640 supplemented with 10% FBS, 100 U/mL penicillin G, and 0.1 mg/mL kanamycin in the same conditions described above.

3.4.4 Western blot analysis

Anti-PARP, Anti-cleaved-PARP and anti-phospho-ERK1/2 were purchased from Cell Signaling Technology (Danvers, MA). Anti-β-catenin was purchased from BD Biosciences (San Jose, CA). Anti-β-actin, HRP-linked anti-mouse IgG, and HRP-linked anti-rabbit IgG were purchased from Sigma-Aldrich. Cells were treated with compounds for 24 h. In the co-treatment test using both 2-DG and an uncoupler, cells were pre-treated with 10 mM 2-DG for 1 h before being treated with the uncoupler. Following treatment, cells were immediately harvested and lysed with RIPA buffer (25 mM HEPES, 1.5% TX-100, 1% sodium deoxycholate, 0.1% SDS, 500 mM NaCl, 5 mM EDTA, 50 mM NaF, 0.1 M Na_3VO_4, and cOmplete Protease Inhibitor Cocktail Tablets (Roche, Germany); pH 7.8). The lysates were centrifuged at 13,000 rpm for 15 min to remove the insoluble fraction. Equal amounts of total protein were subsequently separated by SDS-polyacrylamide gel electrophoresis and probed with the indicated antibodies. The chemiluminescence signal was detected using an Immobilon Western kit (Merck Millipore) and ChemiDoc XRS+ System (Bio-Rad, Hercules, CA).

3.4.5 Cell cycle and apoptosis analysis by flow cytometry

Percentages of cells in different phases of the cell cycle, were analyzed by flow cytometry following staining with propidium iodide (PI; Wako Pure Chemical Industries), modified from a previously reported method[137]. Cells were treated with compounds for 48 h, then were harvested and fixed with 70% EtOH at 4°C, followed by treatment with 10 μg/mL RNase A (Wako Pure Chemical Industries) for 20 min at 37°C. Subsequently, cells were stained with 50 μg/mL PI. PI fluorescence was measured using an EPICS ALTRA Flow Cytometer (Beckman Coulter, Brea, CA).

3.4.6 Growth inhibition assay

Cell growth was measured by a CellTiter-Glo Luminescent Cell Viability Assay (Promega, Madison, WI) according to the manufacturer's protocol. The luminescence was detected by Fluoroskan Ascent FL (Labsystems, Helsinki, Finland), and this was compared to the luminescence recorded at 0 h. The growth rate of each cell type at each concentration of nonactin was calculated using nonactin-treated luminescence at 48 h (X_i), control luminescence at 48 h (X_{ctrl}), luminescence at 0 h ($X_{0\,h}$), and the following formula:

$$\text{If } X_i \geq X_{0\,h}, \text{ Growth rate} = X_i / X_{ctrl}$$

$$\text{If } X_i < X_{0\,h}, \text{ Growth rate} = X_i / X_{0\,h} - 1$$

If nonactin induced cell cycle arrest in the cells, the growth rate would be near zero. On the other hand, if nonactin induced cell death in the cells, the growth rate would be below zero.

3.4.7 Overexpression of wild type and active mutant β-catenin

Transfection of wild type and active mutant β-catenin (S37A, S45A) plasmid vectors and control vector was performed using PLUS Reagent and Lipofectamine LTX (Invitrogen Life Technologies, Carlsbad, CA) according to the manufacturer's protocol.

3.4.8 Monitoring of mitochondrial membrane potential

Loss of mitochondrial membrane potential was assessed using JC-1 (Wako Pure Chemical Industries), modified from a previously reported method[138]. Cells were treated with compounds for 30 min, then were stained with 2.0 μM JC-1 for 30 min at 37°C. Subsequently, cells were harvested and red and green fluorescence was observed using a

fluorescence microscope (IX71, Olympus, Japan). The images were captured with a digital camera (Olympus). Red and green fluorescence was quantified using ImageJ and the red/green ratio was calculated.

3.4.9 Assessment of glycolysis ability

The glycolysis ability of cells were analyzed using the XFe96 Extracellular Flux Analyzer (Seahorse Bioscience, Billerica, MA) according to the manufacturer's protocol[139]. In brief, 20,000 cells were seeded in 96-well plates designed for XFe96 and, following overnight culture, were resuspended in RPMI medium without D-glucose, serum and sodium bicarbonate. After incubation in the absence of CO_2 for 1 h, the extracellular acidification rate (ECAR) was measured using 50 mM 2-DG and 11 mM D-glucose.

3.4.10 Anti-tumor tests in a xenograft model

Specific pathogen-free female nude mice (BALB/cA Jcl-nu) were purchased from CLEA Japan (Tokyo, Japan). A tumor cell suspension (2×10^6 cells/mL) was inoculated subcutaneously into the axillar region of the nude mice on Day 0. Nonactin was dissolved in 10% dimethylacetamide (Wako Pure Chemical Industries), 10% NIKKOL HCO60 (Nikko Chemicals, Tokyo, Japan), and saline (Otsuka Pharmaceutical, Tokyo, Japan) and given daily to the animals by intraperitoneal administration (0.1 mL/10 g body weight). Tumor-bearing nude mice were randomly grouped (six mice/group), and administration of nonactin started on Day 9. Tumor volumes were calculated using a microgauge (Mitsutoyo Corporation, Kawasaki, Japan) according to the following equations: Tumor volume (mm^3) = 1/2 × (tumor length) × (tumor width)^2.

TUNEL staining of xenograft tumor tissue was performed using the FragEL DNA Fragmentation Detection Kit (Merck Millipore) according to the manufacturer's protocol. Tissue sections were viewed at 100× magnification, and images were captured with a digital camera.

3.4.11 Statistical analysis

All statistical analyses in bar plots were performed with a two-tailed paired Student's *t*-test to determine the difference between control and test group. In all cases, statistical significance was set at * $P<0.05$, ** $P<0.01$, and *** $P<0.001$.

Chapter 4 Conclusion

In Chapter 2, I investigated the molecular mechanisms governing the contribution of VCP to the antitumor activity of xanthohumol (XN). XN, a simple prenylated chalcone, can be isolated from hops and has the potential to be a cancer chemopreventive agent against several human tumor cell lines. I previously identified valosin-containing protein (VCP) as a target of XN; VCP can also play crucial roles in cancer progression and prognosis. Several human tumor cell lines were treated with XN to investigate which human tumor cell lines are sensitive to XN. Several cell lines exhibited high sensitivity to XN both *in vitro* and *in vivo*. shRNA screening and bioinformatics analysis identified that the inhibition of the adenylate cyclase (AC) pathway synergistically facilitated apoptosis induced by VCP inhibition. These results suggest there is crosstalk between the AC pathway and VCP function, and targeting both VCP and the AC pathway is a potential chemotherapeutic strategy for a subset of tumor cells.

In Chapter 3, I performed the screening for the compounds, which exhibit synthetic lethality with β-catenin mutation. As β-catenin is mutated in a wide variety of tumors, including up to 10% of all sporadic colon carcinomas and 20% of hepatocellular carcinomas, it has been considered a promising target for therapeutic interventions. Therefore, I screened an in-house natural product library for compounds that exhibited synthetic lethality towards β-catenin mutations and isolated nonactin, an antibiotic mitochondrial uncoupler, as a hit compound. Nonactin, as well as other mitochondrial uncouplers, induced apoptosis selectively in β-catenin mutated tumor cells. Significant tumor regression was observed in the β-catenin mutant HCT116 xenograft model, but not in the β-catenin wild type A375 xenograft model, in response to daily administration of nonactin *in vivo*. Furthermore, I found that expression of an active mutant form of β-catenin induced a decrease in the glycolysis rate. Taken together, our results demonstrate

that tumor cells with mutated β-catenin depend on mitochondrial oxidative phosphorylation for survival. Therefore, they undergo apoptosis in response to mitochondrial dysfunction following the addition of mitochondrial uncouplers, such as nonactin. These results suggest that targeting mitochondria is a potential chemotherapeutic strategy for tumor cells that harbor β-catenin mutations.

In the end, this concept of synthetic lethal has a great potential to target cancer cells with high selectivity. However, it is relatively new in oncology studies, therefore, it has not been resulted in clinical use yet. And also, it is quite difficult to identify synthetic lethal related genes. Our findings would provide clinical usefulness of synthetic lethality for patients with tumors, and contribute to human health more and ever.

References

1 Globocan, I. Estimated cancer incidence, mortality and prevalence worldwide in 2012. (2012).

2 Stewart, B. & Wild, C. P. World cancer report 2014. (2014).

3 Kohn, K. W., Hartley, J. A. & Mattes, W. B. Mechanisms of DNA sequence selective alkylation of guanine-N7 positions by nitrogen mustards. *Nucleic Acids Research* **15**, 10531-10549 (1987).

4 Nurse, D. S. Effect of antimetabolites on epidermal structures. *Archives of Dermatology* **87**, 258-265 (1963).

5 Hande, K. Etoposide: four decades of development of a topoisomerase II inhibitor. *European Journal of Cancer* **34**, 1514-1521 (1998).

6 Jordan, M. Mechanism of action of antitumor drugs that interact with microtubules and tubulin. *Current Medicinal Chemistry-Anti-Cancer Agents* **2**, 1-17 (2002).

7 Vogelstein, B. & Kinzler, K. W. Cancer genes and the pathways they control. *Nature Medicine* **10**, 789-799 (2004).

8 Sawyers, C. Targeted cancer therapy. *Nature* **432**, 294-297 (2004).

9 Druker, B. J. *et al.* Effects of a selective inhibitor of the Abl tyrosine kinase on the growth of Bcr-Abl positive cells. *Nature Medicine* **2**, 561-566 (1996).

10 Hudziak, R. M. *et al.* p185HER2 monoclonal antibody has antiproliferative effects in vitro and sensitizes human breast tumor cells to tumor necrosis factor. *Molecular and Cellular Biology* **9**, 1165-1172 (1989).

11 Carter, P. *et al.* Humanization of an anti-p185HER2 antibody for human cancer therapy. *Proceedings of the National Academy of Sciences of the United States of*

America **89**, 4285-4289 (1992).

12 Cunningham, D. *et al.* Cetuximab monotherapy and cetuximab plus irinotecan in irinotecan-refractory metastatic colorectal cancer. *New England Journal of Medicine* **351**, 337-345 (2004).

13 Escudier, B. *et al.* Sorafenib in advanced clear-cell renal-cell carcinoma. *New England Journal of Medicine* **356**, 125-134 (2007).

14 Llovet, J. M. *et al.* Sorafenib in advanced hepatocellular carcinoma. *New England Journal of Medicine* **359**, 378-390 (2008).

15 Holohan, C., Van Schaeybroeck, S., Longley, D. B. & Johnston, P. G. Cancer drug resistance: an evolving paradigm. *Nature Reviews Cancer* **13**, 714-726 (2013).

16 Hartwell, L. H., Szankasi, P., Roberts, C. J., Murray, A. W. & Friend, S. H. Integrating genetic approaches into the discovery of anticancer drugs. *Science* **278**, 1064-1068 (1997).

17 Lucchesi, J. C. Synthetic lethality and semi-lethality among functionally related mutants of *Drosophila melanogaster*. *Genetics* **59**, 37 (1968).

18 Dobzhansky, T. Genetics of natural populations. XIII. Recombination and variability in populations of *Drosophila pseudoobscura*. *Genetics* **31**, 269 (1946).

19 Sturtevant, A. A highly specific complementary lethal system in *Drosophila melanogaster*. *Genetics* **41**, 118 (1956).

20 Brough, R., Frankum, J. R., Costa-Cabral, S., Lord, C. J. & Ashworth, A. Searching for synthetic lethality in cancer. *Current Opinion in Genetics & Development* **21**, 34-41 (2011).

21 Beijersbergen, R. L., Wessels, L. F. & Bernards, R. Synthetic lethality in cancer therapeutics. *Annual Review of Cancer Biology* **1** (2016).

22 Bryant, H. E. *et al.* Specific killing of BRCA2-deficient tumours with inhibitors of poly (ADP-ribose) polymerase. *Nature* **434**, 913-917 (2005).

23 Farmer, H. *et al.* Targeting the DNA repair defect in BRCA mutant cells as a therapeutic strategy. *Nature* **434**, 917-921 (2005).

24 Puyol, M. *et al.* A synthetic lethal interaction between K-Ras oncogenes and Cdk4 unveils a therapeutic strategy for non-small cell lung carcinoma. *Cancer Cell* **18**, 63-73 (2010).

25 Luo, J. *et al.* A genome-wide RNAi screen identifies multiple synthetic lethal interactions with the Ras oncogene. *Cell* **137**, 835-848 (2009).

26 Rottmann, S., Wang, Y., Nasoff, M., Deveraux, Q. L. & Quon, K. C. A TRAIL receptor-dependent synthetic lethal relationship between MYC activation and GSK3β/FBW7 loss of function. *Proceedings of the National Academy of Sciences of the United States of America* **102**, 15195-15200 (2005).

27 Reinhardt, H. C., Aslanian, A. S., Lees, J. A. & Yaffe, M. B. p53-deficient cells rely on ATM-and ATR-mediated checkpoint signaling through the p38MAPK/MK2 pathway for survival after DNA damage. *Cancer Cell* **11**, 175-189 (2007).

28 Li, B., Gordon, G. M., Du, C. H., Xu, J. & Du, W. Specific killing of Rb mutant cancer cells by inactivating TSC2. *Cancer Cell* **17**, 469-480 (2010).

29 Wang, H. *et al.* Skp2 is required for survival of aberrantly proliferating Rb1-deficient cells and for tumorigenesis in Rb1+/-mice. *Nature Genetics* **42**, 83-88 (2010).

30 Hillenmeyer, M. E. *et al.* The chemical genomic portrait of yeast: uncovering a phenotype for all genes. *Science* **320**, 362-365 (2008).

31 Costanzo, M. *et al.* The genetic landscape of a cell. *Science* **327**, 425-431 (2010).

32 Nijman, S. M. & Friend, S. H. Potential of the synthetic lethality principle. *Science* **342**, 809-811 (2013).

33 Magnaghi, P. *et al.* Covalent and allosteric inhibitors of the ATPase VCP/p97 induce cancer cell death. *Nature Chemical Biology* **9**, 548-556 (2013).

34 Latterich, M. & Patel, S. The AAA team: related ATPases with diverse functions. *Trends in Cell Biology* **8**, 65-71 (1998).

35 Ju, J.-S. *et al.* Valosin-containing protein (VCP) is required for autophagy and is disrupted in VCP disease. *The Journal of Cell Biology* **187**, 875-888 (2009).

36 Tresse, E. *et al.* VCP/p97 is essential for maturation of ubiquitin-containing autophagosomes and this function is impaired by mutations that cause IBMPFD. *Autophagy* **6**, 217-227 (2010).

37 Yamanaka, K., Sasagawa, Y. & Ogura, T. Recent advances in p97/VCP/Cdc48 cellular functions. *Biochimica et Biophysica Acta (BBA)-Molecular Cell Research* **1823**, 130-137 (2012).

38 Ye, Y., Meyer, H. H. & Rapoport, T. A. The AAA ATPase Cdc48/p97 and its partners transport proteins from the ER into the cytosol. *Nature* **414**, 652-656 (2001).

39 Jarosch, E. *et al.* Protein dislocation from the ER requires polyubiquitination and the AAA-ATPase Cdc48. *Nature Cell Biology* **4**, 134-139 (2002).

40 Dai, R.-M., Chen, E., Longo, D. L., Gorbea, C. M. & Li, C.-C. H. Involvement of valosin-containing protein, an ATPase Co-purified with IκBα and 26 S proteasome, in ubiquitin-proteasome-mediated degradation of IκBα. *Journal of Biological Chemistry* **273**, 3562-3573 (1998).

41 Asai, T. *et al.* VCP (p97) regulates NFkB signaling pathway, which is important for metastasis of osteosarcoma cell line. *Japanese Journal of Cancer Research* **93**, 296-304 (2002).

42 Partridge, J. J., Lopreiato, J. O., Latterich, M. & Indig, F. E. DNA damage modulates nucleolar interaction of the Werner protein with the AAA ATPase p97/VCP. *Molecular Biology of the Cell* **14**, 4221-4229 (2003).

43 Mouysset, J. *et al.* Cell cycle progression requires the CDC-48UFD− 1/NPL− 4 complex for efficient DNA replication. *Proceedings of the National Academy of Sciences of the United States of America* **105**, 12879-12884 (2008).

44 Song, C., Wang, Q. & Li, C.-C. H. ATPase activity of p97-valosin-containing protein (VCP) D2 mediates the major enzyme activity, and D1 contributes to the heat-induced activity. *Journal of Biological Chemistry* **278**, 3648-3655 (2003).

45 Yamamoto, S. *et al.* Expression level of valosin-containing protein is strongly associated with progression and prognosis of gastric carcinoma. *Journal of Clinical Oncology* **21**, 2537-2544 (2003).

46 Yamamoto, S. *et al.* Increased expression of valosin-containing protein (p97) is associated with lymph node metastasis and prognosis of pancreatic ductal adenocarcinoma. *Annals of Surgical Oncology* **11**, 165-172 (2004).

47 Tsujimoto, Y. *et al.* Elevated expression of valosin-containing protein (p97) is associated with poor prognosis of prostate cancer. *Clinical Cancer Research* **10**, 3007-3012 (2004).

48 Wang, Q., Li, L. & Ye, Y. Inhibition of p97-dependent protein degradation by Eeyarestatin I. *Journal of Biological Chemistry* **283**, 7445-7454 (2008).

49 Wang, Q. *et al.* The ERAD inhibitor Eeyarestatin I is a bifunctional compound

with a membrane-binding domain and a p97/VCP inhibitory group. *PLoS One* **5**, e15479 (2010).

50 Bursavich, M. G. *et al.* 2-Anilino-4-aryl-1, 3-thiazole inhibitors of valosin-containing protein (VCP or p97). *Bioorganic & Medicinal Chemistry Letters* **20**, 1677-1679 (2010).

51 Chou, T.-F. & Deshaies, R. J. Quantitative cell-based protein degradation assays to identify and classify drugs that target the ubiquitin-proteasome system. *Journal of Biological Chemistry* **286**, 16546-16554 (2011).

52 Chou, T.-F. *et al.* Reversible inhibitor of p97, DBeQ, impairs both ubiquitin-dependent and autophagic protein clearance pathways. *Proceedings of the National Academy of Sciences of the United States of America* **108**, 4834-4839 (2011).

53 Power, F. B., Tutin, F. & Rogerson, H. CXXXV.—The constituents of hops. *Journal of the Chemical Society, Transactions* **103**, 1267-1292 (1913).

54 Sasazawa, Y. *et al.* Xanthohumol impairs autophagosome maturation through direct inhibition of valosin-containing protein. *ACS Chemical Biology* **7**, 892-900 (2012).

55 Dorn, C., Bataille, F., Gaebele, E., Heilmann, J. & Hellerbrand, C. Xanthohumol feeding does not impair organ function and homoeostasis in mice. *Food and Chemical Toxicology* **48**, 1890-1897 (2010).

56 Festa, M. *et al.* Xanthohumol induces apoptosis in human malignant glioblastoma cells by increasing reactive oxygen species and activating MAPK pathways. *Journal of Natural Products* **74**, 2505-2513 (2011).

57 Albini, A. *et al.* Mechanisms of the antiangiogenic activity by the hop flavonoid

xanthohumol: NF-κB and Akt as targets. *The FASEB Journal* **20**, 527-529 (2006).

58 Deeb, D. *et al.* Growth inhibitory and apoptosis-inducing effects of xanthohumol, a prenylated chalone present in hops, in human prostate cancer cells. *Anticancer Research* **30**, 3333-3339 (2010).

59 Lust, S. *et al.* Xanthohumol activates the proapoptotic arm of the unfolded protein response in chronic lymphocytic leukemia. *Anticancer Research* **29**, 3797-3805 (2009).

60 Yoshimaru, T. *et al.* Xanthohumol suppresses oestrogen-signalling in breast cancer through the inhibition of BIG3-PHB2 interactions. *Scientific Reports* **4**, 7355 (2014).

61 Barker, N. & Clevers, H. Mining the Wnt pathway for cancer therapeutics. *Nature Reviews Drug discovery* **5**, 997-1014 (2006).

62 Clevers, H. Wnt/β-catenin signaling in development and disease. *Cell* **127**, 469-480 (2006).

63 Amit, S. *et al.* Axin-mediated CKI phosphorylation of β-catenin at Ser 45: a molecular switch for the Wnt pathway. *Genes & Development* **16**, 1066-1076 (2002).

64 Daniels, D. L. & Weis, W. I. β-catenin directly displaces Groucho/TLE repressors from Tcf/Lef in Wnt-mediated transcription activation. *Nature Structural & Molecular Biology* **12**, 364-371 (2005).

65 Cadigan, K. M. & Liu, Y. I. Wnt signaling: complexity at the surface. *Journal of Cell Science* **119**, 395-402 (2006).

66 Tamai, K. *et al.* A mechanism for Wnt coreceptor activation. *Molecular Cell* **13**, 149-156 (2004).

67 Cselenyi, C. S. *et al.* LRP6 transduces a canonical Wnt signal independently of Axin degradation by inhibiting GSK3's phosphorylation of β-catenin. *Proceedings of the National Academy of Sciences of the United States of America* **105**, 8032-8037 (2008).

68 Hecht, A., Vleminckx, K., Stemmler, M. P., Van Roy, F. & Kemler, R. The p300/CBP acetyltransferases function as transcriptional coactivators of β-catenin in vertebrates. *The EMBO journal* **19**, 1839-1850 (2000).

69 Samowitz, W. S. *et al.* β-catenin mutations are more frequent in small colorectal adenomas than in larger adenomas and invasive carcinomas. *Cancer Research* **59**, 1442-1444 (1999).

70 Polakis, P. Wnt signaling and cancer. *Genes & Development* **14**, 1837-1851 (2000).

71 Van Nhieu, J. T. *et al.* Nuclear accumulation of mutated β-catenin in hepatocellular carcinoma is associated with increased cell proliferation. *The American Journal of Pathology* **155**, 703-710 (1999).

72 Gamallo, C. *et al.* β-catenin expression pattern in stage I and II ovarian carcinomas: relationship with β-catenin gene mutations, clinicopathological features, and clinical outcome. *The American Journal of Pathology* **155**, 527-536 (1999).

73 Voeller, H. J., Truica, C. I. & Gelmann, E. P. β-Catenin mutations in human prostate cancer. *Cancer Research* **58**, 2520-2523 (1998).

74 Forbes, S. A. *et al.* COSMIC: exploring the world's knowledge of somatic mutations in human cancer. *Nucleic Acids Research* **43**, D805-D811 (2015).

75 Klaus, A. & Birchmeier, W. Wnt signalling and its impact on development and cancer. *Nature Reviews Cancer* **8**, 387-398 (2008).

76 Behrens, J. *et al.* Functional interaction of an axin homolog, conductin, with β-catenin, APC, and GSK3β. *Science* **280**, 596-599 (1998).

77 Mori, Y. *et al.* Somatic mutations of the APC gene in colorectal tumors: mutation cluster region in the APC gene. *Human Molecular Genetics* **1**, 229-233 (1992).

78 Powell, S. M. *et al.* APC mutations occur early during colorectal tumorigenesis. *Nature* **359**, 235-237 (1992).

79 Dahmen, R. *et al.* Deletions of AXIN1, a component of the WNT/wingless pathway, in sporadic medulloblastomas. *Cancer Research* **61**, 7039-7043 (2001).

80 Satoh, S. *et al.* AXIN1 mutations in hepatocellular carcinomas, and growth suppression in cancer cells by virus-mediated transfer of AXIN1. *Nature Genetics* **24**, 245-250 (2000).

81 Kim, J.-S., Crooks, H., Foxworth, A. & Waldman, T. Proof-of-Principle: Oncogenic β-Catenin Is a Valid Molecular Target for the Development of Pharmacological Inhibitors. *Molecular Cancer Therapeutics* **1**, 1355-1359 (2002).

82 Kahn, M. Can we safely target the WNT pathway? *Nature Reviews Drug Discovery* **13**, 513-532 (2014).

83 Herr, P., Hausmann, G. & Basler, K. WNT secretion and signalling in human disease. *Trends in Molecular Medicine* **18**, 483-493 (2012).

84 Liu, J. *et al.* Targeting Wnt-driven cancer through the inhibition of Porcupine by LGK974. *Proceedings of the National Academy of Sciences of the United States of America* **110**, 20224-20229 (2013).

85 Gurney, A. *et al.* Wnt pathway inhibition *via* the targeting of Frizzled receptors results in decreased growth and tumorigenicity of human tumors. *Proceedings of the National Academy of Sciences of the United States of America* **109**, 11717-

11722 (2012).

86 Smith, D. C. *et al.* First-in-human evaluation of the human monoclonal antibody vantictumab (OMP-18R5; anti-Frizzled) targeting the WNT pathway in a phase I study for patients with advanced solid tumors. *Journal of Clinical Oncology* **31** (2013).

87 Smith, D. C. *et al.* Abstract B79: A first-in-human Phase 1 study of anti-cancer stem cell (CSC) agent OMP-54F28 (FZD8-Fc) targeting the WNT pathway in patients with advanced solid tumors. *Molecular Cancer Therapeutics* **12**, B79-B79 (2013).

88 Emami, K. H. *et al.* A small molecule inhibitor of β-catenin/cyclic AMP response element-binding protein transcription. *Proceedings of the National Academy of Sciences of the United States of America* **101**, 12682-12687 (2004).

89 El-Khoueiry, A. B. *et al.* A phase I first-in-human study of PRI-724 in patients (pts) with advanced solid tumors. *Journal of Clinical Oncology* **31** (2013).

90 Kiga, M. *et al.* SMK-17, a MEK1/2-specific inhibitor, selectively induces apoptosis in β-catenin-mutated tumors. *Scientific Reports* **5**, 8155 (2015).

91 Cho, Y.-C. *et al.* Differential anti-inflammatory pathway by xanthohumol in IFN-γ and LPS-activated macrophages. *International Immunopharmacology* **8**, 567-573 (2008).

92 Vogel, S., Ohmayer, S., Brunner, G. & Heilmann, J. Natural and non-natural prenylated chalcones: synthesis, cytotoxicity and anti-oxidative activity. *Bioorganic & Medicinal Chemistry* **16**, 4286-4293 (2008).

93 Bhattacharya, S., Virani, S., Zavro, M. & Haas, G. J. Inhibition of *Streptococcus mutans* and other oral streptococci by hop (*Humulus lupulus L.*) constituents.

Economic Botany **57**, 118-125 (2003).

94 Ostrom, R. S., Post, S. R. & Insel, P. A. Stoichiometry and compartmentation in G protein-coupled receptor signaling: implications for therapeutic interventions involving Gs. *Journal of Pharmacology and Experimental Therapeutics* **294**, 407-412 (2000).

95 Huang, D. W., Sherman, B. T. & Lempicki, R. A. Systematic and integrative analysis of large gene lists using DAVID bioinformatics resources. *Nature Protocols* **4**, 44-57 (2009).

96 Huang, D. W., Sherman, B. T. & Lempicki, R. A. Bioinformatics enrichment tools: paths toward the comprehensive functional analysis of large gene lists. *Nucleic Acids Research* **37**, 1-13 (2009).

97 Chijiwa, T. *et al.* Inhibition of forskolin-induced neurite outgrowth and protein phosphorylation by a newly synthesized selective inhibitor of cyclic AMP-dependent protein kinase, N-[2-(p-bromocinnamylamino) ethyl]-5-isoquinolinesulfonamide (H-89), of PC12D pheochromocytoma cells. *Journal of Biological Chemistry* **265**, 5267-5272 (1990).

98 Hall, M., Middleton, R. & Westmacott, D. The fractional inhibitory concentration (FIC) index as a measure of synergy. *Journal of Antimicrobial Chemotherapy* **11**, 427-433 (1983).

99 Chou, T.-C. Theoretical basis, experimental design, and computerized simulation of synergism and antagonism in drug combination studies. *Pharmacological Reviews* **58**, 621-681 (2006).

100 Kase, H. *et al.* K-252 compounds, novel and potent inhibitors of protein kinase C and cyclic nucleotide-dependent protein kinases. *Biochemical and Biophysical*

Research Communications **142**, 436-440 (1987).

101 Gerhauser, C. *et al.* Cancer chemopreventive activity of Xanthohumol, a natural product derived from hop. *Molecular Cancer Therapeutics* **1**, 959-969 (2002).

102 Vanhoecke, B. *et al.* Antiinvasive effect of xanthohumol, a prenylated chalcone present in hops (*Humulus lupulus L.*) and beer. *International Journal of Cancer* **117**, 889-895 (2005).

103 Stevens, J. F. & Page, J. E. Xanthohumol and related prenylflavonoids from hops and beer: to your good health! *Phytochemistry* **65**, 1317-1330 (2004).

104 Yamamoto, S. *et al.* Expression of valosin-containing protein in colorectal carcinomas as a predictor for disease recurrence and prognosis. *Clinical Cancer Research* **10**, 651-657 (2004).

105 Chang, Y. *et al.* Xanthohumol-induced presynaptic reduction of glutamate release in the rat hippocampus. *Food & Function* **7**, 212-226 (2016).

106 Wang, D. *et al.* Loss of cannabinoid receptor 1 accelerates intestinal tumor growth. *Cancer Research* **68**, 6468-6476 (2008).

107 Okazaki, Y. *et al.* CD146 and insulin-like growth factor 2 mRNA-binding protein 3 predict prognosis of asbestos‐induced rat mesothelioma. *Cancer Science* **104**, 989-995 (2013).

108 Morin, P. J. *et al.* Activation of β-catenin-Tcf signaling in colon cancer by mutations in β-catenin or APC. *Science* **275**, 1787-1790 (1997).

109 Stamos, J. L. & Weis, W. I. The β-catenin destruction complex. *Cold Spring Harbor Perspectives in Biology* **5**, a007898 (2013).

110 Ikeda, H., Shikata, Y., Watanapokasin, R., Tashiro, E. & Imoto, M. Metacycloprodigiosin induced cell death selectively in β-catenin-mutated tumor

cells. *The Journal of Antibiotics* **70**, 109-112 (2016).

111 Corbaz, R. *et al.* Stoffwechselprodukte von Actinomyceten. 3. Mitteilung. Nonactin. *Helvetica Chimica Acta* **38**, 1445-1448 (1955).

112 Marrone, T. J. & Merz Jr, K. M. Molecular recognition of potassium ion by the naturally occurring antibiotic ionophore nonactin. *Journal of the American Chemical Society* **114**, 7542-7549 (1992).

113 Graven, S. N., Lardy, H. A., Johnson, D. & Rutter, A. Antibiotics as tools for metabolic studies. V. Effect of nonactin, monactin, dinactin, and trinactin on oxidative phosphorylation and adenosine triphosphatase induction. *Biochemistry* **5**, 1729-1735 (1966).

114 Moore, C. & Pressman, B. C. Mechanism of action of valinomycin on mitochondria. *Biochemical and Biophysical Research Communications* **15**, 562-567 (1964).

115 Chen, L. B. Mitochondrial membrane potential in living cells. *Annual Review of Cell Biology* **4**, 155-181 (1988).

116 Vander Heiden, M. G., Cantley, L. C. & Thompson, C. B. Understanding the Warburg effect: the metabolic requirements of cell proliferation. *Science* **324**, 1029-1033 (2009).

117 Peifer, M. & Polakis, P. Wnt signaling in oncogenesis and embryogenesis--a look outside the nucleus. *Science* **287**, 1606-1609 (2000).

118 Polakis, P. The oncogenic activation of β-catenin. *Current Opinion in Genetics & Development* **9**, 15-21 (1999).

119 Ilyas, M., Tomlinson, I., Rowan, A., Pignatelli, M. & Bodmer, W. β-Catenin mutations in cell lines established from human colorectal cancers. *Proceedings of*

the National Academy of Sciences of the United States of America **94**, 10330-10334 (1997).

120 Polakis, P. The adenomatous polyposis coli (APC) tumor suppressor. *Biochimica et Biophysica Acta (BBA)-Reviews on Cancer* **1332**, F127-F147 (1997).

121 Gupta, P. B. *et al.* Identification of selective inhibitors of cancer stem cells by high-throughput screening. *Cell* **138**, 645-659 (2009).

122 Huczynski, A. Salinomycin–a new cancer drug candidate. *Chemical Biology & Drug Design* **79**, 235-238 (2012).

123 Naujokat, C., Fuchs, D. & Opelz, G. Salinomycin in cancer: A new mission for an old agent. *Molecular Medicine Reports* **3**, 555-559 (2010).

124 Antoszczak, M. & Huczyński, A. Anticancer activity of polyether ionophore-salinomycin. *Anti-cancer agents in medicinal chemistry* **15**, 575-591 (2015).

125 Managò, A. *et al.* Early effects of the antineoplastic agent salinomycin on mitochondrial function. *Cell Death & Disease* **6**, e1930 (2015).

126 Kemler, R. From cadherins to catenins: cytoplasmic protein interactions and regulation of cell adhesion. *Trends in Genetics* **9**, 317-321 (1993).

127 Aberle, H. *et al.* Assembly of the cadherin-catenin complex *in vitro* with recombinant proteins. *Journal of Cell Science* **107 (Pt 12)**, 3655-3663 (1994).

128 Hoschuetzky, H., Aberle, H. & Kemler, R. Beta-catenin mediates the interaction of the cadherin-catenin complex with epidermal growth factor receptor. *The Journal of Cell Biology* **127**, 1375-1380 (1994).

129 Tao, Y. S. *et al.* beta-Catenin associates with the actin-bundling protein fascin in a noncadherin complex. *The Journal of Cell Biology* **134**, 1271-1281 (1996).

130 Molenaar, M. *et al.* Differential expression of the HMG box transcription factors

XTcf-3 and XLef-1 during early Xenopus development. *Mechanisms of Development* **75**, 151-154 (1998).

131 Behrens, J. *et al.* Functional interaction of β-catenin with the transcription factor LEF-1. *Nature* **382**, 638-642 (1996).

132 Yamamoto, M., Bharti, A., Li, Y. & Kufe, D. Interaction of the DF3/MUC1 breast carcinoma-associated antigen and β-catenin in cell adhesion. *Journal of Biological Chemistry* **272**, 12492-12494 (1997).

133 Yu, G. *et al.* The presenilin 1 protein is a component of a high molecular weight intracellular complex that contains β-catenin. *Journal of Biological Chemistry* **273**, 16470-16475 (1998).

134 Aicher, B., Lerch, M. M., Müller, T., Schilling, J. & Ullrich, A. Cellular redistribution of protein tyrosine phosphatases LAR and PTPσ by inducible proteolytic processing. *The Journal of Cell Biology* **138**, 681-696 (1997).

135 Kuroda, S. *et al.* Role of IQGAP1, a target of the small GTPases Cdc42 and Rac1, in regulation of E-cadherin-mediated cell-cell adhesion. *Science* **281**, 832-835 (1998).

136 Yang, W. *et al.* Nuclear PKM2 regulates β-catenin transactivation upon EGFR activation. *Nature* **480**, 118-122 (2011).

137 Takeshima, M. *et al.* Anti-proliferative and apoptosis-inducing activity of lycopene against three subtypes of human breast cancer cell lines. *Cancer Science* **105**, 252-257 (2014).

138 Saito, K., Iioka, H., Kojima, C., Ogawa, M. & Kondo, E. Peptide-based tumor inhibitor encoding mitochondrial p14ARF is highly efficacious to diverse tumors. *Cancer Science* **107**, 1290-1301 (2016).

139 Wu, M. *et al.* Multiparameter metabolic analysis reveals a close link between attenuated mitochondrial bioenergetic function and enhanced glycolysis dependency in human tumor cells. *American Journal of Physiology-Cell Physiology* **292**, C125-C136 (2007).

Acknowledgements

本研究は慶應義塾大学理工学部教授 井本正哉博士のご指導のもと、実施致しました。終始ご指導ご鞭撻賜りましたことに謹んで感謝の意を表します。

また本研究を進めるにあたり、多くのご指導、ご助言を頂きました慶應義塾大学理工学部専任講師　田代悦博士に深く感謝の意を表します。

本研究の執筆にあたり、ご指導、ご助言を頂きました慶應義塾大学理工学部教授 岡浩太郎博士、慶應義塾大学理工学部准教授 土居信英博士、慶應義塾大学理工学部准教授 清水史郎博士に厚く御礼申し上げます。

Xanthohumol に関する研究に際し、*in vivo* 試験を実施して下さいました徳島大学疾患プロテオゲノムセンターゲノム制御分野 片桐豊雅博士、小松正人博士、吉丸哲郎博士、各臓器における組織染色をして下さいました名古屋大学医学部豊國伸哉博士、岡﨑泰昌博士、shRNA スクリーニングを実施して下さいました東京医科歯科大学難治疾患研究所 石川俊平博士、加藤洋人博士、佐藤玲子氏、様々な cell line 間での VCP の発現量を比較検証して下さいました慶應義塾大学理工学部卒業生 金墻周平氏に厚く御礼申し上げます。

Nonactin に関する研究に際し、Extracellular Flux Analyzer をお貸し頂き、またご指導、ご助言を頂きました理化学研究所ケミカルバイオロジー研究グループ 長田裕之博士、二村友史博士、青野晴美氏、*in vivo* 試験を実施して頂きました慶應義塾大学理工学部卒業生 木我真基博士、組織染色法についてご指導、ご助言を頂きました微生物化学研究所 川田学博士、井上裕幸氏、nonactin の構造決定についてご助言を頂きました日本女子大学家政学部 新藤一敏博士に厚く御礼申し上げます。

また、様々な面でサポートして頂きましたケミカルバイオロジー研究室秘書梅崎秀香さん、数々の助言を頂き、相談に乗って下さったケミカルバイオロジー研究室の諸先輩方、後輩、技術員のみなさんに感謝致します。

そして、共に励ましあい、助け合い、活発な議論をした同輩の井岡秀二君、齋藤駿君、溝谷優治君に深く感謝致します。

最後に、大学院まで通わせてくれた家族、応援してくれた友人に感謝します。